TAMPEREEN TEKNILLINEN YLIOPISTO
TAMPERE UNIVERSITY OF TECHNOLOGY

Valtteri Lahtinen

Searching for Frontiers in Contemporary Eddy Current Model Based Hysteresis Loss Modelling of Superconductors

Julkaisu 1231 • Publication 1231

Tampere 2014

Tampereen teknillinen yliopisto. Julkaisu 1231
Tampere University of Technology. Publication 1231

Valtteri Lahtinen

Searching for Frontiers in Contemporary Eddy Current Model Based Hysteresis Loss Modelling of Superconductors

Thesis for the degree of Doctor of Science in Technology to be presented with due permission for public examination and criticism in Tietotalo Building, Auditorium TB109, at Tampere University of Technology, on the 1st of September 2014, at 10:30 am.

Tampereen teknillinen yliopisto - Tampere University of Technology
Tampere 2014

ISBN 978-952-15-3334-1 (printed)
ISBN 978-952-15-3352-5 (PDF)
ISSN 1459-2045

Abstract

Alternating current (AC) or magnetic field leads to heat generation in otherwise lossless superconducting materials. Such heat generation is called AC loss. AC loss of special type that occurs in the superconducting material itself, and not in the normal-conducting parts of the superconducting wire is called hysteresis loss. Hysteresis loss is a restricting factor for the feasibility of many superconducting applications, and hence, having reliable and efficient models for predicting hysteresis losses in devices is crucial for the design process.

In this thesis, we first introduce the readers to the mathematical structures that are essential for simulating AC losses. The level of abstraction deviates from what is typical in this field, but it allows us to present the models and formulations we use in a structured manner and naturally program simulation tools, which are independent of the dimension of the modelling domain. We also discuss the background of the research by presenting important aspects of our research philosophy and the framework inside which the research in this field is conducted. Then, we briefly present two formulations implemented in our AC loss simulation tool, the so called H-formulation and the so called T-φ-Ψ-formulation, and compare their properties through simulations. The latter of the formulations exploits the topology of the modelling domain to reduce the number of required equations, and it is superior to the former in terms of running times of the simulations. Furthermore, we discuss the properties of two widely used models, the critical state model and the eddy current model, through particular case studies of superconductors under direct current bias and an alternating magnetic field. Neither one of the models is fully able to reflect the intrinsic properties of high-temperature superconductors. Finally, the possibilities of our simulation tool are investigated: we study the potential of the tool in question to yield predictions of multifilamentary twisted superconductors with partially coupled filaments in external magnetic field in two dimensions. We present a simple algorithm for this, and the obtained simulation results show good agreement with results of three-dimensional simulations.

Preface

In the late summer of 2007, I, as an excited and a bit frightened freshman, arrived at Tampere University of Technology (TUT) for the first time as a student. Sitting on the stairs of the Festia building, waiting for my first university lecture, I had absolutely no idea what to expect and what the future years would bring. However, as the academic year went on, it became very soon clear that the teachers at the research group of Electromagnetics[1] (EM) were something special. The first basic courses taught by Aki Korpela, Risto Mikkonen and Jari Kangas, and the ones taught by Lauri Kettunen and Saku Suuriniemi the next year, made me realize that one can actually learn something about electromagnetic phenomena and how they are modelled; a subject I had been completely lost with for all my high school years. But not only was I learning, I was getting extremely excited about mathematics and electromagnetic modelling. I took as many courses taught by the people of EM as I could, and sooner than I knew, I was already learning mathematical physics from Timo Tarhasaari and talking to my doctoral thesis supervisor-to-be Antti Stenvall about a suitable subject for bachelor's thesis about mathematical modelling of superconductors in the spring of 2010.

Eventually, I think Antti liked my bachelor's thesis since in the summer of 2011, he hired me for a project that allowed me to first write my master's thesis about superconductor modelling and then continue to write a doctoral thesis about the same subject. The book you are holding in your hands is precisely that. Working on this book has been very challenging, time-consuming, and most importantly, extremely fun and rewarding. The working environment at EM, I believe, is something unique. In no other workplace have I been privileged to work with such inspirational and friendly people. I am utterly sure that the spirit of EM will stay strong in me, whatever the future holds.

So, some thanks for the people of EM are in order. Thank you Antti for your guidance, mentorship and friendship throughout these years. Thank you

[1] At that time, Institute of Electromagnetics.

Timo for sharing your insight and teaching me so much. Thank you Lauri for having created and kept up the extraordinary spirit of EM. Thanks to Aki for taking care that everyone had fun (and coffee) at coffee breaks. Thanks to Erkki Härö for being a great roommate, at the office as well as when travelling, for these past two and a half years. Thanks to Juha Tampio and Mika Lyly for all the great conversations and relaxing moments over a pint of beer during our beer club meetings. Many thanks go to Matti Pellikka as well: not only are you a good friend, but a great young scientist; you helped me a lot with this thesis, even after you left EM for other opportunities. Thanks also to Maija-Liisa Paasonen and Lasse Söderlund for making sure that I have not had to worry about any administrative and bureaucratical issues.

It turns out that the list of people to thank at EM is way too long to be written out in full in this preface. So simply, I would like to thank everyone I have had the privilege to work with here at EM. Luckily, however, it has not been all work. The weekly floorball games and all the other events we have had together have had a great impact on my well-being.

I also had the wonderful opportunity to visit the research group of professor Frédéric Sirois at École Polytechnique de Montréal for six months during the academic year 2013–2014. Most of the actual writing process of this thesis was done there, in the home of hockey. I want to thank Frédéric, professor Marc LaForest and many of their co-workers and students for the warm welcome I received there. Special thanks go to Andy Wan for our lengthy discussions about cohomology and to Roland Rivard for the solver benchmarking project we worked on. I hope to see all of you soon again. Go Habs go!

Finally, thanks to all my family and friends for keeping me sane and reminding me there is more to life than research. Most importantly, thanks to my dear Heidi: there are no words to describe what you mean to me.

In Tampere, July 22, 2014

Valtteri Lahtinen

List of publications and author's contribution

Publication 1

Lahtinen V, Lyly M, Stenvall A and Tarhasaari T 2012
Supercond. Sci. Technol. **25** 115001
"Comparison of three eddy current formulations for superconductor hysteresis loss modelling"

Publication 2

Lahtinen V and Stenvall A 2013
IEEE Trans. Appl. Supercond. **23** 4900505
"The difficulty of modeling ripple field losses in superconductors using the eddy current model"

Publication 3

Lahtinen V and Stenvall A 2014
IEEE Trans. Appl. Supercond. **24** 8200205
"Toward two-dimensional simulations of hysteresis losses in partially coupled superconducting wires"

Publication 4

Lahtinen V and Stenvall A 2014
J. Supercond. Nov. Magn. **27** 641
"Scientific research in the field of mesh method based modeling of AC losses in superconductors: A review"

Publication 5

Lahtinen V, Pardo E, Šouc J, Solovyov M and Stenvall A 2014
J. Appl. Phys. **115** 113907
"Ripple field losses in direct current biased superconductors: Simulations and comparison with measurements"

Publication 6

Lahtinen V, Stenvall A, Sirois F and Pellikka M 2014
Appl. Num. Math. Submitted for peer review.
"A modelling tool for simulating hysteresis losses in superconductors utilizing an H-oriented finite element method formulation with cohomology basis functions"

Author's contribution

The author has written all the text in the publications, with the following exception. E. Pardo wrote substantial parts of sections 3 and 4 and small parts of all the other sections for **Publication 5**. All in all, the writing of **Publication 5** was divided rather equally with E. Pardo, while the author was the corresponding writer all the time.

In all the publications, the discussions with A. Stenvall played a crucial role in all the stages of writing. Furthermore, F. Sirois and M. Pellikka helped to finalize the text in **Publication 6** and discussions with M. Pellikka were crucial for conceiving the paper.

All the simulation and programming work was done by the author, with the exceptions of programming two of the eddy current formulations presented in **Publication 1**, which had been done earlier by A. Stenvall, and the critical state model based simulations of **Publication 5**, which were performed by E. Pardo.

In **Publication 5**, AC loss measurements were performed by J. Šouc, while the author was merely an apprentice. The author post-processed the measurement data. The Hall-probe mapping measurements presented in the same paper were performed by M. Solovyov. He also did the required post-processing to get the current density profile in the superconductor from the measured magnetic field distribution.

Detailed author's contribution for each publication

Publication 1: The author programmed one of the eddy current formulations in MATLAB for the simulation tool used in the publication, wrote the text and performed all the simulations used for comparing the different formulations. Furthermore, he put special effort into writing an informative overview about manifolds and differential geometry in the context of superconductor

modelling.

Publication 2: The author used an in-house AC loss simulation software to simulate ripple field losses in a direct current biased multifilamentary MgB_2 wire and a monofilamentary wire. This led to observations about the applicability of the power law based eddy current model for such simulations. The author programmed the software using C++ programming language and it was implemented as a compact part of an open-source finite element mesh generator software, using its interface for interpreting the pre-processor model files as Riemannian manifolds. An open-source time integrator package was used for time-discretization. This software was used extensively and further developed in all the rest of the publications, too. The author wrote the publication.

Publication 3: The author invented the presented algorithm for simulating hysteresis losses in superconducting wires with partially coupled filaments in two dimensions. He then programmed the necessary additions to his AC loss simulation software and performed the two-dimensional simulations. Furthermore, he simulated the same situations in three dimensions for benchmarking purposes. The author wrote the publication.

Publication 4: The author conducted a wide literature survey related to contemporary research of mesh method based AC loss modelling of superconductors. Furthermore, as a result of various discussions with A. Stenvall, he divided the research into different research directions and carefully scrutinized the terminology often used in such research. The author wrote the publication.

Publication 5: The author performed the eddy current model based computations of the investigated high-temperature superconducting tapes and post-processed AC loss measurement data. As the corresponding author, he also envisioned, supervised and approved, in close collaboration with the co-authors, the different simulation and measurement cases detailed in the publication. He wrote the publication together with E. Pardo, as discussed above.

Publication 6: The author programmed the simulation tool described in the publication and performed all the simulations. The tool was implemented in the same programming environment as the one first used in **Publication 2**. To benchmark the new simulation tool, different AC loss simulation cases were performed by the author in two and three dimensions using both of these tools. The author wrote the publication, putting special emphasis on a readable exposition of the concepts of algebraic topology exploited in the simulation tool.

Contents

Lists of symbols and abbreviations

A	Magnetic vector potential
B	Magnetic flux density
$\mathbf{B}$	Vector field version of magnetic flux density
B^*	Threshold amplitude of varying magnetic flux density for dynamic magneto-resistance
B_a	Amplitude of magnetic flux density
B_c	Critical magnetic flux density
B_c1	Lower critical magnetic flux density
B_c2	Upper critical magnetic flux density
B_p	Magnetic flux density of full penetration
B_ext	Applied magnetic flux density
c	Small positive real number
$\hat{c}$	Curve
C	Coupling degree
C_eff	Effective coupling degree
d	Exterior derivative operator
$\tilde{\mathrm{d}}$	Weak exterior derivative
D	Electric flux density
D	Differential of a mapping
E	Electric field intensity
$\mathbf{E}$	Vector field version of electric field intensity
$E(\Omega)$	Set of mesh edges in the modelling domain Ω
E_c	Electric field criterion
e_m	Energy density of magnetic field
f	Frequency
$\hat{f}$	Smooth function
$\hat{F}$	Smooth mapping between manifolds
$F_p(\Omega)$	The space of differential p-forms on the manifold Ω
g	The metric tensor (or its matrix representation)
G	Solution of an equation, a differential form

G_{app}	Approximative solution of an equation, a differential form
H	Magnetic field intensity
$\mathbf{H}$	Vector field version of magnetic field intensity
$H_1(\Omega)$	The 1-homology space of the manifold Ω
h_i	Real number coefficient
H_m	Magnetic field intensity without the contribution of currents
I	Current
I_i	Current through conductor i, a real number coefficient
I_{a}	Amplitude of alternating current
I_{c}	Critical current
I_{coupled}	Current through a filament in a fully coupled situation
$\hat{I}_{\text{coupled}}$	Positive peak value of current through a filament in a fully coupled situation
$\tilde{I}_{\text{coupled}}$	Negative peak value of current through a filament in a fully coupled situation
$\bar{I}_{\text{coupled}}$	Average of absolute values of $\hat{I}_{\text{coupled}}$ and $\tilde{I}_{\text{coupled}}$
I_{DC}	Value of direct current
I_{fil}	Current through a filament
$\hat{I}_{\text{fil}}$	Positive peak value of current through a filament
$\tilde{I}_{\text{fil}}$	Negative peak value of current through a filament
$\bar{I}_{\text{fil}}$	Average of absolute values of $\hat{I}_{\text{fil}}$ and $\tilde{I}_{\text{fil}}$
i_{m}	Ratio of amplitude of alternating current and critical current
J	Current density
$\mathbf{J}$	Vector field version of current density
$\hat{J}$	Vector valued 3-form current density
J_{c}	Critical current density
k	Arbitrary dimension of a manifold
L	Linear operator
$L^2F_p(\Omega)$	The L^2 inner product space of differential forms on Ω
$L^2F_p(\text{d}, \Omega)$	A Sobolev space of differential forms on Ω
$L^2F_p(\delta, \Omega)$	A Sobolev space of differential forms on Ω
m	Magnetization (1-form)
$\mathbf{m}$	Vector field version of magnetization
$\hat{m}$	2-vector valued 3-form magnetization
M	Magnetic (dipole) moment (2-vector)
$\mathbf{M}$	Magnetic (dipole) moment vector
$\mathbf{n}$	Normal vector
n	n-value of the superconductor
$N(\Omega)$	Set of mesh nodes in the modelling domain Ω
p	Arbitrary non-negative integer

P	Power
p_{d}	Ohmic power density
q	Arbitrary non-negative integer
Q	Total hysteresis loss
Q_{M}	Magnetization loss
Q_{T}	Transport loss
Q_{Υ}	Hysteresis loss obtained after rotating applied field about an angle Υ
$\mathbf{r}$	Location with respect to coordinate system origin
r_{m}	Radius of matrix with round cross-section
r_{SC}	Radius of superconducting filament with round cross-section
S	Surface
T	Current vector potential
$T_p^q(\Omega)$	The space of (q,p)-tensor fields on the manifold Ω
$T_x(\Omega)$	Tangent space at point x
$T_x^*(\Omega)$	Cotangent space at point x
t	Time
t_i	Real number coefficient
u	An oriented subset of a $p+1$-dimensional manifold
U	A subset of the p-dimensional real coordinate space
$\boldsymbol{v}$	a tuple of tangent vectors
V	Vector space
V_{e}	Electromotive force
$\mathbf{v}_x$	Tangent vector at point x
vol^k	Volume form on a k-dimensional manifold
$VT(\Omega_{\mathrm{nc}})$	The set of tunnels through the manifold Ω_{nc}
w_i	Whitney 1-form related to edge i
w_i^p	Whitney p-form related to simplex i
W	Parametrization mapping
W^*	Pullback through W
$W_p(\Omega)$	The space of Whitney p-forms on manifold Ω

$\mathcal{H}$	Hilbert space
$\mathbb{R}$	The set of real numbers
$\mathbb{R}^k$	The k-dimensional real coordinate space
∂	Boundary operator
∂_t	Time-derivative operator
$\frac{\boldsymbol{\partial}}{\boldsymbol{\partial} x^i}$	Basis tangent vector

α	Angle
α_j	Real number coefficient
β	Arbitrary p-form
β_j	Real number coefficient
γ	Arbitrary p-form
Γ	Curve
γ_j	Real number coefficient
δ	Coderivative operator
$\tilde{\delta}$	Weak coderivative
δ^{ji}, δ^j_i	The Kronecker delta
δ^J_I	The Kronecker delta for multi-indices
δ_j	Real number coefficient
ϵ	Material specific part of the permittivity operator
$\epsilon_\star$	Permittivity operator $\epsilon \circ \star$
η	Arbitrary p-form
θ	Temperature
θ_c	Critical temperature
λ_i	Whitney 0-form related to node i
μ	Material specific part of the permeability operator
$\mu_\star$	Permeability operator $\mu \circ \star$
μ_0	Vacuum permeability
ϖ	Arbitrary $p-1$-form
ρ	Material specific part of the resistivity operator
$\rho_\star$	Resistivity operator $\rho \circ \star$
ρ_air	Resistivity of air
ρ_m	Resistivity of matrix
ρ_SC	Material specific part of the resistivity operator in superconductor
τ	Arbitrary q-form
Υ	Angle
σ	Charge density
ς	Arbitrary 0-form
ϕ	Arbitrary 0-form
Φ	Element of a Hilbert space. A p-form in particular.
ϕ_i	Real number coefficient
φ	Magnetic scalar potential
ψ	Arbitrary 1-form
Ψ	Cohomology basis function
Ω	Manifold, modelling domain
Ω_c	Conducting subdomain

Ω_{nc}	Non-conducting subdomain
Ω_{SC}	Superconducting subdomain
χ	Coordinate chart
$\hat{\chi}$	Coordinate chart

$\wedge$	Exterior product
$\star$	Hodge operator
$\sharp$	Metric isomorphism taking p-forms to p-vectors: sharp
$\flat$	Metric isomorphism taking p-vectors to p-forms: flat
$\otimes$	Tensor product

AC	Alternating current
AC field	Alternating magnetic field
Bi-2223	Bismuth based high-temperature superconductor
BVP	Boundary value problem
CSM	The critical state model
DC	Constant current (direct current)
DC field	Constant (non-alternating) magnetic field
DAE	Differential-algebraic equation
DOF(s)	Degree(s) of freedom
ECM	Eddy current model
FCL	Fault current limiter
FDM	Finite difference method
FDTD	Finite difference time-domain
FEM	Finite element method
FIT	Finite integration technique
HTS	High-temperature superconductor
IEM	Integral equation method
LHC	Large Hadron Collider
LTS	Low-temperature superconductor
MgB_2	Magnesium diboride
MMMACL	Mesh method based modelling of AC losses in superconductors
MRI	Magnetic resonance imaging
NbTi	Niobium-titanium
Nb_3Sn	Niobium-tin
PDE	Partial differential equation
SC	Superconducting / Superconductor
SMES	Superconducting magnetic energy storage
YBCO	Yttrium based high-temperature superconductor

Chapter 1

Introduction

We, human beings, make observations about the world around us constantly. But we are not only interested in observing, as we also want to make predictions based on those observations. For example, people have tried to predict the weather based on their observations for ages: if the sky is clear this evening, you might predict that the following night will be cold. Or you may observe someone commuting to his workplace in the same bus at exactly the same time as you commute to your own workplace. Then, the next day you see the same person at exactly the same time of the day in exactly the same situation. When you observe this happening again and again, it is likely that you will, at least implicitely, make the prediction that you will see that person the next morning, too. It is natural for us to build our intuition of things on the orderly behaviour and repetitive occurences we observe. Even though in a much more formal manner, this is also the idea of physics: the repetitive patterns observed in nature are formalized in the language of mathematics, using which we can, often with high accuracy, predict future occurences in the world. We trust that nature is self-consistent and *formalize our intuition* using mathematics.

Sometimes, when we stumble upon something new, the observations we make might not match the intuition we have built and formalized so far. This was also the case with the discovery of *superconductivity* [90], which did not really fit into anything that people had observed before: suddenly, at a temperature low enough, the resistivity of the superconducting material vanished completely. Later on, it was observed that at the same time as the resistivity vanishes, all the magnetic field is expelled from the material [38]. At the time of these discoveries, no known physics could predict such an event. Occurences like this force us to reshape our thinking: our models which we use to predict what happens in the world are not always valid everywhere and give better

predictions in some situations than in others. It does not make sense to claim that a given model yields some kind of an *intrinsic* description of the world as it is: all we have is our observations and the unreasonably effective language of mathematics, which we can use to formalize the intuition we have built based on them.

Eventually, the discovery of superconductivity turned out to be a very useful observation, and today, there are many technologies that benefit from the use of superconducting materials [32]. Also, it turns out that nowadays we have several ways to predict the behaviour of superconductors using mathematical descriptions. This thesis concentrates on mathematical modelling of heat generation in superconductors. The research presented in the thesis targets on searching for and pushing the frontiers in modelling the phenomena related to it. As a general guideline for the research, we have tried to not only present the excellence of the mathematical models we use, but also concentrate on the results that do not always fit in with our observations.

1.1 Motivation

From an engineer's point of view, understanding heat generation is an issue of high importance. Dissipative processes need to be carefully taken into account in the design process of a technological device. This can be done by using simulations based on mathematical models. Simulations form an essential phase in the design process as reliable modelling can significantly reduce the resources wasted on building a prototype after another not matching the specifications.

One of the main motivations to use superconductors in electrotechnical devices stems from the fact that they can carry large currents without producing any heat. This is, however, true only if the current is not time-varying and there is no time-varying magnetic field present. The dissipation related to the time-variation of the electromagnetic quantitites that occurs in superconductors is called alternating current (AC) loss. In this thesis, our particular interest is in mathematical modelling of AC losses in superconductors, and to be even more particular, in the modelling of *hysteresis losses*, which constitute one type of AC loss. This is important, as superconducting applications that do not experience any time-variation of electric current or magnetic field are rare: AC losses can often be a restricting factor for the feasibility of applications.

To predict the heat generation in superconductors, we need models, and essentially, modelling physical phenomena is mathematics. However, the mathematical structures, on which the models are based, are often left without

recognition in engineering. A structural approach provides indispensable tools for the modeller to identify the relevant aspects of modelling in different situations, and understand the models that are used to describe nature. Such an identification can lead to results of high generality and wide usability. Modern mathematical tools of the 20th century are of structural and geometrical nature, as the theory of manifolds and differential geometry unifies mesoscopic modelling of many kinds under the same framework. Modern mathematics offers tools for engineers to identify the structures and invariances in the models, giving rise to creativity and new engineering tools through deeper understanding of the machinery they are using. The identification of structures and invariances is important for getting to the bottom of things: the more unnecessary or unrecognizable structure there is in a model, the further one gets from the fundamental understanding.

The mathematical formalism used to present the theory and models in this thesis is that of manifolds and differential geometry. It is a very natural language for describing electromagnetic phenomena, as it reveals the structure of Maxwell's theory and its models in a way unattainable in the traditional vector field formalism. Such a structural approach is beneficial from not only the point of view of presentation, but also for a programmer working with electromagnetic modelling [100].

1.2 Structure of the thesis

Each chapter of this thesis seeks to find and push the frontiers of the research in this particular field of science in a different way. In chapter 2, the fundamentals of mathematical modelling of AC losses are discussed in a more structural way than what is typical to our field. Then, in chapter 3, we discuss a formulation that is new to our field, exploiting mathematical concepts more familiar from the context of algebraic topology than superconductor technology. Chapter 4 discusses discrepancies between the predictions of two widely used models, as well as between them and measurement results, and chapter 5 presents a new approach for modelling hysteresis losses in certain situations.

Let us summarize the structure of the thesis in more detail. First, in chapter 2, the philosophical and mathematical background for the research of this thesis is presented. We discuss the aspects of mathematical modelling important for this thesis, and furthermore, present the relevant parts of the theory of manifolds and differential geometry. The different aspects of modelling electromagnetic phenomena are discussed and introduced side-by-side

with the mathematics, to emphasize their interconnectedness. Furthermore, we introduce superconductivity and AC losses of superconductors. As an essential part of the background, we also discuss the scientific framework, in which the research of this thesis resides.

After the background, in chapter 3, we discuss the AC loss modelling tool that plays the double role of a research tool and an outcome of the research of this thesis. We present two of the formulations implemented within the tool and discuss their properties. In particular, we present a formulation that is, to our best knowledge, completely new in the field of AC loss modelling. Furthermore, we compare the formulations using simulation examples.

Chapter 4 presents case studies of DC biased superconductors experiencing AC ripple fields. The predictions of two widely used models for such situations are compared with each other as well as with measurements. We also discuss the background and consequences of this research related to physics and research philosophy.[1]

In chapter 5, we investigate the possibility to model superconducting wires, that are partially coupled with respect to external magnetic field, using our modelling tool in two dimensions. We present an algorithm to perform such simulations and compare the results with three-dimensional simulations.

Finally, in chapter 6, we summarize the presented research and draw conclusions.

[1]However, this thesis is not a book about philosophy. For us, the research philosophy means a desire for a thorough understanding of all the terminology related to natural sciences we tend to use, and a will to understand all the aspects of even a particular modelling case via underlying mathematical structures. This research philosophy is heavily influenced by the works of mathematician R. L. Wilder [137, pp. 3-53] and philosopher J. North [89]. Furthermore, our way of approaching and presenting the mathematical aspects related to our research is heavily influenced by J. C. Baez [11]. This is not to say that we would or even could replicate the works of these three scientists, but merely that this thesis would be very different without their influence.

Chapter 2

Background

This chapter provides the mathematical-philosophical and technological framework for this thesis and for the search of frontiers in our branch of science. We discuss the philosophical and mathematical background for modelling nature. First, mathematical modelling is discussed from a philosophical point of view. In a sense, we try to answer the question: 'what is mathematical modelling?'. Consequently, we present the sufficient mathematical background for following the publications of this thesis. Then, electromagnetic phenomena and Maxwell's theory, the models of which predict those phenomena with high precision, are discussed. Furthermore, we introduce superconductivity and AC losses of superconductors in particular. Especially, we discuss hysteresis loss, which is a special type of AC loss. Finally, a framework inside which research is performed in our particular field of science is presented.

2.1 Mathematical modelling of natural phenomena

Mathematics is a construction built on pure reason. Part of the beauty and effectiveness of mathematics is its axiomatic character. Once you establish that the objects you are dealing with fulfill the axioms of some mathematical system, everything that has been proven or that can be proven from the axioms holds for those objects. This is a magnificent property: a detailed identification of the mathematical structures one needs to use can save a few lifetimes of work. However, mathematics is not only a fascinating game of reasoning: it is also the language of nature. The elegance, beauty and effectiveness of mathematics combined with its universal applicability to express the order and tendencies

of the phenomena we make observations of is beyond compare among the creations of mankind. Mathematics is our way to model causality, and as such it is intertwined to our way to model nature, which we call physics. Simply, physics is mathematics, applied for the special purpose of making predictions of the world around us.

Even though none of us can probably claim to completely understand why, the effective use of mathematics allows us to make predictions of the world we live in. Nature seems to work in a consistent manner, and relying on this consistency, we can express the orderly behaviour of nature in the language of mathematics and use it in our favour to predict the future. This is the essence of mathematical modelling. It is the process of applying mathematics to make predictions of our world. In engineering, mathematical modelling constitutes an invaluable tool for predicting the behaviour of devices, as it saves the engineers from building expensive defunct prototypes.

In engineering science, such words as *theory*, *model*, *formulation*, *method* and *modelling tool* are terms that often emerge in the context of mathematical modelling in a multitude of purposes. In this section, we discuss the meaning of those terms from the point of view of technological research and give them definitions to avoid using them simply as meaningless jargon.

2.1.1 Models: instances of theories

In mathematics, a *theory* is a collection of axioms, which is taken as a starting point for deduction [137, pp. 3-53]. Axioms are sentences that concern the *primitives*, the undefined elementary entities, of the theory. Axioms and primitives are not defined, they are just taken for granted, but of course, they are often based on some kind of intuition. Then, anything else considered to be true within this theory, must be purely deductible from the axioms using the rules of mathematical logic.[1] The true statements deduced within the theory are often called *theorems*, not to be confused with theories.

Mathematics is not the only branch of science or arts to use the word theory: in other branches of science, as well as in music and arts, theory is used in different meanings. Also physicists tend to use the word theory, and most often it is the theories of mathematics and physics that are valuable for an engineer. Moreover, theories of physics and mathematics are inseparably intertwined. A theory in physics is typically built within a mathematical one:

[1] However, as Gödel's incompleteness theorems state, there are true statements in a self-consistent theory, that cannot be proven within the theory, and a self-consistent axiomatized system cannot be proven to be self-consistent within the system itself [103].

it postulates a set of *defining properties* for a special set of objects within the framework of a mathematical theory and yields a physical interpretation for them. In some sense, from a mathematical point of view, a theory in physics is thus only a nomenclature within a theory. From a physical point of view, it formalizes the intuition the phycisists have about the behaviour of nature, in terms of an existing mathematical framework.[2]

A theory gives the framework for the modellers to work within. It provides them with the boundaries and rules inside which to build their models. However, it may leave some of the mathematical structures it utilizes uninstantiated: it is the modeller's task and privilege to instantiate them to yield a model describing the reality. *A model* is an instance of a theory obtained by instantiating the uninstantiated structures.[3] For the instance of a theory to be eligible for modelling observed phenomena, it must, of course, yield predictions that are compatible with our observations. Different models match our observations in different situations: if one model yields predictions that deviate from what we observe, we cannot deduce that the physical theory is wrong, as there can be another model, which yields predictions that are perfectly compatible with the observations. Furthermore, even less can we infer about the mathematical theory, inside which our physical theory is built, being wrong, as a mathematical theory is self-consistent and valid without any notion of physical reality and observations. Later in this thesis, in chapter 4, we shall discuss the eligibility of two models of Maxwell's theory [79] for modelling superconductors under certain conditions. Even though their predictions are not always compatible with each other or observations, one cannot say the theory they are based on is wrong. These two models of the theory are merely different descriptions of reality, which may be used to yield predictions of high precision in different situations. This is not to say, however, that there could not be some other model, which would lead to accurate predictions in a wider range of situations.

2.1.2 Formulations of models

Once a model describing reality has been established, the next arising question is how to formulate it efficiently in a way that provides good basis for making predictions. A model can often be formulated in various different ways

[2]This is not to say that mathematics could not be developed for the sole purpose of providing a framework for a theory in physics.

[3]Here, we mean that a model is an instance of a theory in a similar sense as in object oriented programming the final class is an instance of a virtual class. A model should thus not be confused with, for example, a particular modelling case or modelling domain.

using, e.g., different equations and variables, and each formulation has different advantages and disadvantages. Furthermore, different formalisms may be used to present the formulations: some formalisms show the invariances and structures of the models more clearly than others, as we shall later see. However, the formalism we use is not the formulation itself. A *formulation* is a way to present the model using some variables and equations. Often, when using some field quantities, this involves decomposing the quantities into several parts or using *potential functions* to reduce the number of equations and finally form a *boundary value problem* (BVP) using these variables. As an example, which we will later discuss in more detail, models of Maxwell's theory [79] have different, equivalent partial differential equation (PDE) formulations in terms of different field quantities and potentials, leading to equivalent but seemingly different BVPs when analyzing particular cases. The employed formalism does not affect the formulation: the H-formulation of the models of magnetoquasistatics is the same regardless whether we use the formalism of differential forms or vector fields.[4] However, of course the formalism needs to be rich enough to allow us to formulate the model in the first place.

Typically, we want to formulate the model so, that it yields a set of solvable equations. When modelling reality, it is not always possible to solve the equations of the formulation exactly, but an *approximative numerical method* is needed.[5] By implementing a combination of a formulation and a solution method, nowadays typically using computers, we obtain a *modelling tool*, with which predictions of the behaviour of nature can be made for particular cases. In engineering, the term *numerical model* is often also used for the same purpose. The modelling tools programmed during this thesis work employ the finite element method (FEM) to solve the formulations. This method will be discussed in subsection 2.2.3.

Often, a research engineer merely uses already established simulation tools to analyze particular cases of applications. This is naturally important research as the final goal of technological research should be innovative and functional applications. However, new developments on simulation tools, formulations, methods, models and even completely new theories can have a dramatic effect on the innovation process in the long term; this is the fundamental science behind engineering R&D. Hence, for the development of new and innovative

[4]For those not familiar with the terms *H-formulation, magnetoquasistatics, differential form* and *vector field*, they will become clear later in this thesis. The H-formulation is an example of a formulation in the context of the research presented in this thesis.

[5]Numerical does not mean the same as approximative. Sometimes, a numerical method can be exact, when for example, applying Gaussian integration of order high enough to polynomials of order low enough [66].

technology, it is crucial that technological research communities channel their resources on research of all these aspects of mathematical modelling, and do not just settle for the prevalent dogmas.

2.2 The mathematical and physical background for modelling electromagnetic phenomena

Let us begin this section by quoting professor John C. Baez [10]:

"Everyone has to learn differential forms eventually..."

This deliberately exaggarated view of the importance of differential geometry in physics provides a hint about how the contemporary mathematical phycisists view the role of geometric tools in modelling nature: physics is geometry [36, 39, 42, 82]. But why should an engineer dealing with superconductors learn differential geometry? Let us try to answer this from our own experience.

Due to a clear segregation of mathematical structures in the formalism, a manifold-based differential geometric approach provides valuable tools for programming more general and structural simulation software [100] compared to programs that are currently available commercially [31]. The calculus of differential forms, like its more often used counterpart vector analysis, is a form of multivariable calculus. However, it differs from the vector field formalism essentially, by providing more general tools for calculus than the traditional approach. Much of the analysis typical for electromagnetism can be done on manifolds in a manner generalizing and clarifying many coordinate-, metric- and dimension-related issues that remain hidden in the vector field formalism. For example, the dimensional reduction due to helicoidal symmetry in the context of modelling twisted superconducting wires would probably never have occured to the authors of [8, 120, 121, 124] without the use of differential geometric formalism on manifolds. Also, even though the research presented in this thesis would have been possible without it, the use of differential geometry and, in particular, a programming interface providing the services needed for calculus of differential forms on manifolds [100] has facilitated it greatly. For example, programming dimension-independent simulation tools for electromagnetic modelling has been a pleasant task, as the governing equations remain the same independently of the dimension, unlike in the vector field formalism.[6] Not only does this structured, geometrical approach allow one to

[6]When programming the AC loss modelling tools of this thesis, 2D and 3D tools were conceived simultaneously in a natural way, because of the differential geometric tools available

work in spaces of different metric properties and dimensions, but it also yields clearly where each structure is really needed. Furthermore, as geometrization of physics is an evident trend in modern science, we believe that it is time for us engineers to start thinking in a more structured and geometrical manner as well, to be able to utilize the results of modern mathematical physics better in the future.[7]

In this section, we present a motivational and rather informal introduction to manifolds and differential geometry. However, we try to be formal enough, to provide a sufficient mathematical tool-package to follow the publications of this thesis, even though the reader would not have heard of differential geometry before. Furthermore, we try to give enough helpful references for more thorough discussions of the most important concepts; after all, this is not an introductory book to differential geometry, like [128]. Using this formalism, we present Maxwell's theory for mesoscopic modelling of electromagnetic phenomena and introduce new mathematical concepts as they appear in the discussion of the theory. Furthermore, we discuss the solution of BVPs using special type of approximative methods, mesh methods. In particular, we present the mathematical background for FEM, which is a widely used mesh method and also the method mainly used in the research of this thesis.

2.2.1 The domain for field quantities: an informal introduction to manifolds

In mesoscopic[8] models, one often deals with some kind of field quantities. For example, nowadays in electrical engineering the conventional way to write Maxwell's theory is to express it in Euclidean space using the so called vector field[9] formalism. However, we wish to raise the abstraction level and express the theory in a more general setting using different field objects. The theory of manifolds and differential geometry acts as a unifying and generalizing

in the programming interface.

[7]Even though in many fields of science the required tools go much deeper in differential geometry than we do here, we do not need to dive very deep into geometrization of physics in the scope of the research presented in this thesis. We do not, e.g., consider how physics determines the metric, or curvature, for the geometry.

[8]In a sense, the mesoscopic scale is in between macroscopic, the scale at which human beings can make direct observations about phenomena, and microscopic. In mesoscopic models, pointwise quantities are defined without any notion of individual atoms or particles: materials are treated as homogeneous continuum. For example in mesoscopic models of electromagnetic phenomena, current densities are discussed without paying any attention to the individual charge carriers.

[9]Vector fields are objects that assign a vector to each point in space.

framework for a wide range of mesoscopic physics [39] and, in particular, it is the most natural language for electromagnetism known to date [11, 39, 105]. When one presents classical physics using a manifold-based differential geometric approach, one does not need to present different kinds of mathematics separately for different phenomena. Hence, we shall here informally review the structures of topological, differentiable and Riemannian manifolds. The definitions are correct but not all technical details are discussed. For more detailed and rigorous definitions the reader is referred, e.g., to [16, 105].

In a topological space the concept of neighbouring points is well-defined. Thus, even though there is no conception of actually measuring distances, one can in a definite way identify, which points are close to each other and which are not. A set with the structure yielding such an intuitive property is a topological space. *A topological manifold* is a topological space covered completely with a set of local coordinate systems referred to as *charts*, which together constitute *an atlas* of the manifold. These charts map points of the manifold to points in the k-dimensional real coordinate space $\mathbb{R}^k$. These mappings are required to be homeomorphic.[10] Hence, a topological manifold of dimension k is parametrizable with k-tuples of real numbers and is locally topologically the same as $\mathbb{R}^k$. An example of two charts of the same underlying manifold is given in figure 2.1.[11]

From a modeller's point of view, a topological manifold as it is, even though an important mathematical structure as an intermediate construction, is not of much applicability. There is no conception of smooth change, which makes differential calculus impossible. To be able to do analysis, we thus need to introduce differentiability. On a *differentiable manifold*, one can smoothly change from a coordinate system to another. It is required, that there exist differentiable transition mappings between coordinates. Given any two overlapping charts $\chi : \Omega \to \mathbb{R}^k$ and $\hat{\chi} : \Omega \to \mathbb{R}^k$ on the manifold Ω, the mapping $\hat{\chi} \circ \chi^{-1} : \mathbb{R}^k \to \mathbb{R}^k$ defined on the domain mapped through the overlap must be differentiable. Note that since differentiability is a well-defined concept in $\mathbb{R}^k$, one can now define, for example, derivatives of mappings between manifolds: a mapping between two differentiable manifolds is differentiable simply if its representation with some charts of the two manifolds (as a function from $\mathbb{R}^k$ to $\mathbb{R}^k$) is differentiable in the ordinary sense. Hence, on a differentiable manifold, differential calculus may be performed. In short, for a topological manifold to

[10] A homeomorphic mapping is topology-preserving as it is continuous and has a continuous inverse.

[11] Note however, that it makes no sense to speak about round things or Cartesian coordinates on a topological manifold with no extra structure, as such notions require metric information.

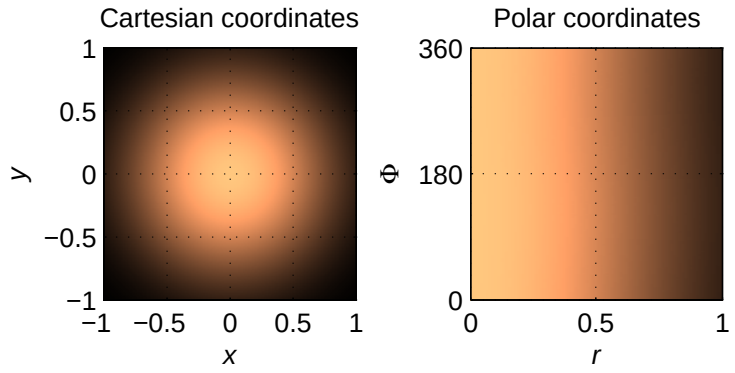

Figure 2.1: A familiar example of two different coordinate charts used for representing the underlying manifold: the Cartesian x-y-coordinate chart and the polar r-Φ-coordinate chart. Round things centered in the origin of the Cartesian coordinates look rectangular in polar coordinates. The Φ-axis has been scaled to represent the angle in degrees.

be a differentiable manifold, it must have an interdifferentiable atlas. In figure 2.2, the idea of interdifferentiable charts on a manifold is demonstrated.

On a differentiable manifold, one can for example write Maxwell's equations. No further structure is required. However, to do any field modelling, we still need metric properties in our space. An *inner product* is a symmetric, linear and positive-definite mapping

$$\langle \cdot, \cdot \rangle : V \times V \to \mathbb{R}, \tag{2.1}$$

taking pairs of elements of a vector space V to elements of the set of real numbers $\mathbb{R}$. *The metric tensor* (from here on *metric*[12]) attaches an inner product smoothly to each point of the manifold. Using the inner product, we obtain a relationship between the basis vectors in a given basis, thus yielding us a tool to measure such things as distances and angles on the manifold: an inner product induces a norm. A *Riemannian manifold* is a differentiable manifold with a positive-definite metric. Such a manifold has sufficient structure to represent space in classical electromagnetism. Note that even though it is often far from obvious, metric is almost always an essential part of field modelling. Without it, we could not, for example, tell whether the coordinate axes are orthogonal to each other or not, or define the constitutive relations between

[12]There are many different concepts related to metric properties of the space. *A metric space* is a set with a distance function [145]. Often, this distance function is also called metric. Note that the metric tensor on a manifold, however, is not a distance function, but it induces one through integration [105, p. 50].

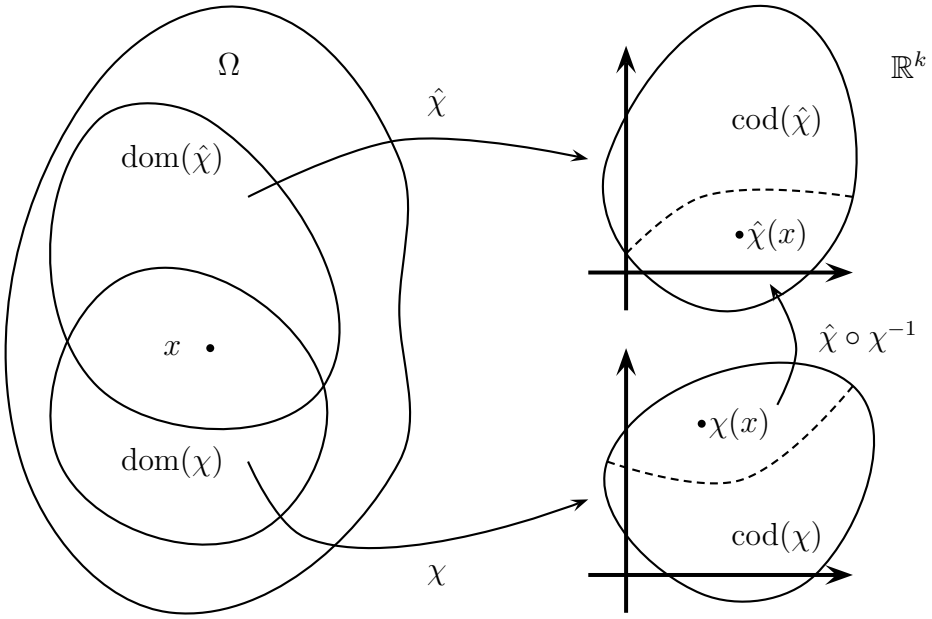

Figure 2.2: Two charts χ and $\hat{\chi}$ map parts of the manifold Ω to $\mathbb{R}^k$. Point $x \in \Omega$ lies in the overlap of the domains of the charts $\mathrm{dom}(\chi) \subset \Omega$ and $\mathrm{dom}(\hat{\chi}) \subset \Omega$. The domains are mapped to the codomains of the charts $\mathrm{cod}(\chi) \subset \mathbb{R}^k$ and $\mathrm{cod}(\hat{\chi}) \subset \mathbb{R}^k$. As Ω is a differentiable manifold, there exists a differentiable transition map $\hat{\chi} \circ \chi^{-1}$ for the change of charts through the overlap.

electromagnetic field quantities, as we shall later discuss.

To summarize, a topological manifold is a topological space covered with a collection of local coordinate systems, charts. A differentiable manifold is a topological manifold with interdifferentiable charts, and a Riemannian manifold is a differentiable manifold with a positive-definite metric tensor. The structures are summarized in figure 2.3.[13] By isolating the structures, it is easier to grasp the essential and intrinsic properties of things [89], which is substantial for obtaining results of high generality. This is the essence of science anyway: science tends to compress things and say more from less.

[13]In modelling, we often use a special type of Riemannian manifold, a Euclidean manifold. A Euclidean manifold is a Riemannian manifold with the conventional Euclidean metric. A metric is Euclidean, if its matrix representation is the identity matrix in some coordinates covering the whole manifold, meaning that the inner product it attaches to each point of the space is the conventional dot product. For example, taking the Cartesian coordinates and the identity matrix as the representation of the metric and transforming the coordinates to cylindrical ones changes the representation of the metric, but we still call this metric Euclidean.

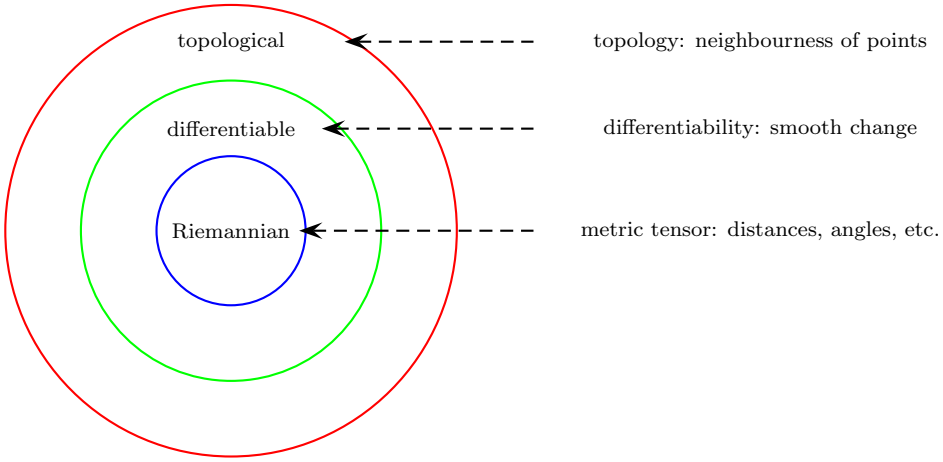

Figure 2.3: A description of structures and requirements for different types of manifolds reviewed here. The larger the radius of the circle, the less requirements there are for such a manifold, and thus, in a sense, the easier it is to find examples of such manifolds. A topological manifold has the structure of topology: the concept of neighbouring points is well-defined on it. A differentiable manifold is a topological manifold with an interdifferentiable atlas: the concept of smooth change is well-defined. A Riemannian manifold is a differentiable manifold with a positive-definite metric tensor: distances, angles, areas and such concepts are well-defined.

2.2.2 Modelling electromagnetic phenomena using differential geometry

It has been observed that the gravitational interaction does not constitute all the forces in nature. Nuclear physics aside, this missing part of nature is *electromagnetism*. Electric and magnetic forces are forces exerted on charged[14] particles. The electric force acts on charges at rest with respect to an observer as well as to charges moving with respect to her. However, a moving charge has been observed to experience also an additional force, which we call the magnetic force. Together these two forces, acting on a moving charge, constitute the electromagnetic force we call *Lorentz force*. Also, it turns out that electric and magnetic forces are not independent of each other but tightly interconnected. Maxwell's theory [79] has been proven to yield models giving a very precise description of reality concerning electric and magnetic phenomena and the connection between them, matching our observations in a wide range of situations.

[14]We do not take a stance on what an electric charge is. It is an undefined primitive in our discussion, yet most of the readers probably have a strong intuition about it.

Here, we introduce the necessary mathematical concepts for Maxwell's theory, as well as the theory itself, which is the mesoscopic theory used for modelling electromagnetic phenomena. First, we discuss what kind of mathematical objects the field quantities of this theory are. Then, we go on to present the defining properties of these quantities, with special emphasis on the magnetoquasistatic version of the theory. Finally, we discuss the two instances of the theory typically used for superconductor modelling, the eddy current model (ECM) (which is presented and discussed extensively in the publications included in this thesis) and the critical state model (CSM) [13]. These two instances are crucially important for the research presented in this thesis: we use them for predicting how the energy stored in the electromagnetic field is converted into thermal energy, which can be observed, for example, as the boiling of the cryogenic liquid used for cooling the superconductor.

The field quantities in Maxwell's theory

Maxwell's theory is a field theory: the interactions observed in nature are modelled using mesoscopic field quantities. Electric and magnetic interactions are accounted for by the introduction of the *electric and magnetic fields.*

In Maxwell's theory, the electric field is the pair $(E,\, D)$, where E is the electric field intensity and D is the electric flux density. Correspondingly, the magnetic field is the pair $(B,\, H)$, where B is the magnetic flux density and H is the magnetic field intensity.[15] The mesoscopic field quantity used for modelling electric currents is the current density J. Most conveniently, these fields are understood as differential forms of different degrees. To get a grasp of what these field quantities are and what this theory says about our world, we will next introduce some necessary mathematical concepts.

Tangent vectors, covectors and differential forms. On a differentiable manifold, *tangent vectors* at a point $x \in \Omega$ constitute the tangent space $T_x(\Omega)$ at that point. In the intuitive special case of a curve embedded in Euclidean space, the tangent space at x is just the line that is tangent to that curve at x. More formally, $T_x(\Omega)$ is the set of all equivalence classes of curves through x. A curve on Ω is defined as a smooth mapping $\hat{c} : \mathbb{R} \to \Omega$. We define any two

[15] In space-time, E and B constitute the electromagnetic field strength. Its decomposition into E and B, usually done in the classical approach, is possible after one defines what is meant by time-differentiation and by local three-dimensional spatial subspaces of space-time. For our purposes, the classical approach is sufficient. For further reading about electromagnetism in space-time, the reader is referred to, e.g., [11, 39].

curves $\hat{c}_1$ and $\hat{c}_2$ through point x, that is curves for which $\hat{c}_1(0) = \hat{c}_2(0) = x$ holds, to be equivalent if and only if the derivatives $(\chi \circ \hat{c}_1)'(0)$ and $(\chi \circ \hat{c}_2)'(0)$ are equal for some chart χ. Note that these mappings are just smooth functions on $\mathbb{R}$. The equivalence classes of curves in this equivalence classification are called tangent vectors and constitute $T_x(\Omega)$. [105, pp. 28-29] Intuitively, this means that two curves through a point, thought of as trajectories of particles moving through space, are equivalent if the particles move at the same velocity and in the same direction at that point. This captures well the intuitive idea of tangent vectors describing instantaneous speeds.

A tangent vector $\mathbf{v}_x$ at a point x acts as a differential operator on a smooth function $\hat{f}$ on the manifold Ω: $\mathbf{v}_x(\hat{f})$ is the directional derivative of $\hat{f}$ in the direction of the curves at x in the equivalence class $\mathbf{v}_x$. [105, pp. 28-29] [11, pp. 27-31] Given local coordinates x^i and the associated coordinate basis, a tangent vector $\mathbf{v}_x$ may be represented as

$$\mathbf{v}_x = \sum_i^k v_x^i \frac{\boldsymbol{\partial}}{\boldsymbol{\partial} x^i}, \tag{2.2}$$

where $\frac{\boldsymbol{\partial}}{\boldsymbol{\partial} x^i}$ denote the basis vectors and v_x^i are the components of $\mathbf{v}_x$ in that basis. Bearing in mind that tangent vectors are differential operators, we can also define the differential D of a smooth mapping $\hat{F} : \Omega_1 \to \Omega_2$ between differentiable manifolds Ω_1 and Ω_2 as the linear mapping

$$\mathrm{D}\hat{F}\left(\mathbf{v}_x\right)\left(\hat{f}\right) = \mathbf{v}_x\left(\hat{f} \circ \hat{F}\right), \tag{2.3}$$

where $\hat{f} : \Omega_2 \to \mathbb{R}$ is a smooth function on Ω_2. Sometimes, $\mathrm{D}\hat{F}\left(\mathbf{v}_x\right)$ is also called the *pushforward* of $\mathbf{v}_x \in T_x(\Omega_1)$ by the mapping $\hat{F}$, as it can be seen taking tangent vectors in $T_x(\Omega_1)$ to tangent vectors in $T_{\hat{F}(x)}(\Omega_2)$. If $\Omega_2 = \mathbb{R}$, we can conveniently define $\mathrm{D}\hat{F}\left(\mathbf{v}_x\right) = \mathbf{v}_x\left(\hat{F}\right)$.

A *covector* is a linear mapping, taking tangent vectors to real numbers. Covectors constitute the dual space of the tangent space, cotangent space $T_x^*(\Omega)$. For the coordinate basis for tangent space, there is a dual basis for cotangent space, the *coordinate cobasis* $\mathrm{d}x^i$, for which it holds $\mathrm{d}x^j(\frac{\boldsymbol{\partial}}{\boldsymbol{\partial} x^i}) = \delta_i^j$, where δ_i^j is the Kronecker delta. A differential 1-form is a covector field, which assigns a covector to each point of the manifold. Thinking of the basis $\frac{\boldsymbol{\partial}}{\boldsymbol{\partial} x^i}$ as coordinate vector fields, we have the corresponding coordinate 1-forms $\mathrm{d}x^i$. Using this basis, we can express any 1-form ψ locally at point x as

$$\psi^x = \sum_i^k \psi_i^x \mathrm{d}x^i, \tag{2.4}$$

where ψ_i^x are the components of the 1-form at the point x.

Furthermore, a tangent p-vector (from now on, usually just a *p-vector*), where p is a non-negative integer, is an ordered tuple of tangent vectors, such that a permutation interchanging the places of two vectors in the tuple changes the sign of the p-vector.[16] Then, a *p-covector* is a multilinear, totally antisymmetric mapping, taking p-vectors to real numbers. Just like we can construct vector fields and covector fields by assigning a vector or covector to each point of the manifold, we can construct p-covector fields as well. Hence, a differential form of degree p (from here on a *p-form*), is a p-covector field, which assigns a p-covector to each point of the manifold.[17] The requirement that a p-form η be totally antisymmetric means simply that

$$\eta(\mathbf{v}_1, ..., \mathbf{v}_j, ..., \mathbf{v}_m, ...) = -\eta(\mathbf{v}_1, ..., \mathbf{v}_m, ..., \mathbf{v}_j, ...), \tag{2.5}$$

for all pairs of entries ($\mathbf{v}_j$, $\mathbf{v}_m$). We denote the set of differential p-forms on a manifold Ω as $F_p(\Omega)$.

Integrating differential forms. On a three-dimensional (3D) manifold, we can write E, $H \in F_1(\Omega)$ and B, D, $J \in F_2(\Omega)$.[18] As an example, E, given a vector in any direction, yields a real number representing the virtual work required to move a unit charge in that direction. The degrees of the forms also bear information valuable for integration. For those acquainted with the vector field formalism of Maxwell's theory, it is clear that one just somehow knows that, e.g., it only makes sense to integrate B over surfaces. In the differential form formalism, this is true by definition: a p-form may only be integrated over a p-dimensional integration domain. E is integrated over paths to yield voltages, J over surfaces to yield net electric currents, and so on. For example, the integral of E over a path on Ω is, intuitively, an addition operation of the virtual works in the direction of the path. This integral yields the voltage

[16] Any two p-vectors that span a parallelopiped of the same p-volume and orientation are equivalent.

[17] In a more general setting, a p-form is a totally antisymmetric *(0,p)-tensor field*, meaning that pointwise it is a mapping taking 0-covectors and p-vectors to real numbers. As for all tensors, the resulting real number is coordinate system independent. Note also that a 0-form is simply a scalar field.

[18] Note that, for example in typical two-dimensional (2D) situations, one often has $E \in F_0(\Omega)$, B, H, $D \in F_1(\Omega)$ and $J \in F_2(\Omega)$. Formally, the forms have been *contracted* to the direction of one dimension [39, p. 89]. Even though the manifolds one is dealing with in time-dependent problems are essentially $k+1$-dimensional, having k spatial dimensions and one temporal dimension, we are content with the notion of p-forms on a k-dimensional manifold. Different instants of time form *foliations* in space-time, on which the forms can be treated as we have done here [52].

between those two points, which represents the total work required to move the unit charge from the point to another.

The integral of a p-form η over a p-dimensional oriented[19] subset of Ω, parametrized by a smooth mapping $W : U \subset \mathbb{R}^p \to \Omega$ is defined as

$$\int_{W(U)} \eta := \int_U W^* \eta \tag{2.6}$$

where the mapping W^* is the linear map called pullback of η through W taking p-forms from one manifold to another. In this case, we pullback $\eta \in F_p(\Omega)$ to $W^*\eta \in F_p(\mathbb{R}^p)$:

$$\left(W^*\eta\right)_x \left(\mathbf{v}_x^1, ..., \mathbf{v}_x^p\right) = \eta_{W(x)} \left(\mathrm{D}W(\mathbf{v}_x^1), ..., \mathrm{D}W(\mathbf{v}_x^p)\right). \tag{2.7}$$

Hence, when evaluating integrals, everything can be done in the familiar $\mathbb{R}^p$ by pulling back the p-form there first using the smooth parametrization mapping W. Note, however, that the notion of pullback is not restricted only for parametrization mappings of the above type, but can be defined for any smooth mapping between two manifolds in the manner of (2.7). Note also, that even if we would need several parametrization mappings (essentially, several coordinate charts) to express our integration domain, integration could still be performed, and the value of the integral is always independent of the parametrizations. [105, pp. 46-48]. Furthermore, the integration domain needs to be *Lebesgue measurable* [41] through a covering of charts [105, pp. 46-48]. That is, the codomains of the charts of the covering need to be Lebesgue measurable in $\mathbb{R}^p$.

[19] Note that some of our field quantities require an *inner orientation* for their integration and some require an *outer orientation*. For example, for a surface, an outer orientation, i.e., a sense of positive crossing direction, is obtained by giving an inner orientation, i.e., a sense of positive propagation direction for a curve piercing it. For integrating J, for instance, the concept of outer orientation of the surface is obviously important, and for integrating E, the inner orientation of the curve is needed. For more on these concepts, see e.g. [21].

Maxwell's theory in the language of differential geometry

Having seen what kind of objects the electromagnetic field quantities are, we are ready to move on to present Maxwell's equations. In the formalism of differential geometry, the familiar vector differential operators will be replaced with a single differential operator, the *exterior derivative*, and the cross and dot products are replaced by the *exterior product*. Furthermore, the metric-dependence of the material operators becomes more evident through the *Hodge operator* than in the traditional vector field formalism.

The defining properties. The pairs of differential forms (E, D) and (B, H) are defined in Maxwell's theory through a set of defining properties. First of all, on a differentiable manifold, they are defined to satisfy Maxwell's equations

$$\mathrm{d}E = -\partial_t B, \tag{2.8}$$

$$\mathrm{d}H = J + \partial_t D, \tag{2.9}$$

$$\mathrm{d}B = 0, \tag{2.10}$$

$$\mathrm{d}D = \sigma, \tag{2.11}$$

namely Faraday's law, Ampère-Maxwell's equation and Gauss's laws for magnetic and electric fields, respectively. In these equations $\sigma \in F_3(\Omega)$ is the charge density, a mesoscopic field quantity used for modelling electric charges, ∂_t denotes the ordinary time-differentiation operator and d: $F_p(\Omega) \to F_{p+1}(\Omega)$ is the exterior derivative operator [39, pp. 73-77]. In the magnetoquasistatic version of Maxwell's theory we assume that changes in the fields are slow enough so that no packing of charges takes place. Thus, only J is a relevant source quantity and only E is relevant for the electric field. Hence, in our discussion, we drop out (2.11) from the set of equations and drop the time-derivative of D out of (2.9) to yield Ampère's law

$$\mathrm{d}H = J. \tag{2.12}$$

Thus, relevant Maxwell's equations for magnetoquasistatics are (2.8), (2.10) and (2.12). Note that we are not instantiating any structures here: we are altering the *defining properties* of Maxwell's theory to obtain the magnetoquasistatic Maxwell's theory. That is, in our terminology, magnetoquasistatics without any instantiated structures is not a model but a theory.

Now, the energy density of the magnetic field e_m, as well as the Ohmic dissipative power density p_d, which are both 3-forms in 3D[20], can be defined

[20] In 2D they are 2-forms.

as

$$e_{\mathrm{m}} = \frac{1}{2} B \wedge H, \tag{2.13}$$

$$p_{\mathrm{d}} = E \wedge J, \tag{2.14}$$

where $\wedge\colon F_p(\Omega) \times F_q(\Omega) \to F_{p+q}(\Omega)$ is the exterior product of differential forms, the product operation of the exterior algebra[21] [39, pp. 66-73]. The integrals of (2.13) and (2.14) over Ω yield the energy stored in the magnetic field and the Ohmic dissipative power P, respectively, the latter of which is interpreted as instantaneous heat generation in the current-carrying subdomains of Ω. Note that to interpret (2.13) as energy density, we assume a linear relationship between B and H, but for example in ferromagnetic materials this relation is not even a function. However, we do not consider ferromagnetic materials in this thesis.

The new formalism in Maxwell's theory: defining $\wedge$ and d. The exterior product $\wedge$ exhibited in (2.13) and (2.14) is a generalization of the familiar vector products. In $\mathbb{R}^3$ with Cartesian coordinates, the exterior product of two 1-forms can be identified with the cross product in vector analysis and the exterior product of a 1-form and a 2-form, which is the case in (2.13) and (2.14) in 3D, can be identified with the dot product. However, the components of the exterior product make sense in any coordinates. The exterior product of a p-form η and a q-form τ is defined as

$$(\eta \wedge \tau)(\boldsymbol{v}_{\hat{I}}) = \sum_{\hat{K}} \sum_{\hat{J}} \delta_{\hat{I}}^{\hat{J}\hat{K}} \eta(\boldsymbol{v}_{\hat{J}}) \tau(\boldsymbol{v}_{\hat{K}}), \tag{2.15}$$

where we have used the *multi-index notation*. A multi-index I is an ordered tuple of indices $(i_1, i_2, ..., i_m)$. If the indices in the tuple are in increasing order, we shall denote the multi-index as $\hat{I}$. In (2.15), $\hat{J}\hat{K}$ is the concatenation of the indices in multi-indices $\hat{J}$ and $\hat{K}$. The symbols $\boldsymbol{v}_{\hat{I}}$, $\boldsymbol{v}_{\hat{J}}$ and $\boldsymbol{v}_{\hat{K}}$ denote the tuples of vectors indexed by $\hat{I}$, $\hat{J}$ and $\hat{K}$, respectively. Furthermore, the *multi-index Kronecker delta* δ_I^J is defined as

$$\delta_I^J = \begin{cases} 1 & \text{when } I \text{ is an even permutation of } J. \\ -1 & \text{when } I \text{ is an odd permutation of } J. \\ 0 & \text{when } I \text{ is not a permutation of } J. \end{cases} \tag{2.16}$$

[21] Here, exterior algebra has been applied to differential forms, but like many abstract algebraic systems, it has also other application domains. Similarly, we obtain, e.g., p+q-vectors from p-vectors and q-vectors by forming their exterior product.

The exterior product also gives us a way to present any p-form η in a given basis. Again, given the coordinate cobasis, if we denote $\mathrm{d}x^I = (\mathrm{d}x^{i_1} \wedge ... \wedge \mathrm{d}x^{i_p})$, we can write

$$\eta = \sum_{\hat{I}} \eta_{\hat{I}} \mathrm{d}x^{\hat{I}}. \tag{2.17}$$

So, for example, the current density J, as a 2-form, can be written as

$$J = \sum_{i<j} J_{ij} \mathrm{d}x^i \wedge \mathrm{d}x^j. \tag{2.18}$$

The exterior product is not commutative but satisfies $\eta \wedge \tau = (-1)^{pq} \tau \wedge \eta$. Furthermore, it is associative and bilinear and for every η, $1 \wedge \eta = \eta$. Note that if p is odd, $\eta \wedge \eta = 0$.

The differential operator d present in all Maxwell's equations is a metric- and dimension-independent generalization of such familiar vector differential operators as gradient, curl and divergence. Formally, d: $F_p(\Omega) \to F_{p+1}(\Omega)$ is uniquely determined by the following properties:

1. $\mathrm{d} : F_0(\Omega) \to F_1(\Omega)$ is the ordinary differential of a function.
2. Linearity: $\mathrm{d}(\eta + \gamma) = \mathrm{d}\eta + \mathrm{d}\gamma$, $c\mathrm{d}(\eta) = \mathrm{d}(c\eta), \quad \forall \eta, \gamma \in F_p(\Omega), c \in \mathbb{R}$.
3. The Leibniz rule: $\mathrm{d}(\eta \wedge \tau) = \mathrm{d}\eta \wedge \tau + (-1)^p \eta \wedge \mathrm{d}\tau, \quad \forall \eta \in F_p(\Omega), \tau \in F_q(\Omega)$.
4. $\mathrm{d} \circ \mathrm{d} = 0$.

For a 0-form, d has similar nature as the gradient has for a scalar function, for a 1-form its nature is similar to curl and for a 2-form to divergence. However, d does not necessarily say anything about the steepest ascent, as that requires metric information. Note also, that as d satisfies $\mathrm{d} \circ \mathrm{d} = 0$, such familiar formulae as $\mathrm{curl} \circ \mathrm{grad} = 0$ and $\mathrm{div} \circ \mathrm{curl} = 0$ are immediately generalized by d. In local coordinates, $\mathrm{d}\eta$ is computed as

$$\mathrm{d}\eta = \sum_{\hat{I}} \sum_{i}^{k} \frac{\partial \eta_{\hat{I}}}{\partial x^i} \mathrm{d}x^i \wedge \mathrm{d}x^{\hat{I}}. \tag{2.19}$$

Together with integration, the exterior derivative also generalizes all the different boundary integral theorems of vector analysis under one powerful theorem, (generalized) Stoke's theorem, which may be written as [39, pp. 111-114]

$$\int_u \mathrm{d}\eta = \int_{\partial u} \eta. \tag{2.20}$$

This simply states that the integral of a $p+1$-form, which is the exterior derivative of η, over a $p+1$-dimensional oriented subset u of Ω is equal to the integral of η over its p-dimensional boundary. The Leibniz rule and Stoke's theorem also give us the integration by parts formula for differential forms, written as

$$\int_u \mathrm{d}\eta \wedge \tau = (-1)^{p+1} \int_u \eta \wedge \mathrm{d}\tau + \int_{\partial u} \eta \wedge \tau, \tag{2.21}$$

for a p-form η and a q-form τ. Here, u is of course $q+p+1$-dimensional.

The Hodge relations of Maxwell's equations and the metric isomorphisms $\flat$ and $\sharp$. Even though Maxwell's equations can be written on a differentiable manifold, we are still missing the links between different field quantities. We need the *constitutive equations* to relate B to H and E to J. In Maxwell's theory, there is also a constitutive equation relating E to D, but as we are concerned with magnetoquasistatics, we will not be needing it. However, differentiability is not enough for the constitutive equations. To understand this, consider the connection between $E \in F_1(\Omega)$, which is related to paths and $J \in F_2(\Omega)$, which is related to surfaces. We must be able to connect things related to geometric objects of different dimensions. We need, not just a real number, but an *operator* to connect paths to areas. Such an operator can be constructed using the metric on the Riemanian manifold.

On a Riemannian manifold, we are able to write the constitutive equations, also known as the Hodge relations of Maxwell's equations as

$$B = \mu_\star H \tag{2.22}$$

$$E = \rho_\star J, \tag{2.23}$$

where $\mu_\star = \mu \circ \star$ and $\rho_\star = \rho \circ \star$ are the permeability and resistivity operators, respectively. The operators μ and ρ are mappings that do not alter the degrees of the forms. However, the operator they are composed with, the Hodge operator $\star$: $F_p(\Omega) \to F_{k-p}(\Omega)$, where k is again the dimension of the manifold, relates forms of different degrees with each other [39, pp. 361-375]. It is derived from the metric, using the Riesz representation theorem [145, p. 90] to yield a formal tool for giving a relation between quantities related to geometric entities of different dimensions.

The Riesz representation theorem is a theorem in functional analysis related to the theory of Hilbert spaces. For this particular purpose, it states that

$$\forall \gamma \in F_p(\Omega) \quad \exists_1 \star\gamma \in F_{k-p}(\Omega) : \beta \wedge \star\gamma = \langle \beta, \gamma \rangle \, \mathrm{vol}^k, \tag{2.24}$$

where $\mathrm{vol}^k \in F_k(\Omega)$ is the *volume form* of the k-dimensional Riemannian manifold Ω, and $\beta \in F_p(\Omega)$.[22] This theorem defines the Hodge operator $\star$ completely and guarantees, for example, that in a linear material, for a given H there is a unique B, and vice versa. Furthermore, it yields a formula for computing the matrix representation of $\star$ in a given basis. The inner product here is the local inner product of p-forms given in a basis as

$$\langle \beta, \gamma \rangle = \sum_{\hat{I}} \sum_{\hat{J}} \beta_{\hat{I}} \gamma_{\hat{J}} \langle \mathrm{d}x^{\hat{I}}, \mathrm{d}x^{\hat{J}} \rangle, \tag{2.25}$$

where the inner product of the basis p-forms is given by the determinant

$$\langle \mathrm{d}x^{\hat{I}}, \mathrm{d}x^{\hat{J}} \rangle = \det((g^{-1})^{\hat{I}\hat{J}}). \tag{2.26}$$

Here, $(g^{-1})^{\hat{I}\hat{J}}$ is the matrix containing the rows $\hat{I}$ and $\hat{J}$ of the matrix representation of the inverse of the metric tensor [98, p. 29].

This differential geometric representation of the constitutive equations is much more informative than its counterpart in the vector field formalism, in which the operator character of the material operators is completely hidden: there, it seems as if one would connect, say, E to J simply by scalar multiplication. Here, all the metric information in Maxwell's theory is packed in $\star$: it is needed nowhere else. This is convenient, as changes in the representations of metric can be accounted for simply by changes in the representations of $\star$. We can also use $\star$ to relate all this to the vector field formalism. We can define the traditional 1-vector field versions of the differential forms E, B, H and J in 3D as

$$\mathbf{E} := E^\sharp, \quad \mathbf{B} := (\star B)^\sharp, \quad \mathbf{H} := H^\sharp, \quad \mathbf{J} := (\star J)^\sharp, \tag{2.27}$$

respectively, where $\sharp$ denotes the metric isomorphism from 1-forms to 1-vectors. Note that such 1-vector representations are not even possible in all dimensions.

One more question may arise. What exactly is this $\sharp$ in (2.27)? On a Riemannian manifold, there is a natural isomorphism between differential forms and vector fields induced by the metric tensor. As an example, given a basis for vector fields and its dual basis for 1-forms, this isomorphism yields the correspondence between the gradient of a scalar field ϕ, denoted as $\nabla\phi$ and its exterior derivative $\mathrm{d}\phi$ as $(\nabla\phi)^i = \sum_j g^{ij}(\mathrm{d}\phi)_j$, where g^{ij} are the components of the inverse of the metric tensor. In fact, on a Riemannian manifold $\nabla\phi$ can

[22] Volume form is also induced naturally by the metric, up to the choice of orientation, even though metric is not a necessity for having a volume form. In an orthonormal cobasis $\mathrm{d}x^i$, we can write the volume form on a Riemannian manifold as $\mathrm{vol}^k = \mathrm{d}x^1 \wedge ... \wedge \mathrm{d}x^k$ up to the orientation. In a non-orthonormal cobasis $\mathrm{d}y^i$, the expression is $\mathrm{vol}^k = \sqrt{\det(g)}\mathrm{d}y^1 \wedge ... \wedge \mathrm{d}y^k$, where g denotes the matrix representation of the metric tensor. [39, pp. 86-88].

be *defined* as the vector field counterpart of $\mathrm{d}\phi$ obtained through the metric isomorphism [39, p. 45]. This isomorphism is often denoted as $\flat$ and its inverse as $\sharp$, so that $\nabla\phi = (\mathrm{d}\phi)^\sharp$ and $\mathrm{d}\phi = (\nabla\phi)^\flat$. More generally, $\sharp$ and $\flat$ are used to denote the metric isomorphisms between any vector space and its dual. This definition of the gradient clearly highlights the metric-dependent nature of the vector field formalism. Given the Cartesian metric, where $g^{ij} = \delta^{ij}$, δ^{ij} denoting the Kronecker delta, the definition simplifies to $(\nabla\phi)^i = (\mathrm{d}\phi)_i$. However, in our case there is no reason to use the complicated metric-dependent formalism, when we can always write Maxwell's equations using differential forms in the same way: regardless of the coordinate system or metric, their component representations stay exactly the same. The metric comes into play only through $\star$ in the constitutive equations. This is not only convenient, but also a valuable asset for programming structural and general simulation tools. If vector fields are needed for visualization purposes, there is always the metric isomorphism available. This is in many ways in contrast to the traditional approach employing the vector field formalism, in which the differential operators and Maxwell's equations have different representations in different coordinate systems and metrics. However, it is true that Laplace operator expressed with only partial derivatives, will always have different representations in curvilinear coordinate systems. Note also, that in spite of the formalism, we will always end up solving the same equations.

Concluding remarks about the magnetoquasistatic Maxwell's theory. Now, we have introduced the magnetoquasistatic Maxwell's theory and the necessary mathematics for it. As discussed, the theory sits naturally in the context of Riemannian geometry. The defining properties for the field quantities E, B, H and J are the metric-independent Maxwell's equations (2.8), (2.10), (2.12) and the metric-dependent constitutive equations (2.22), (2.23). By instantiating, for example, different metric tensors or different material operators, one obtains different models of this theory, valid in different situations. Note, however, that by performing a coordinate transformation, for example from Cartesian to cylindrical coordinates, one does not instantiate a different metric, even though its matrix representation will be different.

Two models of the magnetoquasistatic Maxwell's theory: ECM and CSM

When modelling superconductors, two instances of Maxwell's theory are typically used: CSM [13, 26, 45, 88, 95, 102] and ECM [23, 44, 45, 56, 86, 122, 123, 146]. The difference in these models is that the resistivity operator is instantiated differently at superconducting regions in them, even though the metric-

induced part is based on the Euclidean metric in both of them. However, this subtle difference can alter the resulting description of reality dramatically, as we shall later discuss.

In CSM, the relation is assumed to be sharp: any E will produce J of magnitude J_c, with $\star J$ in the direction of E.[23] This J_c is called the critical current density. However, this does not mean that whenever there exists a J, there would also be E. In ECM, however, the relation is assumed to be smooth. The resistivity operator is instantiated as $\rho_{SC} \circ \star$, where ρ_{SC} can be given pointwise as a real number

$$\rho_{SC} = \frac{E_c}{J_c} \left(\frac{||J||}{J_c} \right)^{n-1} . \tag{2.28}$$

In this equation, $||J||$ denotes the Euclidean norm of the current density and n is the n-value of the superconductor, which is related to macroscopically observed slanted shapes of current-voltage curves in superconductors [25] and microscopically to a quantum scale phenomenon called flux creep [4]. Note that there is thus plenty of macroscopic and microscopic information packed into this mesoscopic model. The symbol E_c denotes the electric field criterion defining J_c. In all the research presented in this thesis, we have used the typical value of $E_c = 10^{-4}$ V/m. The E-J-relations of CSM and ECM are plotted in figure 2.4 as a summary, as well as to clarify the roles of n, E_c and J_c in the models. Note, however, that despite of their similarity, the models are essentially different: CSM leads to a multi-valued E-J-relation, whereas in ECM, there is a definite way to relate any J to a unique E. The relation is not bijective in CSM, while in ECM it is. Hence, power law resistivity with inifinite n does not correspond to ECM, as at $n \to \infty$ the nature of the constitutive relation becomes completely different. Therefore, CSM and ECM are truly two distinct models. In chapter 4, we shall discuss the properties, assumptions and differences of these models in more detail.

2.2.3 Solving boundary value problems approximatively using FEM

Models of the magnetoquasistatic Maxwell's theory can be formulated as partial differential equations. To solve such equations uniquely, relevant boundary conditions are needed. This leads to boundary value problems of PDEs. However, solving BVPs of PDEs is possible analytically only in certain very simple

[23] Two p-forms γ and η are parallel if there exists a scalar field ϕ such that $\gamma = \phi\eta$. If $\phi > 0$, γ and η are in the same direction.

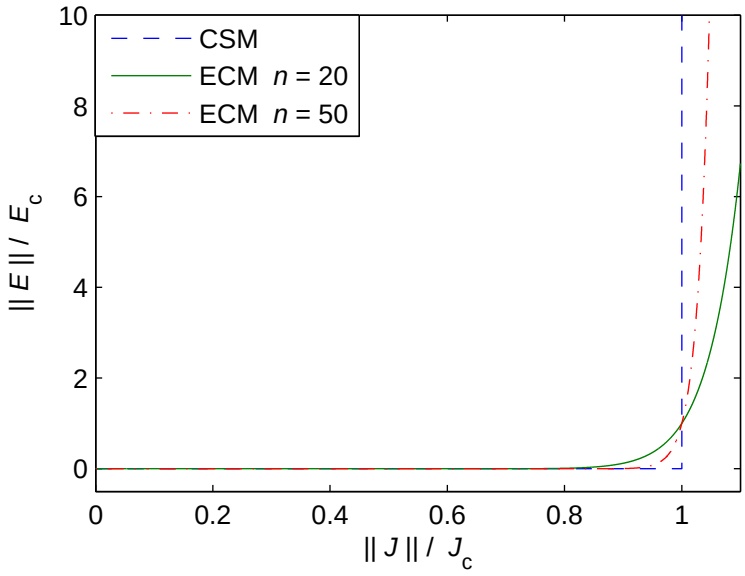

Figure 2.4: The E-J-relations of ECM and CSM.

cases, in which, for example, the modelling domain is very simple. This is why we often use *mesh methods*. Mesh methods are approximative solution methods, in which one meshes[24] the modelling domain wholly or partially, to find a finite-dimensional subspace of the function space, from which to seek the solution: eventually, we always want to solve matrix equations, as that is what computers are capable of. Popular mesh methods for solving the formulations arising from electromagnetic modelling include FEM, finite difference (time-domain) method (FDM, FDTD) [144], finite integration technique (FIT) [136] and various integral equation methods (IEM) [51], to name a few.

Let us walk through the workflow of a mesh method of one kind. When solving the BVP, we are generally solving for a tensor field. In the simplest case, we are looking for a (0,0)-tensor field, i.e., a scalar field. To approximate the tensor field, one defines a finite set of basis functions. This is what the mesh is used for: the basis functions are defined on the mesh entities. *The basis functions, defined on the mesh, span the finite-dimensional space, from which the approximative solution is sought.* Finding the basis can be relatively simple, as is the case when solving for a scalar field, or on the other hand, a bit more complicated when solving for a p-form with $p \geq 1$, or even more complicated, if solving for a mixed (q,p)-tensor with $q \geq 1$ and $p \geq 1$. Nonetheless, in this kind

[24]To mesh the modelling domain is to represent it with a cell complex, which is a finite collection of convex polyhedra. For a definition, see e.g. [78].

of mesh methods the fundamental idea is the same: mesh the domain, define a basis for the finite-dimensional space from which to search the solution, and find the approximative tensor field solution of the original problem.

Probably the most widely used method among physicists and engineers for solving problems arising from formulations of models in physics is (Galerkin) FEM [24, 107]. It is also the method mainly used in the research of this thesis. In FEM, one formulates the equations to be solved into a so called *weighted residual formulation*, in which the equations are weighted by some suitably chosen functions and integrated over the whole modelling domain Ω. The mesh is then formed by dividing Ω into a finite number of non-overlapping polyhedra covering it completely. After this, to find a finite-dimensional subspace of the function space, from which to seek the solution, each unknown to be solved for is approximated as a sum of a set of basis functions attached to the mesh. This, together with a finite number of weighting functions, yields a finite set of equations, which can be expressed in matrix form. Then, with proper boundary conditions, the matrix equation is solved to yield an approximative solution to the problem. [24, 107]

Next, we will take a brief look at the theoretical and practical sides of FEM and give a short introduction to the method. First, we will briefly discuss its mathematical background, and after that, some implementation-related issues are considered.

The mathematical foundations of FEM

In the following discussion, Ω denotes a bounded open subset of a Riemannian manifold with a sufficiently regular boundary $\partial\Omega$.

The structure of Hilbert space is an essential ingredient for FEM. In short, a Hilbert space $\mathcal{H}$ is an inner product space, complete with respect to the norm induced by its inner product [145]. Formally, this means that $\mathcal{H}$ is a vector space accompanied with an inner product, such that each Cauchy-sequence[25] in $\mathcal{H}$ converges to a limit in $\mathcal{H}$. Intuitively, we can think of this simply as securing us from not getting out of the space we are in when performing analysis in it.[26]

The existence of the weighted residual formulation, and thus the existence of FEM, is based on a simple but powerful theorem valid in Hilbert spaces.

[25]For a Cauchy-sequence, the distance between all the elements of the sequence is smaller than an arbitrarily small positive $c \in \mathbb{R}$ after a given index in the order of the index set.

[26]As an example of a set that is not complete, consider the open interval $(0, 1) \subset \mathbb{R}$ with the standard Euclidean norm of $\mathbb{R}$. The sequence having $1/p$, as the p:th term, is indeed a Cauchy-sequence in this set, while its limit as p approaches infinity is $0 \notin (0, 1)$.

The theorem states that [145]

$$\Phi \in H, \quad \Phi = 0 \quad \Leftrightarrow \quad \langle \Phi, \Phi' \rangle = 0, \quad \forall \Phi' \in \mathcal{H}. \tag{2.29}$$

To utilize this theorem, we introduce a global inner product of p-forms Φ and Φ' as

$$\langle \Phi, \Phi' \rangle = \int_\Omega \Phi \wedge \star \Phi'. \tag{2.30}$$

It is easy to check that (2.30) indeed defines an inner product. Intuitively, one immediately relates this inner product to energy as it reminds us of, for example (2.13), and hence, it is often called the *energy inner product*. We have used the same symbol Φ for the p-forms here as we did for elements of an arbirtary Hilbert space in (2.29) to emphasize that we indeed are in a Hilbert space. This is not, however, a trivial issue; in fact it is far from it. Not even the space of smooth square-integrable p-forms is a Hilbert space by construction. Such a space still needs to be *completed* [39, p. 361], [145]. However, such issues are not in the scope of this book, and from here on in our discussion of FEM, we shall *assume*, that the set of piecewise smooth p-forms accompanied with (2.30) and with the property $\langle \Phi, \Phi \rangle < \infty$, for all Φ, has the structure of a Hilbert space. This inner product space is denoted as $L^2F_p(\Omega)$.

In $L^2F_p(\Omega)$, the exterior derivative d is not defined everywhere, and it must be replaced by the *weak exterior derivative* $\tilde{\mathrm{d}}$, defined to satisfy [68]

$$\langle \tilde{\mathrm{d}}\Phi, \eta \rangle = \langle \Phi, (-1)^p \star^{-1} \mathrm{d} \star \eta \rangle, \quad \forall \eta \in \mathcal{D}F_{p+1}(\Omega), \tag{2.31}$$

where $\mathcal{D}F_{p+1}(\Omega) \subset F_{p+1}(\Omega)$ is the space of smooth $p+1$-forms with their supports in Ω. For smooth p-forms in $L^2F_p(\Omega)$, d and $\tilde{\mathrm{d}}$ coincide. From now on, we shall denote $\tilde{\mathrm{d}}$ also with d, as is customary. The operator $\delta := (-1)^p \star^{-1} \mathrm{d} \star : F_p(\Omega) \to F_{p-1}(\Omega)$ is called the *coderivative*, which can also be defined in the weak sense to satisfy

$$\langle \tilde{\delta}\Phi, \varpi \rangle = \langle \Phi, \mathrm{d}\varpi \rangle, \quad \forall \varpi \in \mathcal{D}F_{p-1}(\Omega). \tag{2.32}$$

Again, it is customary not to make a difference between the weak coderivative $\tilde{\delta}$ and δ in the notation. Now, the Sobolev space $L^2F^p(\mathrm{d}, \Omega)$ of p-forms may be defined as [68]

$$L^2F^p(\mathrm{d}, \Omega) = \left\{ \Phi \in L^2F_p(\Omega) \quad | \quad \mathrm{d}\Phi \in L^2F_{p+1}(\Omega) \right\}, \tag{2.33}$$

where, d is now the weak exterior derivative. In this space, we can do finite element modelling. Note that not only the p-forms need to be piecewise smooth and square-integrable but also their weak exterior derivatives. By employing

the weak exterior derivative here instead of the strong one, we ensure that, for example, we can have normal jumps across material boundaries in potentials. Such discontinuities among others are essential in electromagnetic modelling. Another important Sobolev space of differential forms is [68]

$$L^2F^p(\delta,\Omega) = \left\{\Phi \in L^2F_p(\Omega) \quad | \quad \delta\Phi \in L^2F_{p-1}(\Omega)\right\}, \tag{2.34}$$

where the coderivative is now understood in the weak sense. The Hodge operator extends to Sobolev spaces and acts as an isomorphism between them: $\star : L^2F^p(\mathrm{d},\Omega) \to L^2F^{k-p}(\delta,\Omega)$.

Now, suppose we are working in $L^2F_p(\mathrm{d},\Omega)$. Using (2.29), a p-form equation of the form $\Phi := \mathrm{L}G - \gamma = 0$, where L is a linear operator and G is the unknown differential form, can be equivalently expressed as

$$\int_\Omega (\mathrm{L}G - \gamma) \wedge \star\Phi' = 0 \Leftrightarrow \int_\Omega \mathrm{L}G \wedge \star\Phi' = \langle\gamma, \Phi'\rangle, \quad \forall\Phi' \in L^2F_p(\mathrm{d},\Omega). \tag{2.35}$$

This is the weighted residual formulation of $\Phi = 0$. The equation $\Phi = 0$, on the other hand, is called the strong form of the equation, which, in its equivalent weighted residual formulation, is said to be *weighted* with *weighting functions* Φ'. Sometimes, one refers to the weighting functions as *test functions* as well. From the weighted residual formulation, one obtains the *weak formulation* of the problem through partial integration of (2.35) [19]. It is weaker than the weighted residual and strong formulations in the sense that the requirement of differentiability is dropped as a consequence of partial integration [24, pp. 1-19], but not in the sense that we would be introducing any approximativity to the solution at this stage [19]. After the partial integration, one typically arrives at a situation, where the equation may be written as

$$a(G,\Phi') = \langle\gamma,\Phi'\rangle, \quad \forall\Phi' \in L^2F_p(\mathrm{d},\Omega), \tag{2.36}$$

where $a(\cdot,\cdot)$ is a bounded, coercive bilinear form on $L^2F_p(\mathrm{d},\Omega)$ [24].

As an example, consider magnetostatics in 3D. We want to solve the equation

$$\mathrm{d}{\mu_\star}^{-1}\mathrm{d}A - J = 0 \Leftrightarrow \star\mathrm{d}{\mu_\star}^{-1}\mathrm{d}A - \star J = 0, \tag{2.37}$$

where the unknown $A \in L^2F_1(\mathrm{d},\Omega)$ is the magnetic vector potential and J is known beforehand as a source term. In the context of (2.35), we have $\mathrm{L} = \star\mathrm{d}{\mu_\star}^{-1}\mathrm{d}$, $G = A$ and $\gamma = \star J \in L^2F_1(\delta,\Omega)$. The weighted residual formulation of (2.37) can now be written as

$$\int_\Omega \star\mathrm{d}{\mu_\star}^{-1}\mathrm{d}A \wedge \star A' = \int_\Omega \star J \wedge \star A', \quad \forall A' \in L^2F_1(\mathrm{d},\Omega). \tag{2.38}$$

Using the properties of $\wedge$ and the facts that $\eta \wedge \star\gamma = \gamma \wedge \star\eta$ and $\star \star \eta = (-1)^{p(k-p)}\eta$ for p-forms η and γ, (2.38) is equivalent with

$$\int_\Omega \mathrm{d}{\mu_\star}^{-1}\mathrm{d}A \wedge A' = \int_\Omega \star J \wedge \star A', \quad \forall A' \in L^2F_1(\mathrm{d}, \Omega). \tag{2.39}$$

Integrating the left-hand side by parts, one obtains the weak formulation

$$\int_\Omega {\mu_\star}^{-1}\mathrm{d}A \wedge \mathrm{d}A' + \int_{\partial\Omega} {\mu_\star}^{-1}\mathrm{d}A \wedge A' = \int_\Omega \star J \wedge \star A', \quad \forall A' \in L^2F_1(\mathrm{d}, \Omega). \tag{2.40}$$

If we have, for example, $\mu_\star^{-1}\mathrm{d}A = 0$ on $\partial\Omega$, the boundary integral has no contribution to the equation and we can drop it out to yield

$$a(A, A') := \int_\Omega {\mu_\star}^{-1}\mathrm{d}A \wedge \mathrm{d}A' = \int_\Omega \star J \wedge \star A', \quad \forall A' \in L^2F_1(\mathrm{d}, \Omega), \tag{2.41}$$

which is simply

$$a(A, A') = \langle \star J, A' \rangle \quad \forall A' \in L^2F_1(\mathrm{d}, \Omega). \tag{2.42}$$

In short, this is the foundation of FEM. Next, we shall turn our attention to more implementation-related matters.

The implementation of FEM

As $L^2F_p(\mathrm{d}, \Omega)$ is not finite-dimensional, equation (2.36) is not of much use as it is. We need to find a finite-dimensional subspace of $L^2F_p(\mathrm{d}, \Omega)$, from which to seek the solution. To do this, we form a mesh to Ω. This mesh can consist of, for example rectangular or hexagonal elements. However, here we consider a finite element mesh consisting of simplices.[27] Hence, on a k-dimensional Ω, we form a mesh consisting of k-simplices. Then, we attach a suitable set of basis functions to, for example, the nodes, edges, faces or volumes of the finite element mesh and seek the solution from the finite-dimensional subspace spanned by these basis functions.

Whitney forms form a family of basis functions especially suitable for electromagnetic modelling [17]. Whitney forms are defined on simplices: a Whitney p-form is related to a p-simplex in the finite element mesh. Whitney 0-forms are often also referred to as nodal basis functions. In a tetrahedron

[27] A 0-simplex is a point, 1-simplex is an edge, 2-simplex is a triangle and 3-simplex is a tetrahedron.

with nodes j, k, l and m and with coordinates $(x, y, z) \in \mathbb{R}^3$, the (linear) Whitney 0-form attached to the node j is defined as

$$\lambda_j = \alpha_j + x\beta_j + y\gamma_j + z\delta_j, \tag{2.43}$$

where the coefficients α_j, β_j, γ_j and δ_j are found from

$$\begin{bmatrix} x^j & y^j & z^j & 1 \\ x^k & y^k & z^k & 1 \\ x^l & y^l & z^l & 1 \\ x^m & y^m & z^m & 1 \end{bmatrix} \begin{bmatrix} \beta_j \\ \gamma_j \\ \delta_j \\ \alpha_j \end{bmatrix} = \begin{bmatrix} 1 \\ 0 \\ 0 \\ 0 \end{bmatrix}. \tag{2.44}$$

Here, (x^j, y^j, z^j), (x^k, y^k, z^k), (x^l, y^l, z^l), $(x^m, y^m, z^m) \in \mathbb{R}^3$ denote the coordinates with which the nodes of the tetrahedron are identified. The same formulae work for 1- and 2-simplices as well, by simply setting the rows and columns containing merely redundant coordinates to zero. Using the definition of Whitney 0-forms, a Whitney 1-form (often referred to as edge element) attached to the edge i is then obtained as

$$w_i = \lambda_j \mathrm{d}\lambda_k - \lambda_k \mathrm{d}\lambda_j, \tag{2.45}$$

where edge i is oriented from node j to node k. The support of w_i is restricted to those tetrahedra, which contain edge i as one of their edges. Moreover, the integral of w_i over i equals one, and the integral of w_i over any other edge in the mesh equals zero. More generally, the same properties hold for the integrals and supports of Whitney p-forms, for the corresponding p-simplices. By looking at the formula (2.44) for obtaining the coefficients for the nodal basis functions, we easily notice that these properties hold for Whitney 0-forms. The integral property of Whitney forms is also easy to grasp from the geometrical interpretation demonstrated in figure 2.5 for Whitney 0-forms and 1-forms on a 2-simplex.

A general simplified guideline is that if the unknown to be solved for is a p-form, it is suitable to use Whitney p-forms as basis functions. So if we were to solve for a 0-form, we would approximate the solution as a sum of Whitney 0-forms. Or if we would like to solve for an unknown 1-form, we would probably be better off using Whitney 1-forms. Thus, in the case of 0-forms, one attaches a Whitney 0-form to each node of the finite element mesh, and correspondingly, in the case of 1-forms, a Whitney 1-form to each edge of the mesh. Solving for a p-form, one attaches a Whitney p-form to each p-simplex of the mesh.

For some problems, however, it can be beneficial to use basis functions of higher polynomial order than one. In that case, to accurately represent such

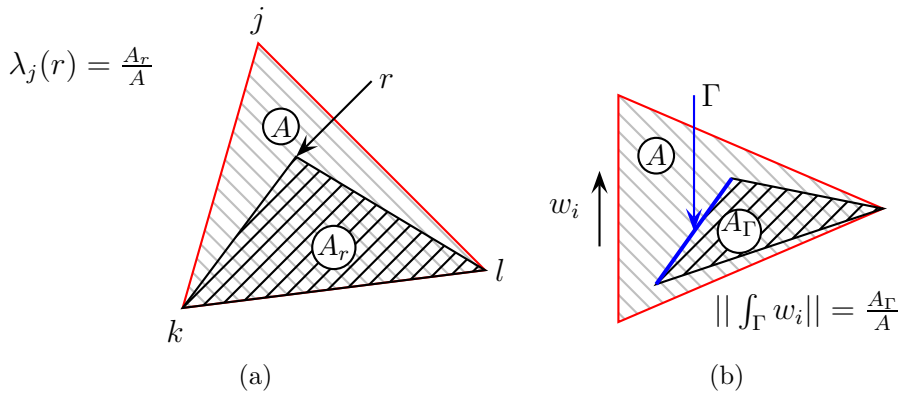

Figure 2.5: A geometrical interpretation for (a) Whitney 0-forms and (b) Whitney 1-forms on a 2-simplex. The integrals of the forms are related to the areas of the 2-simplices they are defined on.

basis functions, one will have more unknowns than just those attached to, for example, nodes or edges of the mesh. The use of such bases can capture different properties of the solution than the simple linear basis functions. For more information on Whitney forms of higher polynomial degrees, see [18], [104]. In the scope of this thesis, we are dealing only with linear Whitney 0-forms and 1-forms as defined above.

Finally, to find the approximative solution of the weak formulation of the problem from $W_p(\Omega) \subset L^2F_p(\mathrm{d}, \Omega)$ spanned by Whitney p-forms w_i^p attached to the p-simplices of the finite element mesh, we approximate the unknown p-form to be solved for as a finite sum of w_i^p with unknown real number coefficients. These coefficients are called the *degrees of freedom* of the problem. Furthermore, we weight the discretized equation with elements of $W_p(\Omega)$ as well.[28] Now, we thus require (2.35) only for all $w_i^p \in W_p(\Omega)$ with unknown coefficients.[29] This way, we obtain a finite number of equations: there will be as many equations as there are unknown coefficients for the Whitney p-forms. Thus, we can combine all this into a matrix equation, impose relevant boundary conditions and finally obtain an approximative solution of the problem by solving the matrix equation. The matrix equation can be a system of algebraic equations, a normal form ordinary differential equation system or their combination: a differential-algebraic equation (DAE) system.

[28] FEM, in which the space of weighting functions is the same as the space of basis functions is called Galerkin FEM.

[29] Note that not all coefficients are necessarily degrees of freedom. For some w_i^p the coefficient may be known beforehand due to, e.g., boundary conditions, and such w_i^p are not used for weighting either.

Concluding remarks

Essentially, we have now covered the most important fundamentals, as well as some implementation details of FEM. Naturally, in real implementations there are many more issues to be considered related to, for example, numerics, programming and physical interpretation, but the basic idea and the foundation are the same regardless of the application or the implementation. In the next chapter, we shall see more concrete examples of FEM formulations in the context of superconductor modelling.

Even though we know that the infinite-dimensional weighted residual formulation is equivalent to the strong form, one more question may arise: how can we know that our approximative solution obtained using FEM is any good? This is a difficult issue and cannot be thoroughly answered within the scope of this book, but we can shed some light on it to at least build up some intuitive credibility. One of the intuitively appealing properties of FEM is that it in some sense minimizes the difference between the approximative solution, found from the finite-dimensional space, and the exact solution. This can be said, because the error is orthogonal to the finite-dimensional $W_p(\Omega)$. To see this, consider the approximative solution G_{app} of (2.36) obtained using FEM and the exact solution G. Then, it holds that [24, p. 58]

$$a(G - G_{\text{app}}, w_i^{p'}) = a(G, w_i^{p'}) - a(G_{\text{app}}, w_i^{p'}) = \langle \gamma, w_i^{p'} \rangle - \langle \gamma, w_i^{p'} \rangle = 0, \quad (2.46)$$

for all $w_i^{p'} \in W_p(\Omega)$. This orthogonality means that we have, in a sense, an optimal approximation with respect to the induced norm. An intuitive analogy (not to be taken too literally in this context, though) is finding the shortest route in $\mathbb{R}^k$ from a point to a straight line: the obvious answer is that the shortest route is the one orthogonal to the line with respect to the Euclidean norm. In a similar manner, we are searching for an approximative solution from $W_p(\Omega)$, which is, in some sense, closest to the exact solution. Note that gauge selection is not taken into account here. The bilinear form $a(\cdot, \cdot)$ induces only a *semi-norm* to $L^2F_p(\mathrm{d}, \Omega)$. However, it induces a norm to the quotient space, which sees different gauge selections equivalent.

2.3 Superconductors

The target application of the research presented in this thesis is superconductor technology. In particular, all the research is related to mathematical modelling of superconductors in situations involving a time-varying magnetic

field. In this section, we discuss superconductors and their fundamental properties from an engineer's viewpoint. First, we give a brief introduction to superconductivity in general, including a historical overview and then we go on to discuss phenomena related to superconductors in time-varying magnetic fields. In particular, we discuss the undesirable heat generation, AC loss, that occurs in superconductors in such situations.

2.3.1 A brief history of superconductivity

Superconductivity has been known as a natural phenomenon for over 100 years. In 1911 Heike Kamerlingh Onnes discovered superconductivity in his low-temperature experiments following his research on the liquification of helium [90]. His remarkable observation was that below a certain threshold temperature the resistivity of mercury vanished completely: electric current could flow through the material without producing any heat. This threshold temperature is called the critical temperature of the superconducting material θ_c. This is the first of the two magnificent properties of superconducting materials. The second property that characterizes superconductors, and distincts them from ideal perfect conductors in the classical sense, is the so called Meissner effect [38]: as a superconducting material is cooled below θ_c, it expells all the magnetic field from its interior. Even though an ideal perfect conductor, once at the perfectly-conducting state, does not permit any magnetic field inside it, such expelling behaviour is not predicted by the classical Maxwell's theory in *the transition* from normal-conducting to perfectly conducting state. As it turns out, superconductivity is a quantum phenomenon, and a more thorough description of the mechanisms of superconductivity can be presented within the framework of quantum mechanics. However, such discussion is not in the scope of this thesis.

It was not until 1950s when a reliable and widely accepted quantum mechanical theory of superconductivity was conceived. The BCS theory, named after its discoverers Bardeen, Cooper and Schrieffer [12] has stood the test of time and is still today *the* theory of superconductivity at low temperatures. However, once again nature turned out to be even more fascinating: in 1986 Bednorz and Müller observed superconductivity above the temperature $\theta = 30$ K, the limit set for superconductivity by the BCS theory [14]. Superconductivity at such high temperatures could not be predicted in the framework of any existing physical theory. This finding introduced a natural division of different types of superconducting materials: the ones in which superconductivity could be predicted by the BCS theory would be called low-temperature

superconductors (LTS), whereas the materials exhibiting superconductivity at higher temperatures were named high-temperature superconductors (HTS). And as if this inconsistency between the theoretical description and observations was not enough, superconductor scientists have recently been puzzled by the discovery of superconductivity in iron-based compounds [62], in which superconducting phenomena were thought to be impossible as well. Still today, we lack a consistent theory of superconductivity in HTS materials, let alone a theory unifying different types of superconductivity. However, for an engineer mainly interested in the modelling of superconductors at the mesoscopic scale in power engineering applications, this is usually not an issue, as microscopic models are often too detailed for modelling such applications, anyway.

Eventhough the phenomenon has been known for a century, commercial breakthrough[30] of superconductivity has been relatively slow [32]. The use of superconductors is usually motivated by their ability to carry large currents and produce high magnetic fields, as well as their lossless behaviour in certain situations. Because of these properties, they often allow size and mass reductions, increases in efficiency and act as an enabling technology for many applications. Ways of utilizing superconductor technology are numerous, but only few have lived up to the expectations of their commercial potential. Commercially speaking, the biggest, and probably the most well-known application of superconductivity is magnetic resonance imaging (MRI) [70]. In the MRI scanners, superconducting coils provide the required high magnetic fields. Other large-scale applications include motors [61, 114, 125], generators [59, 91, 117], transformers [40, 60, 69], power transmission cables [58, 74], induction heating [110], fault current limiters (FCL) [87] and superconducting magnetic energy storages (SMES) [142], to name a few. However, such power applications are mainly on the level of demonstrations, still too far from commercialization. Also, superconductors act as an enabling technology for such big science projects as large-scale particle accelerators [5, 34, 131], like the Large Hadron Collider (LHC) in CERN [108]. In the long run, the need for 20 T range magnets in such applications keeps on boosting the superconductor research [134]. Another such application is fusion, the largest ongoing demonstration of which is the ITER project [83]. Hence, even though the commercialization of superconductivity has not been very fast, the need and interest for superconducting technology has not died out. Still today, we need new research to boost existing technology, and to come up with new innovative applications.

[30] By commercial breakthrough of a technology, we mean that such products exploiting the technology, that continuously create financial value for their producers, are introduced to the market.

2.3.2 Different types of superconductors

The most obvious categorization of superconductors is the categorization by the critical temperature θ_c, which divides superconductors into LTS and HTS materials. However, it is not only the temperature θ, which needs to be low enough for a superconducting material to stay in the superconducting state. In fact, superconductivity is maintained, as long as three quantities stay below their critical values. In addition to θ_c, critical current density J_c and critical magnetic flux density, or simply the critical field, B_c, which denote the maximal Euclidean norms of J and B the superconductor can withstand, characterize the surface of transition between superconducting and normal-conducting states. The critical value of each of the quantities depends non-linearly on the two other ones, and often also on the directions of the fields. This is a major difficulty for the numerical modelling of superconductors. Typically, for precise simulations, the critical quantity that enters the model must be expressed as a function of the two others. The transition surface defined by critical quantities, the critical surface, is depicted in figure 2.6. Furthermore, J_c of HTS materials tends to behave extremely anisotropically with respect to magnetic field, which can be a nuisance for modelling but must be accounted for in application design. In some materials, J_c can vary orders of magnitude between different magnetic field orientations [75]. Of course, as J_c is merely a mesoscopic model of electric currents, one has the corresponding macroscopic obervable quantity, the critical current I_c, as well. Hence, even though materials exhibit practically no resistivity in the superconducting state, we still cannot, for example, drive an infinite electric current into the conductor, or produce an infinite magnetic field with a superconducting coil.

The eligibility of a superconducting material for the purposes of applications, such as electromagnets, is often determined by its B_c and J_c. Another convenient categorization of superconductors is that of type-I and type-II superconductors. Type-I superconductors exhibit Meissner effect in its pure sense: no magnetic flux can enter the material, except for a very small surface layer of the order of few tens of nanometers. As soon as B_c is exceeded, flux enters the superconductor, and the material loses its superconductivity.[31] As magnetic field penetrates the superconductor merely in the thin surface layer, the electric currents are restricted to this layer as well. Hence, the B_c and I_c

[31] However, even though external field would remain below B_c, effects due to the sample shape may cause the field in the type-I superconducting sample to locally exceed B_c, and the superconductivity may be lost there while the rest of the sample remains superconducting. Thus, the field can penetrate the sample partially. This is called the *intermediate state* [113, p. 5].

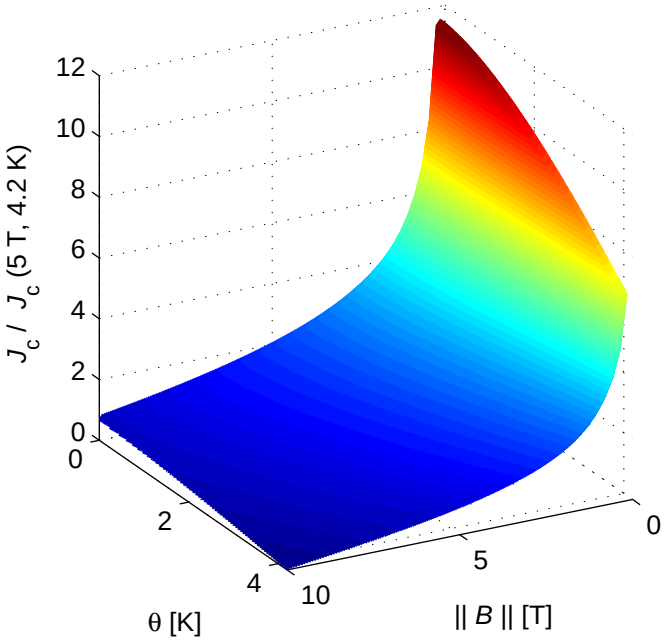

Figure 2.6: The critical surface defined by the critical quantities of a superconductor shows J_c as a function of $||B||$ and θ. We have used the fitting formula and fitting parameters presented in [22] for niobium titanium.

values of type-I superconductors are far too low for most practical applications, with B_c typically of the order of 10 mT. [80, pp. 12-13] Type-II superconductors, on the other hand, are characterized by two critical field values: the lower critical field B_{c1} and the upper critical field B_{c2}. Below B_{c1} a type-II superconductor acts similarly as a type-I superconductor. However, between B_{c1} and B_{c2}, type-II superconductors exhibit so called mixed state, in which magnetic flux enters the superconductor in quantized flux vortices[32]. In this state, however, the material stays superconducting. Finally, as the upper critical field B_{c2} is reached, all the flux vortex cores overlap, and the superconducting state is lost. [80, pp. 13-17]

Superconductors of type-II are also much more promising for applications than type-I superconductors as their B_{c2} and J_c can reach much higher values than those of type-I. However, when a current-carrying type-II superconductor is exposed to magnetic field, the Lorentz force exerted on the flux vortices

[32]These elementary building blocks of magnetic flux each contain exactly one flux quantum, the smallest possible value of magnetic flux. These tubes of flux are often called flux vortices as supercurrents circulate the tubes to shield the superconductor. However, they are also sometimes called flux tubes, fluxoids or flux quanta.

because of the flowing current causes the vortices to move through the material viscously generating heat. This phenomenon, called *flux flow resistance* thus means that type-II superconductors generate heat *even in DC (direct current) use* when they are subject to a magnetic field [65], [80, p. 17]. However, the flux movement due to the Lorentz force can be significantly reduced by the presence of anomalities, so called *pinning centers*, in the material, in which J_c is lower with the same B and θ than in its surroundings, or even zero. The vortices get stuck in the pinning centers, thus remaining motionless and generating no heat. Hence, it is advantageous to artificially add impurities to the crystal structure of the superconductor to reach higher critical currents in fixed external field [113, p. 82]. The release of flux vortices from their pinning centers due to, for example, thermal energy is called *flux creep*, and it is more prominent for HTS than LTS materials, partially due to their higher operating temperatures [4]. Also this can be reduced by strong pinning.

Type-II superconductors with considerably strong pinning are called *hard superconductors* [80, pp. 17-23]. Hard superconductors possess the most favourable properties for power applications: high critical current and critical field values. For example in superconducting wires made of the LTS material niobium-tin (Nb_3Sn), critical current densities reach 3000 - 4000 A/mm^2 in magnetic fields of the order of 10 T [141]. However, the favourable properties of hard superconductors come with a downside as well: hysteresis loss, towards which we will turn our attention in the next subsection. In table 2.1, values of the upper critical fields and critical temperatures in some typical hard superconductor materials are presented. I_c and thus J_c are very much affected by wire manufacturing process and thus, are not such intrinsic properties of the materials as θ_c and B_{c2}. However, critical current density data as a function of applied field for some state-of-the-art conductors can be found in [6]. To give an idea of the high-field performance of LTS and HTS materials, we make a few remarks from this data for YBCO and Nb_3Sn wires in 20 T applied field. A coated conductor YBCO tape can sustain a current density of 3000 A/mm^2 on average in the cross-section of a technical product, when the applied field is parallel to the tape plane, and 400 A/mm^2, when the field is perpendicular to it. A Nb_3Sn wire is not affected by the direction of the field but can only reach approximately similar values as YBCO in perpendicular field. Note that for HTS materials, the upper critical fields can reach extremely high values, and therefore, they are promising for high-field magnets. However, there are difficulties in using HTS materials for applications, too: along with other material scientific challenges, they are relatively expensive and their ceramic structure makes them brittle, making it difficult to wind them into coils [37]. On the other hand, the winding and fabrication difficulties are prominent for Nb_3Sn,

too [80, p. 30].

Table 2.1: Typical critical temperatures and upper critical field values for some hard superconducting materials [27, ch.B3.3.1,ch.B3.3.4], [47, 132]. YBCO stands for yttrium barium copper oxide, MgB_2 for magnesium diboride, NbTi for niobium-titanium and Bi-2223 is a Bismuth based superconducting compound.

Material type	Material	θ_c @ 0 A, 0 T [K]	B_{c2} @ 4.2 K, 0 A [T]
HTS	Bi-2223	110	> 100
	YBCO	92	> 100
	MgB_2	39	20
LTS	Nb_3Sn	18	29
	NbTi	9	12

2.3.3 AC losses in superconductors

Hard superconductors can carry electric currents without generating any heat in the process, even under a *constant* magnetic field, since strong pinning prevents the movement of vortices. However, this property, which is naturally very attracting from the application design's point of view, holds unfortunately only for DC, when no *varying* magnetic field is present. Whenever the magnetic field experienced by the superconductor changes, an associated heat generation occurs. This can, of course, happen due to the magnetic field produced by a changing current flowing through the superconductor, as well as due to changes in the external field it experiences. This heat generation is one of the greatest restricting factors for the use of superconducting technology in applications, and hence, this phenomenon deserves a name: AC loss of the superconductor.

Magnetization behaviour of hard superconductors and hysteresis loss

As discussed, magnetic field can penetrate type-II superconductors in quantized flux vortices. As seen from the outside, superconductors subject to magnetic field *magnetize*, which is caused by the non-decaying supercurrents circulating in the material. The magnetization process of an ideal type-II superconductor is fully reversible, but for a hard superconductor, the magnetization behaviour is strongly hysteretic [80, pp. 17-23].

Consider a specimen of hard superconducting material subject to an external oscillating magnetic field. As the magnitude of the magnetic flux density

exceeds B_{c1}, magnetic field enters the material. However, the flux vortices are trapped in the pinning centers present in hard superconductors. Now, even though the magnetic flux density is reduced back to zero, the vortices remain trapped in the pinning centers, and the material remains magnetized: *the magnetization of the material lags behind the external field.* The (net) magnetic moment of the sample will always return to zero only at a magnetic field with inverse polarity. This irreversible behaviour is associated to heat generation: the oscillating movement of flux vortices entering and exiting the specimen, or depinned from the pinning center, produces frictional heat. If we have a cyclic external magnetic field and we plot the magnetic moment of the specimen as a function of the magnetic flux density of the external field, we obtain a *hysteresis loop*, the area of which corresponds to the heat generated during the cycle of the field. This heat is called hysteresis loss.[33] A typical shape of a hysteresis loop for a superconducting wire in such a case is depicted in figure 2.7. Note that after any penetration of B in the superconductor, the virgin state of zero magnetic moment at zero applied field may only be reached by means of first losing the superconducting state completely.

But what exactly is meant by the magnetization and magnetic moment of the superconductor? The intuitive picture that probably many of us share is that they somehow reflect how some elementary magnets, atomic-level current loops in the material line up in the presence of external magnetic field to magnetize the material. Why is magnetic moment then expressed as a single real number, when the intuitive picture clearly suggests that directional information is needed as well? Let us try to clarify this a little. There are actually two different quantities related to magnetization, one defined locally and another one only globally. Here, we shall call the former the magnetization m, which may be understood as the magnetic (dipole) moment density and the latter is the magnetic moment M. Again, consider a superconductor in applied field carrying screening currents with density J. Then, the local magnetization m is a 1-form, such that in the presence of no other currents, the field quantities satisfy

$$\mathrm{d}m = J, \quad \mathrm{d}H_m = 0, \quad \mathrm{d}B = 0, \quad B = \mu_\star(H_m + m) \tag{2.47}$$

where the contribution of currents in the superconductor has been removed from H to yield H_m, and they have been accounted for by the introduction of m. Note that for simplicity, we do not consider here the exciting currents outside the superconductor. Thus, J and m are merely two different ways of stating that a magnetic flux density B is produced outside the superconductor:

[33] This is not to say that hysteresis losses could *only* be evaluated after a full cycle of the magnetic field. In the case of superconductor magnetization, they can be computed momentarily, too.

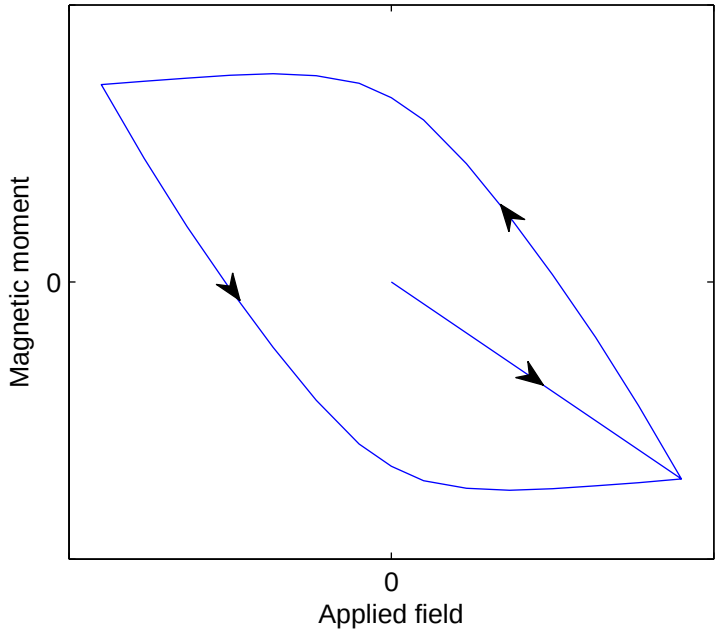

Figure 2.7: Typical shape of a diamagnetic hysteresis loop for a superconducting wire, obtained from a simulation employing CSM and constant J_c. The graph starts from the origin. As the magnetic moment exceeds zero, it will not return to zero until at a magnetic field of inverse polarity with a derivative of different sign.

J and m are completely interchangeable in that sense. Of course, (2.47) does not determine a unique m, but an equivalence class of magnetizations: m is defined up to an additive closed[34] 1-form. What about the constitutive relation for B then? If we alter the gauge[35] condition for m, do we not alter B as well? This is not problematic, as actually both m and H_m are defined only up to an additive closed 1-form. If $B = \mu_\star(H_0 + m_0)$ for some H_0 and m_0, and we choose $m = m_0 + \mathrm{d}\varsigma$, $\varsigma \in F_0$, we must have $H_m = H_0 - \mathrm{d}\varsigma$. After all, there is no method to measure H_m or m directly without utilizing the defining properties.

On the other hand, J can be interpreted in 3D as a *vector-valued* 3-form $\hat{J}$. Intuitively, one can picture current density as the charge density σ equipped with a velocity vector. That is, having σ in C/s and a velocity vector $\mathbf{v}$ in m/s,

[34] A differential form, whose exterior derivative vanishes is called *closed*. A form that is an exterior derivative of another form is called *exact*. Every exact form is closed as $\mathrm{d} \circ \mathrm{d} = 0$, however, whether a closed form is exact depends on the topology of the manifold. Note, that exactness and closedness of forms is where the potential formulations of mesoscopic modelling arise from.

[35] Gauging is the selection of a unique representative from the equivalence class.

we obtain current density in units $(\mathrm{Cm})/(\mathrm{sm}^3) = \mathrm{C}/(\mathrm{sm}^2) = \mathrm{A}/\mathrm{m}^2$. Interpreted this way, we can define the magnetic moment of the superconducting sample Ω_{SC} as

$$M = \frac{1}{2}\int_{\Omega_{\mathrm{SC}}} \left(\mathbf{r} \wedge (\star J)^\sharp\right) \otimes \mathrm{vol}^3 = \frac{1}{2}\int_{\Omega_{\mathrm{SC}}} \left(\mathbf{r} \wedge (\star \mathrm{d}m)^\sharp\right) \otimes \mathrm{vol}^3, \tag{2.48}$$

where $\mathbf{r}$ denotes the location with respect to a coordinate system origin, $\otimes$ is the tensor product [39, pp. 58-66], $\sharp$ denotes the metric isomorphism taking 1-forms to vectors as earlier and vol^3 is the volume form of the manifold. We can also make the interpretation

$$\hat{J} = (\star J)^\sharp \otimes \mathrm{vol}^3 \in T^1_3(\Omega). \tag{2.49}$$

By $T^q_p(\Omega)$, we denote the set of (q,p)-tensor fields on Ω.[36] Now, M is a 2-vector and the integrand in (2.48) can be interpreted as the 2-vector valued 3-form $\hat{m}$, the 2-vector magnetic moment density

$$\hat{m} = \left(\mathbf{r} \wedge (\star J)^\sharp\right) \otimes \mathrm{vol}^3 \in T^2_3(\Omega). \tag{2.50}$$

Note that in the language of vector fields in $\mathbb{R}^3$ with Cartesian metric, equation (2.48) is usually expressed as

$$\mathbf{M} = \frac{1}{2}\int_{\Omega_{\mathrm{SC}}} \mathbf{r} \times \mathbf{J} dV = \frac{1}{2}\int_{\Omega_{\mathrm{SC}}} \mathbf{r} \times \mathrm{curl}(\mathbf{m}) dV, \tag{2.51}$$

where $\mathbf{M}$ is the 1-vector version of M, $\mathbf{m} = m^\sharp$ is the vector field version of m and $\times$ denotes the cross product of vectors. M is independent of the choice of gauge for m as well as the choice of origin for the coordinate system [20]. The former is clear, as M depends on $\mathrm{d}m$ and not directly on m. The latter can be seen by making an arbitrary translation of origin by $\mathbf{r}_0$, in which case we obtain

$$\frac{1}{2}\int_{\Omega_{\mathrm{SC}}} \left((\mathbf{r}+\mathbf{r}_0) \wedge (\star J)^\sharp\right) \otimes \mathrm{vol}^3 = M + \frac{1}{2}\left(\mathbf{r}_0 \wedge \int_{\Omega_{\mathrm{SC}}} (\star J)^\sharp \otimes \mathrm{vol}^3\right) = M. \tag{2.52}$$

The last equality is true as

$$\int_{\Omega_{\mathrm{SC}}} (\star J)^\sharp \otimes \mathrm{vol}^3 = 0, \tag{2.53}$$

[36] Note that the metric in $\sharp$ and $\star$ cancels out, so actually we do not need metric for obtaining the isomorphism between J and $\hat{J}$. In the end, we need to only make use of the *Poincaré isomorphism* between 2-forms and 1-vectors [68].

since in orthonormal coordinates x^i assuming positive orientation

$$\mathrm{d}m = J \Rightarrow \mathrm{d}J = 0 \Rightarrow \left(\mathrm{d}\left(x^i J\right) = \mathrm{d}x^i \wedge J + x^i \mathrm{d}J = \mathrm{d}x^i \wedge J = J_i \mathrm{vol}^3\right), \tag{2.54}$$

where J_i is the component of J corresponding to x^i. Integrating over Ω_{SC} and utilizing Stoke's theorem (2.20), we infer

$$\int_{\Omega_{\mathrm{SC}}} J_i \mathrm{vol}^3 = \int_{\partial\Omega_{\mathrm{SC}}} x^i J = 0, \tag{2.55}$$

assuming no current flows through $\partial\Omega_{\mathrm{SC}}$, or more precisely, the restriction of J to $\partial\Omega_{\mathrm{SC}}$ is 0.[37] This means that (2.53) must be true component-wise.

Now, having seen an interpretation for M, we conclude that it is then the magnitude of M and the magnitude of the applied magnetic flux density, B_{ext}, that are usually plotted in the magnetization loops of superconductors, as in figure 2.7. This can be done, if the situation has enough symmetry for $\mathbf{M}$ to be parallel to the applied field [20].

The hysteresis losses are proportional to the area of the hysteresis loop and, to an extent, independent of the frequency of the oscillating field. However, it is well-known, that the energy loss associated to the diamagnetic hysteresis of a hard superconductor can also be interpreted simply as Ohmic heat generation in a material with highly non-linear resistivity. We refer the reader to [20] for the equivalence of these two pictures. Hence, from an engineer's point of view, AC losses can be mesoscopically modelled using models of the classical Maxwell's theory, such as CSM and ECM presented in the previous section. The electric field and magnetic field are connected as predicted by Maxwell's equations and constitutive relations. A varying magnetic field causes a varying electric field and vice versa. This means that E and J can coexist in a superconducting material in a varying magnetic field. Then, if p_{d} calculated using (2.14) is positive, Ohmic power loss occurs locally. However, one should note that hysteresis has nothing to do with the mesoscopic constituve relations of superconductors per se. It is a macroscopic observation: the whole superconductor acts hysteretically with respect to applied magnetic field [20]. Its magnetization is not independent of its history.

[37] Often, the restriction of a form γ to the boundary of the modelling domain is called trace of γ, denoted as $\mathrm{tr}(\gamma)$. Formally, it is the pullback of the inclusion map [39, p. 79]. As an example, the boundary condition stating that the tangential component of E vanishes on $\partial\Omega$, would be written $\mathrm{tr}(E) = 0$ on $\partial\Omega$. There, the trace operator states that we have restricted the domain of E to the vectors that are tangent to the boundary. We usually omit the trace operator in our notation when it is implicitely clear from the context that it is used.

Categorization of AC losses

AC losses of superconductors occuring at the frequencies of power applications are often divided into three sub-categories: *hysteresis loss*, which is precisely the loss associated to the diamagnetic hysteresis exhibited by hard superconductors, and *eddy current loss* and *coupling loss*, which both are losses of the normal-conducting materials present in a superconducting wire. None of the loss types can be fully eliminated except by not exposing the superconductor to any changes of magnetic field, but they can be reduced by careful wire design. The only way to effectively reduce hysteresis losses is to subdivide the superconducting wire into small filaments [139]. However, a fine filamentary subdivision is effective only when the magnitude of the magnetic field is above the penetration field B_p, which is the magnitude of the applied magnetic flux density required for the field to fully penetrate the superconductor. If the field is clearly weaker than B_p, it can be more beneficial to have large superconducting filaments to shield the interior of the superconductor from the field [139].

Eddy current losses are simply associated with the inductive heating occuring in a normal conductor when it is exposed to a varying magnetic field. They can be reduced using a highly resistive matrix material, in which the filaments of the wire are typically embedded. The higher the matrix resistivity the faster the eddy currents decay. On the other hand, the dynamic stability of the wire increases with decreasing matrix resistivity [138, p. 136]. In essence, this means that the wire is less vulnerable in the occurence of a local transition to normal-conducting state: the matrix is supposed to offer a low-resistive path for current in such a case, allowing the local normal-conducting zone in the superconductor to cool down. Hence, when choosing the matrix material, the designer has to compromise between low eddy current losses and high stability. Naturally, the magnitude of such losses also depends, for example, on the frequency and amplitude of the magnetic field, as predicted by Maxwell's equations.

Coupling losses occur in multifilamentary superconducting wires due to the mutual coupling of the filaments in magnetic field. In an uncoupled situation, the screening currents induced to shield the interior of the wire flow in both directions in each filament of the wire. However, as the filaments start to couple, currents will flow through the matrix from one filament to another. In the fully coupled situation, the screening current pattern looks similar as it would do in the case of a monofilamentary wire. Hence, coupling increases AC losses by two means: firstly, the currents flowing in the normal-conducting matrix material from filament to another generate heat. Secondly, the advan-

tages of the multifilamentary structure in terms of hysteresis losses are lost in the coupled situation. Coupling can, however, be reduced by twisting the filaments of the wire: for a twisted filament the induced electric field reverses its polarity every half twist pitch and the current loops created by the screening currents are reduced in length to the order of the twist pitch. The effect of twisting on coupling is demonstrated in figure 2.8. Note, however, that twisting is not an effective way to reduce losses in self-field [139]. Another obvious way to decrease the coupling between filaments is to increase the transversal resistivity of the matrix. This can be done, for example, by surrounding the superconducting filaments by highly resistive barriers. These barriers can be made of such materials as nickel or manganese [139].

Finally, in figure 2.9 a so called 3-component niobium-titanium (NbTi) wire is presented. The name stems from the wire structure: it has the superconducting component, the barrier component and the matrix component. It has been especially designed for AC use, consisting of three different materials: niobium-titanium as the superconductor, copper as matrix and copper-nickel barriers between filament bundles to reduce coupling. Note also the large number of small filaments for achieving low hysteresis losses.

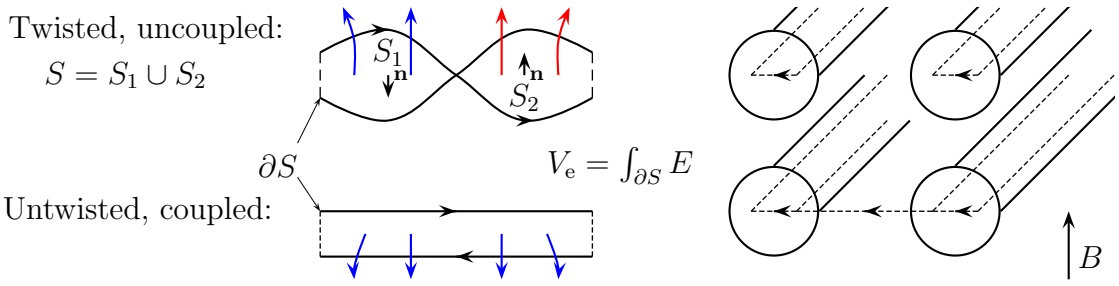

Figure 2.8: On the left: An electromotive force V_e is induced due to varying magnetic flux density B through the surface S. In the twisted situation, the coupling currents are restricted to the smaller loops S_1 and S_2. The normal vectors $\mathbf{n}$ define the orientations of S_1 and S_2. On the right: Screening currents in a two-filament conductor experiencing a varying magnetic flux density B. In the uncoupled situation the screening currents flow in both directions in both filaments whereas when the filaments are coupled, screening currents flow through the matrix metal from one filament to another.

Hysteresis loss is often the most dominant component of the AC loss [138, p. 197]. Hence, in this thesis, we will mainly be dealing with the mathematical modelling of hysteresis losses. However, the formulations of ECM we will present in the scope of this book are also suitable for evaluating the losses in normal-conducting materials.

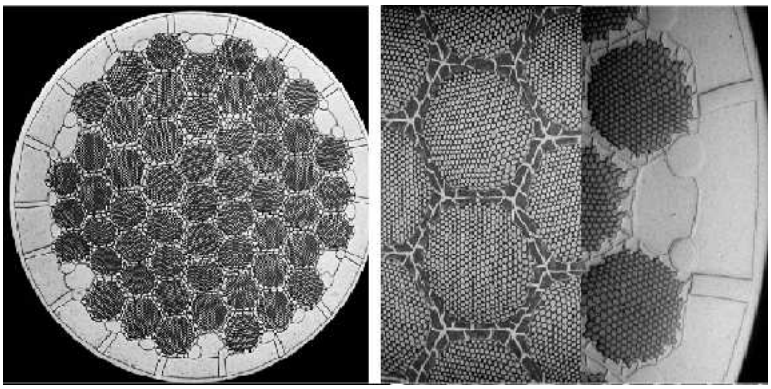

Figure 2.9: A 3-component wire designed for AC use. A large number of small filaments reduces hysteresis losses and copper-nickel barriers between filaments reduce coupling in external magnetic field. [139]

2.4 The framework for scientific research in the field of mesh method based modelling of AC losses in superconductors

As the title of this thesis suggests, we are trying to search for and push the frontiers in the field of superconductor modelling. More precisely, our field of interest in this thesis is the *mesh method based modelling of AC losses in superconductors* (MMMACL). It is not reasonable to assume that the frontiers are found by starting the research from scratch. As in any established field, there is a natural framework constructed by earlier research performed in the field. This kind of a framework is crucial as it answers the question 'Where can the frontiers in our field of science be found?': the research in the field is not completely unstructured. But of course, having a clear framework does not mean that research must not be creative and innovatively combine concepts in new ways. Here, we discuss this framework and present a classification of research in MMMACL. Furthermore, we discuss the publications included in this thesis in terms of this classification. A review of contemporary research in MMMACL in the context of the presented framework can be found in **Publication 4**.

One can view MMMACL to be comprised of seven different, but in many ways equally important research directions: *theory development*, *model development*, *formulation development*, *method development*, *tool development*, research on the *possibilities of existing tools* and analyses of *particular cases*. Research in the directions of theory and model development has not been as

active as in the other directions, which is understandable as working on such subjects is fundamental research and it may take years to get any results, let alone the results to have any actual impact. However, there certainly are issues to be scrutinized in these directions as well, such as the problematics of the superconductor E-J-relation in 3D [9, 30], and in general, as we discuss in **Publication 2** and **Publication 5**. Formulation development, on the other hand, has been rather vivid. Different formulations of ECM [23, 56, 122, 123] as well as CSM [26, 93, 95, 102, 111, 119] have been investigated extensively. However, it is still currently unclear, which formulations of the models are the most suitable for superconductor modelling, especially in 3D. So research on existing formulations as well as on completely new ones is of continuous interest in the community.

In method development, one considers the solution methods for the problems arising from the formulations. Naturally, such research can be mathematically very involved, but on the other hand, tailoring methods for specific problems can be very beneficial. Such research is not very common in MMMACL, but recently interest for mesh methods with an eye for superconductor AC loss modelling has arised [115, 135]. The fully space-time adaptive finite element method of [135] is of particular interest because of its potential in computational speed. In tool development, one develops simulation tools, which are just combinations of formulations and solution methods. This, of course, includes development of completely new tools [124], as well as enhancement of existing ones [121]. Finally, the two research directions that are left, investigation of the possibilities of the simulation tools and using the tools in analyses of particular cases can sometimes be cumbersome and even unnessecary to distinct from each other: possibilities of the tools are often best investigated through particular examples. Nonetheless, these two directions are the ones in which most of the research articles in our field are currently published [1, 2, 48, 57, 73, 86, 92, 94, 140]. Such research is extremely important, but on some other fields, most of the particular case analyses would be left for the industry. This, however, is not the case in MMMACL, due to the fact that commercial applications of superconductors are still so few.

Of course, it is not reasonable to think that every publication could be associated with exactly one of these research directions. It is often the case, that a publication can easily be viewed to belong to many of them. However, it seems that most of the research can be identified to belong to at least one of the directions. Naturally, the research presented in this thesis sits in the context of this framework as well. In figure 2.10, the research directions and the publications of this thesis have been located between different steps on the path from theory to simulations of applications. **Publication 1** and **Publication 6**

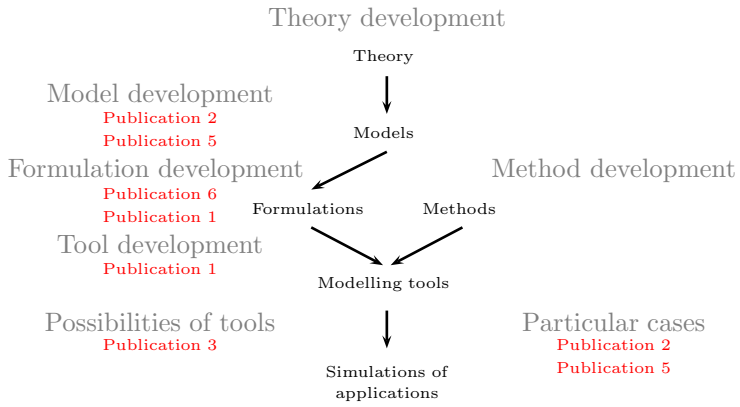

Figure 2.10: The framework for research in MMMACL. The different research directions are located as natural steps on the path from theory to applications. Furthermore, the publications of this thesis have been placed below the research directions to which they contribute the most.

fall naturally into the research direction of formulation development, whereas **Publication 2** and **Publication 5**, while being presented as particular case analyses on one hand, discuss observations suggesting that there still exists a need in the direction of model development, too, on the other. **Publication 3** presents new possibilites for creative use of an existing and already established hysteresis loss modelling tool, while also hinting that tool development is still called for to fully benefit from the speed advantage of 2D simulations compared to 3D ones.

This classification gives a framework for the research presented in this thesis. It also concludes our background chapter: in the following chapters, we turn our attention to the search for frontiers within this framework.

Chapter 3

Searching for frontiers: a simulation tool and formulations

One of the most concrete results of the research presented in this thesis has been the AC loss simulation code we have developed. Simultaneously, even though still a work-in-progress, it has provided a valuable tool for performing some of the research, as well. In a wider context, the code is to be integrated into our in-house superconductor stability analysis software, consisting of quench[1] and AC loss simulation modules, developed in the group of Electromagnetics at Tampere University of Technology using the C++ programming language. At this stage, the AC loss simulation code provides three different FEM formulations of ECM both in 2D and 3D: the H-formulation, the T-φ-formulation (with conducting air regions) and yet another H-oriented formulation, with non-conducting air regions, which makes use of so called cohomology basis functions to impose current constraints. Here, we shall call this formulation the T-φ-Ψ-formulation. An introduction to the concepts of homology and cohomology required for the T-φ-Ψ-formulation is presented in **Publication 6**. More rigorous definitions in connection with engineering applications may be found, for example, in [39, ch.13], [99]. The solvers have been implemented as a compact part of Gmsh[2] [43] using its Riemannian manifold interface [100]. The SUNDIALS time-stepping package [126], which has already been demonstrated to be suitable for superconductor modelling [116], has been used for

[1] A superconducting magnet is said to quench, when part of the superconductor loses its superconducting state, which leads to heat generation, which in turn makes the normal-conducting part of the magnet expand further in a chain reaction -like manner.

[2] Gmsh is an open-source finite element mesh generator with pre- and post-processor facilities. Available online at `http://geuz.org/gmsh/`.

time-discretization of the problems.[3] In addition, in **Publication 1** an in-house FEM based AC loss simulation tool implemented in MATLAB [77] providing three different formulations of ECM in 2D was used for comparing the properties of different formulations.

In this chapter, we briefly present the two FEM formulations of ECM implemented in our in-house AC loss simulation code used in the research: the H-formulation and the T-φ-Ψ-formulation. The FEM discretization and the weak formulations of the A-v-J- and T-φ-formulations, compared with the H-formulation in **Publication 1**, are detailed in [122] and [123]. The weak formulations of the H-formulation and the T-φ-Ψ-formulation are discussed in **Publication 1** and **Publication 6**, respectively. We pay special attention to modelling decisions related to the air regions of the modelling domain based on the research presented in **Publication 1** and **Publication 6**. As is well-known, continuous and discrete symmetries can sometimes be utilized to obtain a dimensional reduction or reduce the size of the modelling domain [8, 105, 106]. This is also the case in many particular cases simulated in this chapter, but we do not focus on such issues here, as they are not relevant for the research presented in thesis.

3.1 The H-formulation

Currently, the H-formulation is probably the most widely used formulation among the AC loss modelling community [23, 44, 56, 146]. This is especially due to the commercial FEM software Comsol Multiphysics [31], that has enabled the researchers and engineers to easily implement such a formulation by providing, for example, Whitney 1-forms for its FEM discretization and time-stepping algorithms for solving stiff DAE systems. Further advantages, to which lot of the appeal of the formulation is based on, include the intuitivity of setting the driving quantities of the problem through constraints, and the lack of responsibility related to gauging, as the problem is formulated directly using H. Even though the formulation has its drawbacks, so far the positive sides have outshadowed the negative ones, and the popularity of the formulation has grown rapidly.

[3] In particular we use IDA, which is a time-integrator suitable for stiff DAE systems provided by the SUNDIALS package. It is based on variable order and variable coefficient backwards differentiation formulae, the application of which results in a non-linear algebraic equation system to be solved at each time-step. This non-linear system is solved using Newton iteration, for which we use a preconditioned Krylov subspace method. [55]

3.1.1 The formulation

In the H-formulation, one combines Maxwell's equations and constitutive laws (2.8), (2.12), (2.22) and (2.23) to yield a single equation in terms of H:

$$\partial_t \mu_\star H + \mathrm{d}(\rho_\star \mathrm{d}H) = 0. \tag{3.1}$$

This is the strong form of the PDE, from which H is solved. Typically, one ignores the possible numerical instabilities related to satisfying the Gauss's law (2.10) in long simulations, and trusts that it is satisfied automatically, as long as the initial condition is consistent with it. To force net currents I_i through the superconducting surfaces S_i, one imposes the algebraic constraints

$$\int_{\partial S_i} H = I_i. \tag{3.2}$$

To set external applied fields as well, one can simply fix H on the boundary of the modelling domain to equal the desired ${\mu_\star}^{-1} B_{\mathrm{ext}}$.

After forming the corresponding weak formulation of (3.1) and (3.2), one approximates H in the finite element mesh introduced to the modelling domain Ω as a sum of Whitney 1-forms

$$H \approx \sum_{i \in E(\Omega)} h_i w_i, \tag{3.3}$$

where $h_i \in \mathbb{R}$ are the degrees of freedom of the problem and $E(\Omega)$ is the set of edges in the mesh. Plugging the approximation into the weak formulation and using Galerkin's weighting, one obtains the DAE system consisting of a finite number of equations to be solved.

3.1.2 Discussion

As one might guess by observing (3.1), the resistivity $\rho_\star$ needs to be defined in all of Ω in the H-formulation. Thus, the regions that would be normally considered non-conducting, such as air regions, must be modelled as conducting regions with very high resistivity. This means, that there is a possibility for currents to flow in the "non-conducting" regions, too! This property of the formulation is especially prominent, when simulating situations, which require setting up both an applied magnetic field and a net current. When one fixes H on the boundary of the domain to apply the external field, one implicitely forces a net current constraint for the whole modelling domain, and this might not

be the same as the current constraint given for the conductors of the domain. Hence, as Ampère's law still needs to be satisfied, one actually forces a net current into the air region to balance out the contradictory current constraints. This is demonstrated in figure 3.1.

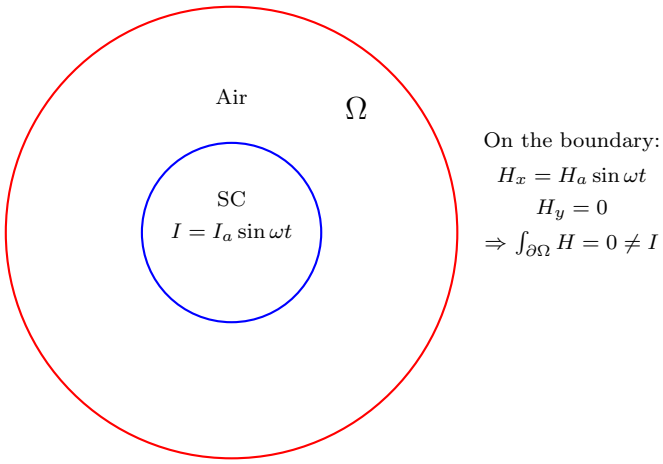

Figure 3.1: The outer boundary represents the boundary of the modelling domain Ω and the inner boundary represents the boundary of the superconducting (SC) region. The boundary conditions used for setting up the applied field and the net current constraints for the conductor do not match from Ampère's law's point of view.

In terms of the field solution, large currents in regions where there should be no currents at all sounds a little bit scary: this means there can be a huge Ohmic loss in the air region. However, according to the results in **Publication 1**, the resistivity chosen for the air regions affects the loss behaviour of the superconducting subdomains surprisingly little. There, a standard AC-AC situation, with an alternating applied field and an alternating current both present, was simulated using the H-formulation using different values of resistivity for the air region: lowering the air resistivity from 1 Ωm to 10^{-8} Ωm did not notably affect the losses in the superconductors. The modeller is free to choose the resistivity of the air regions from a large scale of values to best suit, for example, the numerical performance of the simulation code. Still, it is reasonable to pay extra attention to the results of such simulations, as the behaviour observed in them is clearly unphysical.

3.2 An H-oriented formulation with cohomology basis functions: the T-φ-Ψ-formulation

The H-formulation suffers from unphysical currents in the regions that should be practically non-conducting. As there are currents in all of Ω, $\mathrm{d}H = 0$ nowhere, which implies that we cannot even locally express H using solely a scalar potential function φ, so that $H = \mathrm{d}\varphi$. In the H-formulation, H is discretized using Whitney 1-forms in all of Ω, but a scalar potential could be discretized using Whitney 0-forms. As there typically are notably more edges than nodes in a finite element mesh, the scalar potential representation of H would yield an advantage in terms of the number of degrees of freedom.

In traditional T-φ-formulations, where T is the current vector potential for which $J = \mathrm{d}T$, air regions are usually considered as truly non-conducting [15]. As H is decomposed into $H = T - \mathrm{d}\varphi$, if there are no net currents flowing in the conductors of Ω, it is indeed possible to express H in the non-conducting part of Ω as $H = \mathrm{d}\varphi$ and T is needed only in the conducting regions. However, if the conductors do carry net currents, de Rham's theorem tells us that they need to be accounted for in the representation of H in the non-conducting parts of Ω, too [39, pp. 356-357]. The traditional way to do this is to introduce cuts into Ω to make φ discontinuous [67]. However, this makes the scalar potential multi-valued, and it might be cumbersome to define cuts for certain topologies.

There does, however, exist a technique for expressing H in the non-conducting regions without breaking the continuity of φ. By exploiting the cohomology of the modelling domain Ω, the missing part of H can be constructed efficiently [53, 63, 99]. The edge-based cohomology basis functions, often called *thick cuts*, which are introduced as a part of the decomposition of the discretized H, provide a tool for this. The function space from which H will be sought in the non-conducting regions will then be spanned by Whitney 0-forms and the edge-based cohomology basis, which tends to have a relatively small support. Thus, the number of degrees of freedom is significantly reduced from the typical H-formulation, and φ becomes single-valued. Net current constraints for the conducting parts of Ω can be set simply by fixing the degrees of freedom related to the cohomology basis, leading to a simple ordinary differential equation system to be solved. Even though such an approach is known to the electromagnetic modelling community, according to our best knowledge, it has not been used for simulating superconductor hysteresis losses before.

In the following, we shall briefly discuss this formulation. Especially the decomposition and discretization of H is discussed.

3.2.1 Briefly about edge-based cohomology basis functions

In essence, homology and cohomology are related to holes in manifolds. Homology captures the quantity and quality of holes in the manifold: how many tunnels and how many voids it has, whereas cohomology assigns scalar values to the voids and tunnels of the manifold. That is, cohomology space consists of linear mappings from the homology space to real numbers.

The conducting subdomains Ω_c of Ω can be considered as holes in the non-conducting subdomain Ω_nc. That is, Ω_nc has non-trivial homology. Following the path of the traditional T-φ-formulation, we would like to express H as a sum of T and φ in Ω_c. In Ω_nc, we have $\mathrm{d}H = 0$, and we would like to have a scalar potential representation for H. Unfortunately, de Rham's theorem tells us that

$$(\mathrm{d}H = 0 \Rightarrow H = \mathrm{d}\varphi) \Leftrightarrow \int_z H = 0, \quad \forall z \in H_1(\Omega_\mathrm{nc}), \tag{3.4}$$

where $H_1(\Omega_\mathrm{nc})$ denotes the 1-homology space of Ω_nc, which includes all the loops around the tunnels in Ω_nc. That is, we cannot express H in the non-conducting regions solely using scalar potential when a net current flows in the tunnels of Ω_nc: in such a case, H is closed but not exact in Ω_nc. In FEM setting, the missing part of H in the non-conducting regions can be expressed using the edge-based cohomology basis functions [64]. The edge-based cohomology basis functions are expressed as a sum of a set of Whitney 1-forms in the mesh. The supports of the basis functions are in some way similar to traditional cuts, but they have a finite thickness of one layer of mesh elements: their supports are small in comparison with the total number of edges in the finite element mesh. Such cohomology basis functions can be generated using the (co)homology solver of Gmsh [99], which we have used in our implementation of the formulation. For a given mesh, the basis computation needs to be done only once, which makes the computation time negligible in comparison to the total solution time of a time-dependent AC loss modelling problem. A demonstration of a cohomology basis function can be seen in figure 3.2.

3.2.2 The formulation

Basically, we are solving for exactly the same PDE as in the H-formulation, but here, we add also Gauss's law to our PDE system:

$$\partial_t \mu_\star H + \mathrm{d}E = 0, \tag{3.5}$$

$$\mathrm{d}\mu_\star H = 0. \tag{3.6}$$

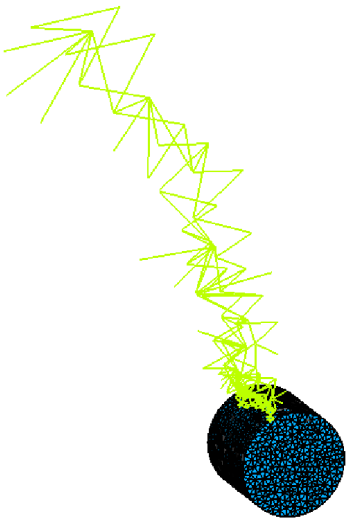

Figure 3.2: A conducting cylinder can be seen as a tunnel in the non-conducting region. Here, the mesh in the conductor and those edges of the mesh outside the conductor, which constitute the cohomology basis function are depicted. In a k-dimensional mesh, the edges take up a finite thickness of one layer of k-simplices.

In addition, we have again some current constraints

$$\int_{\Gamma_i} H = I_i, \tag{3.7}$$

where Γ_i are boundaries of surfaces that each enclose one conductor S_i, through which a current is forced. As there are no currents in Ω_{nc}, we also have the constraint

$$\mathrm{d}H = 0 \tag{3.8}$$

there.

After forming the corresponding weak formulations of (3.5) and the time-derivative of (3.6), we must find the appropriate approximation of H in the finite element mesh. This can be written as

$$H \approx \sum_{i \in N(\Omega)} \varphi_i \mathrm{d}\lambda_i + \sum_{i \in E(\Omega_{\mathrm{c}})} t_i w_i + \sum_{i \in VT(\Omega_{\mathrm{nc}})} I_i \Psi_i, \tag{3.9}$$

where $N(\Omega)$ denotes the set of nodes in the mesh, $E(\Omega_{\mathrm{c}})$ denotes the set of edges in the mesh in Ω_{c}, $VT(\Omega_{\mathrm{nc}})$ is the set of tunnels in Ω_{nc} transporting a net current, $\varphi_i \in \mathbb{R}$, $t_i \in \mathbb{R}$, Ψ_i are the representations of the cohomology basis, and $I_i \in \mathbb{R}$ are the degrees of freedom related to them. Substituting

(3.9) into the weak formulations and using Galerkin's weighting, one obtains the ordinary differential equation, from which an approximative solution for H can be found. In terms of the traditional T-φ-formulation, one can think that the first part of the summation represents $\mathrm{d}\varphi$, the second part T and the third part is the part of H arising from the non-trivial homology of the modelling domain. To select the gauge, we zero φ_i from Ω_c up to $\partial\Omega_\mathrm{c}$ and in one arbitrary node in Ω_nc, instead of, for example, employing a tree-co-tree decomposition of the mesh, which is another popular way to do this [122]. On $\partial\Omega_\mathrm{c}$, the tangential continuity of H is ensured by setting $t_i w_i = I_i \Psi_i$ on all the edges $i \in \partial\Omega_\mathrm{c}$, as the support of Ψ_i is restricted to Ω_nc.

Generally, the selection of the (co)homology space does require some involvement from the modeller, but by a wise decision I_i are exactly the net currents flowing in the tunnels through Ω_nc. We would like the representation of the homology basis to be such that each representative loops exactly once around exactly one tunnel. Having obtained such a basis, we can adjust the cohomology basis accordingly and have a clear interpretation for the corresponding coefficients I_i as the net currents through the tunnels. Hence, we can constrain the net currents as we wish by fixing the coefficients I_i equal to the desired current: no algebraic constraints are needed, like typically in the H-formulation. Fortunately, the Gmsh (co)homology solver allows the user to adjust the basis representation as he/she wishes [99]. Hence, in our implementation, we can always obtain a basis representation, for which we have a clear interpretation. For driving the applied magnetic field B_ext, one can set up a Neumann-type boundary condition on $\partial\Omega$ to drive magnetic flux through the boundary of the domain [72].

3.3 Comparing the formulations in simulation cases

As suggested in the previous section, the T-φ-Ψ-formulation does have certain advantages over the traditional H-formulation. To demonstrate this, we investigate and compare the performance and simulation results of the two formulations in a few example cases. For all the simulations we used $n = 25$ in the power law E-J-relation for the superconductor, and for each pair of simulations, we used exactly the same numerical parameters for the time-stepping algorithm, to ensure a fair comparison. Furthermore, we used $\mu = \mu_0$ everywhere, μ_0 being the vacuum permeability. All the simulations were perfomed on the author's laptop computer utilizing a single processor core. The resistivity of the air regions in the simulations employing the traditional H-formulation was $\rho_\mathrm{air} = 0.1\ \Omega\mathrm{m}$. Each case was solved in time for 0.75 cycles of the AC

quantity for obtaining the steady-state hysteresis loss: losses were integrated from 0.25 to 0.75 cycles and multiplied by two to yield the loss per cycle [123]. When deciding the suitable mesh density to ensure convergence, we relied on experience, part of which was gained in the documented convergence studies of **Publication 1**

3.3.1 2D simulations

Our first simulation case is a 2D simulation of a superconductor with two filaments embedded inside a normal-conducting matrix. The filaments are round with radius $r_{\mathrm{sc}} = 0.178412$ mm. The matrix is also round, with a radius of $r_{\mathrm{m}} = 0.56419$ mm, which gives a 1 mm^2 total cross-sectional area for the wire. $J_{\mathrm{c}} = 500$ A/mm^2 yielding an I_{c} of 100 A for the total superconducting area of 0.2 mm^2. The resistivity of the matrix is $\rho_{\mathrm{m}} = 10^{-8}$ Ωm. We set $B_{\mathrm{ext}} = 0$, that is, no flux exits or enters Ω, which means that we have no applied field. For the T-φ-Ψ-formulation, we compute the cohomology basis of Ω_{nc}, which sees the matrix and the filaments inside them as a single tunnel. Then, we fix the real number coefficient of the cohomology basis function to $I = 0.8 I_{\mathrm{c}} \sin(2\pi f t)$, where $f = 50$ Hz. In the H-formulation, we fix the algebraic constraint for current accordingly. This is the **case 1**.

The second simulation case in 2D is a system of four round superconductors, each of them carrying their own sinusoidal net currents with an amplitude of $0.8 I_{\mathrm{c}}$ at $f = 50$ Hz. The cross-sectional area of each conductor is 0.1 mm^2 and $I_{\mathrm{c}} = 100$ A. This gives a critical current density $J_{\mathrm{c}} = 1000$ A/mm^2 for each wire. First, we have $B_{\mathrm{ext}} = 0$ and in the T-φ-Ψ-formulation we fix the coefficients of the cohomology basis functions equal to the desired net currents of the corresponding superconductors. In the H-formulation, we fix the algebraic current constraints accordingly. This is the **case 2**. Furthermore, we simulate the same situation but with $B_{\mathrm{ext}} = 0.1 \sin(2\pi f t)$ T, set through non-homogeneous Neumann type boundary condition (T-φ-Ψ) or a boundary condition of Dirichet type (H). This is the **case 3**.

The results of the simulations are listed in table 3.1. The most striking fact about the results is the clear advantage in the number of degrees of freedom as well as in the running times of the simulations for the T-φ-Ψ-formulation. The computed AC losses, however, are very accurately the same for all the cases. The speed advantage of the T-φ-Ψ-formulation is most prominently shown in **case 3**, which is the most difficult one for the time-integrator. In that case, the computation time was reduced by almost 50 %. the reason behind this requires further investigation. Looking at figure 3.3, in which the

Table 3.1: The results of the 2D simulations for **case 1**, **case 2** and **case 3**. For **case 1** the mesh consisted of 2494 triangular elements and for **case 2** and **case 3**, it consisted of 3274 triangular elements. The decrease in the number of degrees of freedom (DOFs) and CPU time are also listed in the table.

		T-φ-Ψ	H	Decrease
case 1	DOFs	3194	3756	15 %
	CPU time [s]	211	283	25 %
	AC loss [mJ/m/cycle]	4.821	4.823	
case 2	DOFs	3237	4925	34 %
	CPU time [s]	364	411	11 %
	AC loss [mJ/m/cycle]	6.662	6.608	
case 3	DOFs	3237	4925	34 %
	CPU time [s]	553	1092	49 %
	AC loss [mJ/m/cycle]	14.368	14.428	

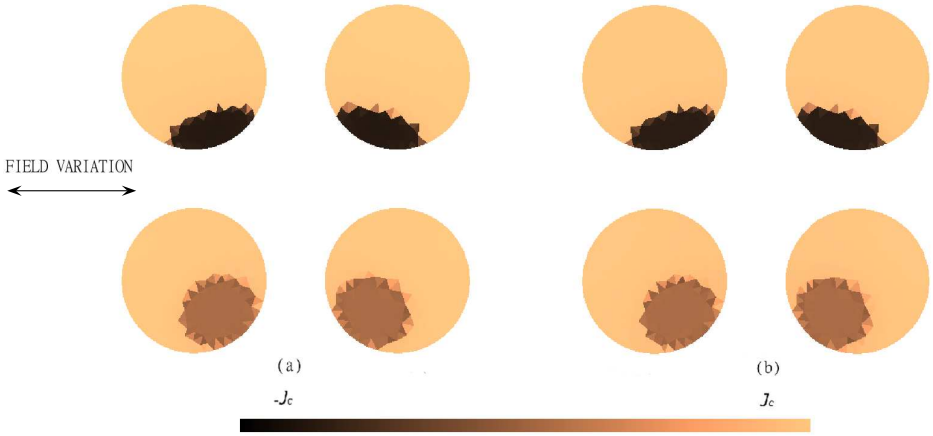

Figure 3.3: The current density profiles for **case 3** at the peak of the in-phase sinusoidal net current and applied field obtained using (a) the T-φ-Ψ-formulation and (b) the H-formulation. The direction of the field variation is indicated in the figure.

current density profiles at the peaks of the current and external field are shown for **case 3**, ensures us that the solutions obtained from both formulations are practically the same.

3.3.2 3D simulations

In 3D simulations, it can be especially advantageous to get rid of the excessive degrees of freedom exhibited by the H-formulation in the air regions. To compare the H-formulation and the T-φ-Ψ-formulation in 3D, we simulated the AC losses of a round superconducting cylinder with transverse cross-sectional area of 1 mm^2. The cylinder carries a sinusoidal current with a peak value of $0.5I_\mathrm{c}$, and $I_\mathrm{c} = 1000$ A, giving a constant $J_\mathrm{c} = 1000$ A/mm^2. This is the **case 4**. The cohomology basis function used in the T-φ-Ψ-formulation was a sum of the edge elements attached to the edges depicted earlier in figure 3.2. For this case, we also compare the computed AC losses with the CSM based analytical formula for an ellpitical wire by Norris, written as

$$Q = \frac{I_\mathrm{c}^2 \mu_0}{\pi} \left[(1 - i_\mathrm{m}) \ln(1 - i_\mathrm{m}) + \frac{(2 - i_\mathrm{m}) i_\mathrm{m}}{2} \right], \tag{3.10}$$

where I_c is the critical current of the wire and i_m denotes the ratio $I_\mathrm{a}/I_\mathrm{c}$, where I_a is the amplitude of the alternating current [88].

The results are listed in table 3.2. For this mesh, the number of degrees of freedom drops considerably (by 43 %) from the H-formulation to the T-φ-Ψ-formulation. The speed advantage for the T-φ-Ψ-formulation is also prominent (decrease of computation time by 23 %). The AC losses obtained using the formulations are almost equal. Furthermore, the loss predicted using the Norris formula (3.10) is close to the losses obtained from the numerical simulations. Even though we used the Norris formula for benchmarking, the numerical computations should not give the same result necessarily even at the limit of mesh with infinite amount of elements, as they are based on ECM whereas Norris formula is based on CSM. However, around 50 Hz they should result into losses very close to each other, which makes the Norris formula eligible for benchmarking.

Table 3.2: The results of the simulations for the round cylinder in 3D (**case 4**). The mesh consisted of 19431 tetrahedral elements.

		T-φ-Ψ	H	Decrease	Norris formula
case 4	DOFs	14211	24778	43 %	
	CPU time [s]	2191	2840	23 %	
	AC loss [mJ/m/cycle]	10.772	10.804		11.370

3.3.3 Concluding remarks

The H-oriented T-φ-ψ-formulation leads to a smaller number of degrees of freedom and up to 50 % faster running times of the simulations than the traditional H-formulation, while keeping equal prediction accuracy. In the T-φ-ψ-formulation the air regions of the modelling domain are considered as truly non-conducting, whereas in the H-formulation, resistivity is finite everywhere. This leads to currents also in the air regions in the H-formulation, while no such currents are possible in the T-φ-Ψ-formulation. The latter formulation also provides a natural way to constrain the net currents of the conductors by fixing the degrees of freedom related to the edge-based cohomology basis functions constituting a part of the approximation of H.

Chapter 4

At the frontier: AC losses in DC biased superconductors

A characteristic feature of contemporary superconductor modelling is that mesoscopic scale models, justified by macroscopic observations, are applied, often with great success. Often even the validity of the mesoscopic model in question is justified by arguments of microscopic or macroscopic scale nature. However, such arguments are, of course, based only on intuition: they merely suggest that such a model *could* be eligible, and hence, should be tested against measurements. It is difficult or even impossible make direct observations on the mesoscopic or microscopic scale, so in that sense, a macroscopic observation is all we have to judge whether the model is eligible or not, at least in the context of power engineering applications. We should constantly remind ourselves that the models we use do not say anything about nature as it is: they are just imaginary descriptions of reality that yield better predictions in some situations than others. Still, as time passes, the models do sometimes become reality in everyday language: it is hard to bear in mind that they are merely models, not the fundamental truth. In the case of hysteresis loss modelling, this has in some sense happened with ECM. The slanted voltage-current curves obtained from measurements [25], as well as the observed decay of magnetic moment in high-temperature superconductors [85], which is manifested as flux creep [4] in microscopic models, speak for the validity of the power law based ECM. On the other hand, also CSM seems to be an eligible model for AC loss simulations in many situations, and the ECM based simulation tools are often even benchmarked against solutions of CSM. This all can be very confusing. To get to the bottom of the issue, we must scrutinize the models we are using.

In this chapter, we discuss the predictions of ECM and CSM based AC

loss simulation tools in the context of DC biased superconductors. Such a concept is important in terms of application design, for superconductors in such applications as motors or generators with superconducting windings or some superconducting power transmission cables experience AC fields (alternating magnetic fields) and a DC bias: different combinations of transport DC, DC field (non-alternating magnetic field) and AC field are possible. It is thus important to be able to reliably predict the heat generation in such situations, as AC losses are often a restricting factor for superconducting applications. However, analyzing such situations can provide deeper insights to modelling as well: we claim, that neither CSM or ECM are truly intrinsic properties of superconducting wires, but they both reflect different properties of superconductors.

The research presented in this chapter is detailed in **Publication 2** and **Publication 5**, the former of which discusses merely the predictions of ECM for DC biased superconductors and mainly provides an introduction to this theme. The latter presents a more thorough comparison of the use of ECM and CSM in such cases, as well as some enlightening measurement results. In the following, we shall present a rationale for such research and show the similarities and discrepancies of the predictions obtained using the two models. Furthermore, measurement results based on **Publication 5** will be compared with simulations. The measurement methods we have used are presented in more detail in **Publication 5**. Our simulation tools based on ECM and CSM employ the H-formulation and minimum magnetic energy variation (MMEV), respectively. The latter one is a formulation of nature's minimum energy principle, which, coupled with CSM, results in a reliable and well-documented approach for modelling hysteresis losses in superconductors [93, 96, 102, 111, 119]. The details of the AC loss computations are also presented in **Publication 5**.

4.1 The considered coated conductor tapes

We analyze the predictions of the models for HTS coated conductor tapes. Through 2D simulations, we analyze two tapes: a coated conductor tape with a superconducting layer of 4 mm $\times$ 1 μm and a constant $I_c = 100$ A (tape 1), and a real YBCO tape sample with cross-sectional dimensions 4 mm $\times$ 90 μm with a superconducting layer of approximately 4 mm $\times$ 1.4 μm (tape 2) [127]. In ECM, we have used $n = 40$ for tape 1 unless otherwise mentioned. Measurement results for tape 2 are compared with the simulations. All the measurements were performed in liquid nitrogen at the temperature of 77 K. In all the simulations involving tape 2, we have used the experimentally obtained

B-dependence of J_c, and those simulations that are based on ECM take also into account the B-dependence of n [97]. In all the simulations, we checked that the field variation penetrates several mesh elements even at the lowest applied AC fields. Furthermore, the meshes were dense enough in the sense that increasing the mesh density did not appreciably alter the results anymore. For the AC loss simulations employing ECM, we had two to three triangular mesh elements over the thickness of the tape and 1000 or 2000 elements altogether in the superconducting region. For the CSM based tool, we had 500, 1000 or 8000 rectangular elements in the superconductor.

First, we discuss how the prediction of ECM differs from the measured behaviour in terms of current penetration, when a direct current is injected into tape 2. We also point out the frequency-dependence of hysteresis losses predicted by ECM in tape 1 and discuss how it is related to the observations made in the current penetration measurement. Finally, we compare the predictions of the models for tape 1, as well as measurements and simulations for tape 2, in situations involving an AC magnetic field and a DC bias. The simulated tapes are summarized in table 4.1.

Table 4.1: Summary of the coated conductor tapes used in the simulations. The height and width are for the transverse cross-sections of the superconducting layers.

	tape 1	tape 2
I_c	100 A	Experimental $J_c(B)$
n	40	Experimental $n(B)$
Height	1 μm	1.4 μm
Width	4 mm	4 mm

4.2 Current penetration into a coated conductor tape: simulation versus measurement

We measured, and simulated using ECM, the current penetration and the time-evolution of current density distribution in tape 2. A current of 70 A was injected into the tape. The tape has self-field I_c of 128 A.[1] The current was ramped up in 40 s and kept constant afterwards. The component of the magnetic field perpendicular to the tape width was measured using the Hall-probe mapping technique right above the sample and the current penetration

[1]Here, self-field I_c means the measured critical current of the tape in zero external field, with $E_c = 10^{-4}$ V/m.

pattern was obtained by an inversion procedure. Further details about the measurement technique can be found in [76, 118].

The measured and simulated current penetration patterns at different instants of time are depicted in figure 4.1. We observe, that in the measurement, the current density profile remains almost exactly the same from 110 s to 1111 s. However, the simulation result obtained using ECM shows substantial homogenization of the current density profile already during the time interval from 110 s to 360 s: the relaxation of the local current density is exaggerated at the peaks of the distribution in the simulation result. Of course, using CSM, no such homogenization would happen at all.

Why does ECM then over-estimate the homogenization? Models of Maxwell's theory predict that the current density in the conductor distributes in a way that produces the minimal amount of heat. If the resistivity is non-zero, the minimal heat generation is achieved when the current density is distributed uniformly over the cross-section of the conductor. In the power law E-J-relation of ECM, whenever J deviates from zero, so does E, meaning that the local resistivity is non-zero, whenever the local $J \neq 0$: there is loss associated to any non-zero J. This leads to continuous redistribution of the current density as long as the distribution is not completely uniform. Naturally, this can be

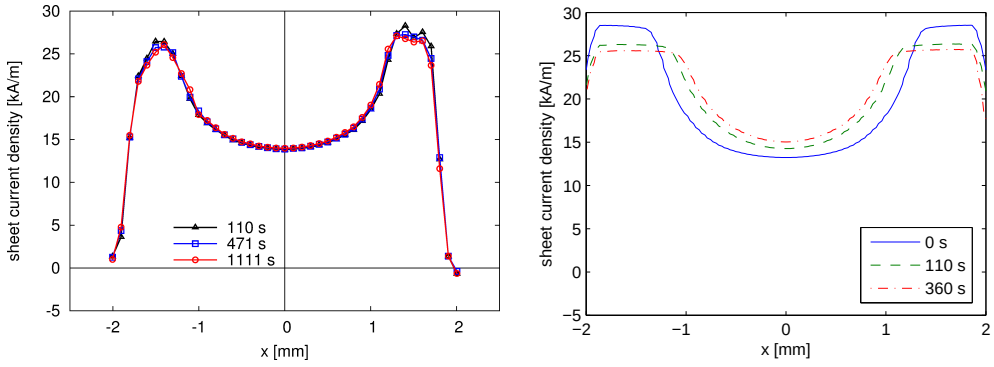

(a) (b)

Figure 4.1: The sheet current density obtained from (a) measurement and (b) ECM based simulation. The x-axis is in the direction parallel to the tape width. The superconducting tape is located roughly from -2 mm to 2 mm on the x-axis. The legend indicates (a) the time at which the field scan reaches the superconductor edge and (b) the time which the simulation has reached. The time $t = 0$ is defined as the moment at which the current ramp reached its target value 70 A. In the simulation, we used the J_c-B and n-B dependences extracted from measurements for the tape.

thought of as a mesoscopic manifestation of flux creep, but as we observe, the associated current density relaxation is vastly over-estimated when ECM used. *The power law E-J-relation does not describe this property of the superconductor in a way that would match our observations.* This exaggeration manifests as discrepancies in AC loss predictions between ECM and CSM, especially in DC biased superconductors, as we shall show in the upcoming sections.

4.3 Frequency-dependence of AC loss predictions of ECM

The smooth E-J-relation of ECM does not only cause losses and homogenization of the current density distribution at DC, but also leads to frequency-dependence of hysteresis losses. Since we observed that ECM actually over-estimates the rate of the homogenization, one could suspect, that also the losses are over-estimated in DC or low-frequency use. The frequency-dependence of hysteresis losses in HTS conductors has been experimentally studied in the past with different conclusions [28, 35, 54, 101, 129, 130, 133]. In particular, there exist data suggesting that the hysteresis losses are rather independent of frequency, especially for alternating currents substantially below I_c [28, 54]. The frequency-dependence of the predictions of ECM has also been studied in many publications [3, 112, 129, 130]. In [143], it was noted that the power law based ECM does not necessarily reflect the frequency-dependent properties of HTS well enough, but a generalized critical state model was suggested instead. In such a model, a non-zero J is not necessarily associated to heat generation unless J is adequately close to J_c.

To investigate the frequency-dependence of the predictions, we performed simulations on tape 1 transporting a sinusoidal current of amplitude $0.5I_\mathrm{c}$ at different frequencies ranging from 0.1 Hz to 100 Hz. Two n-values, $n = 40$ and $n = 80$ were used in ECM. Furthermore, the losses obtained using ECM were compared to the analytical formula derived from CSM for a thin superconducting strip by Norris:

$$Q = \frac{\mu_0 {I_\mathrm{c}}^2}{\pi} \left[(1 + i_\mathrm{m}) \ln (1 + i_\mathrm{m}) + (1 - i_\mathrm{m}) \ln (1 - i_\mathrm{m}) - {i_\mathrm{m}}^2 \right], \tag{4.1}$$

where Q is the loss per cycle of AC [88]. The results are presented in figure 4.2.

As expected, the higher the n-value is, the smaller is the frequency-dependence. CSM, corresponding to infinite n, exhibits of course no frequency-dependence. For ECM, the losses tend to increase as the frequency is decreased. Qualita-

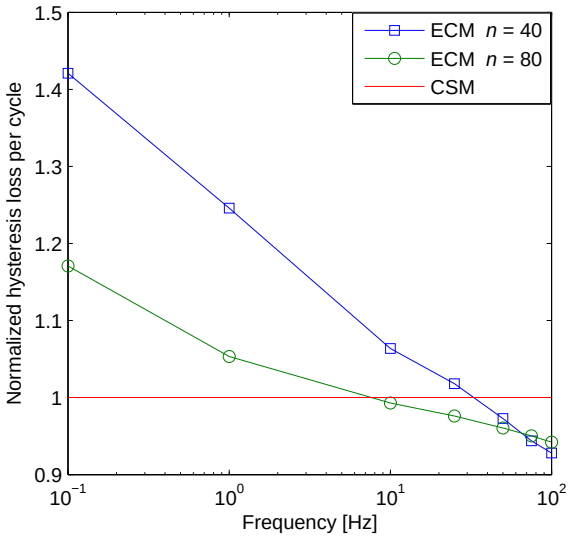

Figure 4.2: Hysteresis losses predicted by ECM for AC transport current of $0.5I_c = 50$ A with $n = 40$ and $n = 80$ for tape 1 as functions of frequency, normalized to the CSM based Norris loss obtained using (4.1), which is 46.50 μJ/m/cycle for this case.

tively, this kind of behaviour is suggested by experimental data, for example in [101, 129]. In the quantitative sense, however, even though the discrepancy is not extremely large, the frequency-dependence of this magnitude is an overstatement. At the typical frequencies of the power applications (around 50 Hz), it seems that CSM and ECM yield very similar predictions, which, in a sense, justifies the use of either one of them for such simulations. However, as the homogenization rate of the current density profile in DC use is over-estimated by ECM, so are the losses at low frequencies, too. ECM yields two loss components: the loss related to the stationary state, the stationary loss, and the loss related to time-varying magnetic field, the variation loss. The lower the frequency is, the larger is the relative contribution of the stationary loss over a cycle of AC field. Homogenization of the current density profile is associated to the fact that this stationary loss component tends to minimize over time.

4.4 Ripple field losses in a DC biased tape

A DC component in the current flowing through the superconductor or in the magnetic field it experiences is associated to over-estimated homogenization of

the current density profile in ECM based simulations. As this is furthermore associated to over-estimated heat generation in the superconductor, the question of validity of ECM based AC loss predictions in DC biased superconductors arises. In addition, one could ask whether CSM and ECM provide similar AC loss results in such cases, as both models have previously been used for such simulations [57, 94]. To investigate this, we have performed simulations using both models for tape 1 and tape 2. In the following, we first scrutinize the predictions of the models for tape 1, which has constant I_c, to better isolate the properties of the models themselves. Then, we compare similar simulations for tape 2 with AC loss measurements.

In our simulations of DC biased tapes in AC ripple fields, we can separate the contribution of *magnetization losses* Q_M and *transport losses* Q_T to the total AC loss per cycle Q [46]. The former is related to the magnetization of the superconductor and computed as the area of the magnetization loop, while the latter is associated to the transport current in the superconductor and it is the difference between the total loss and the magnetization loss. When a superconductor carries DC in AC magnetic field, voltage is produced over the superconducting sample, as long as the amplitude of the AC field is sufficient. Hence, there will be a transport loss associated to a flowing direct current even substantially below I_c. This phenomenon is called dynamic magneto-resistance. The threshold value of the AC field amplitude for dynamic magneto-resistance to occur in a thin superconducting strip may be evaluated as [81]

$$B^* = \frac{\mu_0 J_c d}{2\pi}\left[\frac{1}{i}\ln\frac{1+i}{1-i} + \ln\frac{1-i^2}{4i^2}\right], \tag{4.2}$$

where d is the thickness of the strip and and $i = I_{DC}/I_c$. I_{DC} denotes the value of the direct current.

4.4.1 Comparison of models: losses over a cycle of AC field

We have simulated AC losses in tape 1 using our ECM and CSM based modelling tools under different combinations of transport DC, DC field and AC field, for several amplitudes B_a of applied AC ripple field of the form $B_{ext} = B_a \sin(2\pi f t)$, where the frequency $f = 50$ Hz. The field variation was in the direction perpendicular to the tape width. In the simulations, the DC quantities were ramped up to their target values simultaneously in 5 ms, and the AC ripple field was applied on top of them, after they had remained constant for 15 ms. We integrated the problem in time for 10 cycles of the AC field and computed the AC losses over the tenth cycle. The results are presented in

table 4.2.

Large discrepancies between the predictions of the models for 1 mT AC field can be seen when a DC quantity, current or field, is involved. For the 5 mT AC fields and for the pure AC cases with 1 mT and 5 mT AC fields the models predict approximately equal losses. The contributions of the magnetization and transport losses were segregated only for CSM based simulations here. This is because the magnetization loops did not close for ECM even after 10 cycles if DC field was involved, especially in the 1 mT cases. The reason for this will become apparent in the next subsection, where we scrutinize the instantaneous power loss in these cases. Using CSM, the loops closed to a reasonable extent in all the simulations.

Table 4.2: The AC losses in tape 1 for different values of DC field, transport DC and AC field computed using the CSM and ECM. The AC field values denote their amplitudes B_a. To make the comparison more explicit, the losses obtained using ECM have been normalized to the losses obtained using CSM.

DC field [mT]	Transport DC [A]	AC field [mT]	Total loss (CSM) [J/m/cycle]	Total loss (ECM) / Total Loss (CSM)	Magnetization loss (CSM) [J/m/cycle]
0	0	1	7.013×10^{-8}	0.949	7.012×10^{-8}
		5	3.677×10^{-5}	0.922	3.677×10^{-5}
	50	1	7.036×10^{-8}	4.644	7.012×10^{-8}
		5	3.680×10^{-5}	0.972	3.677×10^{-5}
10	0	1	7.397×10^{-8}	10.930	7.012×10^{-8}
		5	3.690×10^{-5}	0.947	3.677×10^{-5}
	50	1	7.344×10^{-8}	35.849	7.019×10^{-8}
		5	3.704×10^{-5}	1.000	3.677×10^{-5}
20	0	1	7.601×10^{-8}	32.29	7.012×10^{-8}
		5	3.696×10^{-5}	0.979	3.677×10^{-5}
	50	1	7.662×10^{-8}	70.937	7.018×10^{-8}
		5	3.707×10^{-5}	1.094	3.677×10^{-5}
60	0	1	7.761×10^{-8}	42.935	7.012×10^{-8}
		5	3.700×10^{-5}	0.993	3.677×10^{-5}
	50	1	8.841×10^{-8}	79.387	7.019×10^{-8}
		5	3.712×10^{-5}	1.128	3.677×10^{-5}
80	0	1	7.763×10^{-8}	42.996	7.012×10^{-8}
		5	3.700×10^{-5}	0.993	3.677×10^{-5}
	50	1	8.951×10^{-8}	78.966	7.019×10^{-8}
		5	3.712×10^{-5}	1.128	3.677×10^{-5}
100	0	1	7.763×10^{-8}	43.002	7.012×10^{-8}
		5	3.700×10^{-5}	0.993	3.677×10^{-5}
	50	1	9.022×10^{-8}	78.590	7.019×10^{-8}
		5	3.712×10^{-5}	1.128	3.677×10^{-5}

4.4.2 Comparison of models: instantaneous AC loss

The difference of the predictions of CSM and ECM in DC biased cases for low fields can be further studied by scrutinizing the power loss P per unit length of the wire as a function of time. Figure 4.3 shows $P(t)$ obtained from the simulations using CSM and ECM for cases of 100 mT DC field, 50 A transport DC and 1 mT and 5 mT AC Fields. In the 5 mT case, the losses over the tenth cycle of AC field given by the models were close to each other, and so are the shapes and magnitudes of the $P(t)$ curves as well. Note also that there is an observable transient in both curves (ECM and CSM) lasting for several cycles. In the 1 mT case, however, there is a substantial difference between the curves. Both of the curves exhibit very long transients but the one obtained using ECM is of completely different magnitude than the CSM one. Furthermore, there is a substantial, very slowly descending offset in the curve obtained using ECM. This is due to the heat generation associated to the DC component: the steady-state will not be fully achieved in ECM until the homogenization of the current density distribution is complete. However, this is not prominent in the 5 mT case, as the AC field is large enough for the offset to be negligible in comparison to the AC component of the loss. As steady-state has not yet been achieved after 10 cycles in the 1 mT case, the magnetization loop over the tenth cycle is not closed either, and one cannot separate the contributions of transport and magnetization losses.

In figure 4.4, close-ups of the curves presented in figure 4.3 are shown. In the close-ups the difference in the magnitude of the losses is even more obvious than in figure 4.3. In the results of both models, the ascending half of the cycle generates a substantially higher peak than the descending one.

4.4.3 Comparison of simulations and measurements

We performed simulations and measurements for tape 2 under several combinations of AC field and transport DC to shed light on the issues raised in the previous sections. The simulation results obtained using ECM and CSM are presented in figure 4.5. As expected, large discrepancies occur at the lowest values of applied AC field amplitude, 1 mT to 2 mT. However, for larger fields, both total and magnetization losses predicted by the models are in good agreement. It should be noted, that for low fields, ECM predicts especially much larger tranport losses than CSM, while the magnetization losses are indeed higher as well.

The AC loss measurements for tape 2 were performed at two frequencies:

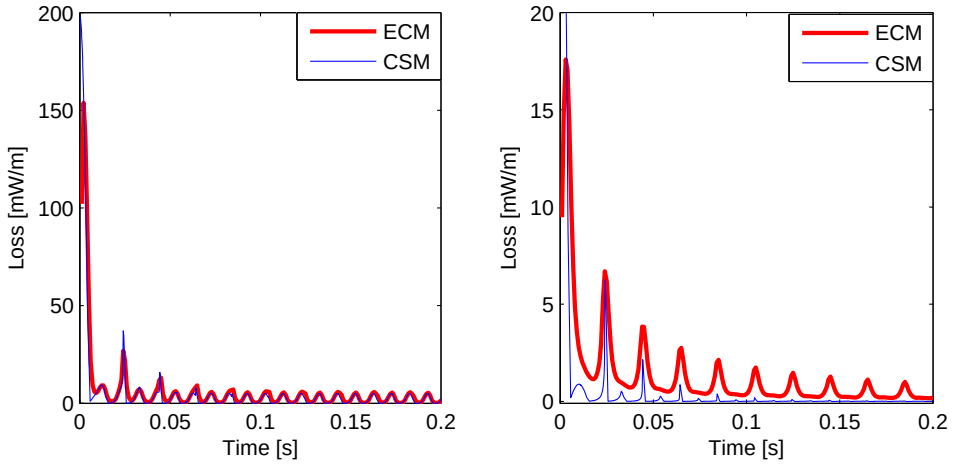

(a) (b)

Figure 4.3: The dissipated power as a function of time for (a) 50 A transport DC, 100 mT DC field and 5 mT AC ripple field and (b) 50 A transport DC, 100 mT DC field and 1 mT AC ripple field, obtained from the simulations. The time instant $t = 0$ marks the start of the ripple field.

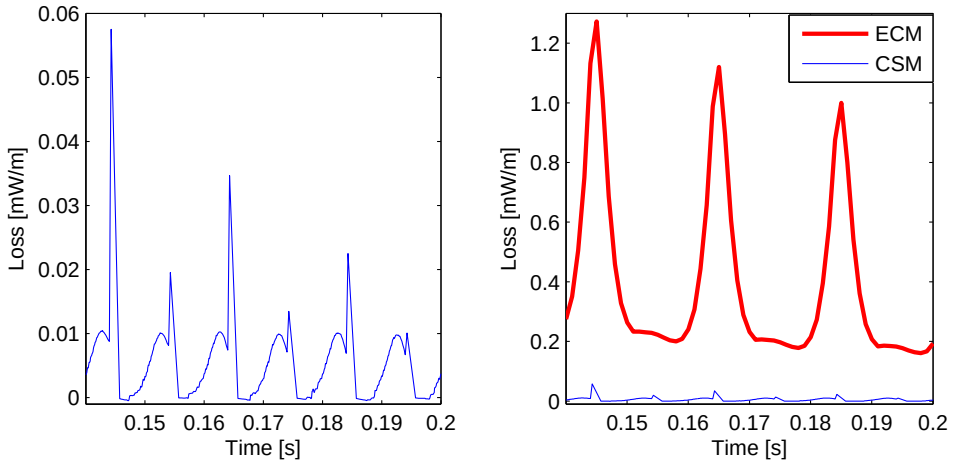

(a) (b)

Figure 4.4: Close-ups of the curves of figure 4.3 near 0.2 s. (a) CSM based simulation. (b) ECM and CSM based simulations.

36 Hz and 72 Hz. The measurement results for both frequencies are presented in figure 4.6. The total losses were interpolated and summed from the measured transport and magnetization loss data, and the total loss for $I = 0$ A was taken

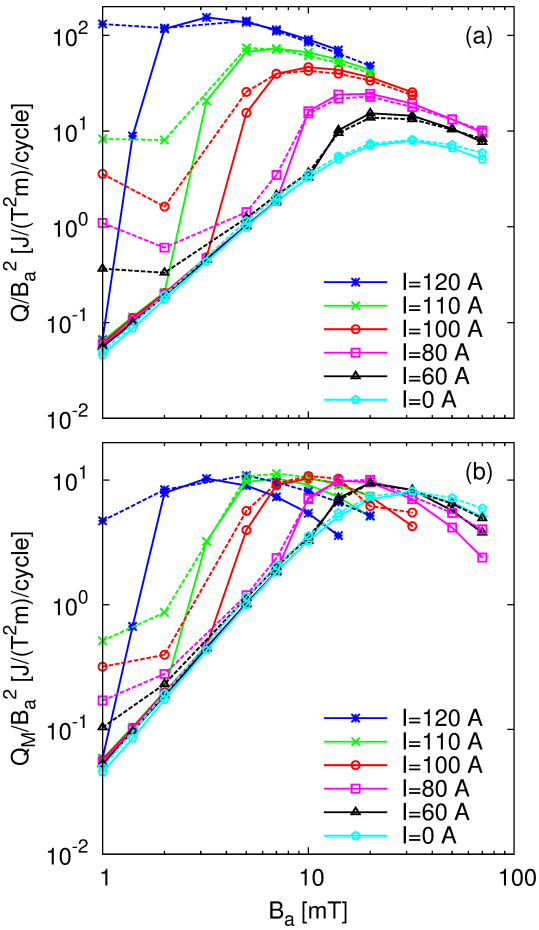

Figure 4.5: (a) The total losses and (b) the magnetization losses obtained from the simulations for tape 2 carrying several values of transport DC I. The losses are normalized by the amplitude of the applied field squared. The solid and dashed lines represent losses obtained using CSM and ECM, respectively.

to be directly the magnetization loss. Unfortunately, at the lowest fields the tranport loss measurements were too noisy and thus transport loss was not measured for those cases. Hence, we could not obtain reliable information about the total losses for the lowest field values, either. A slight frequency-dependence is observed in the results. However, the frequency-dependence is especially substantial for the highest values of DC and applied fields. This is natural, since the critical current of the tape decreases with increasing B_{a}: at high applied fields and DC the transport current is over-critical, at least for part of the cycle. Hence, the loss is then mostly of resistive nature and thus frequency-dependent. Furthermore, we observe that the magnetization loss increases with transport DC at low fields, as expected [29], but at high

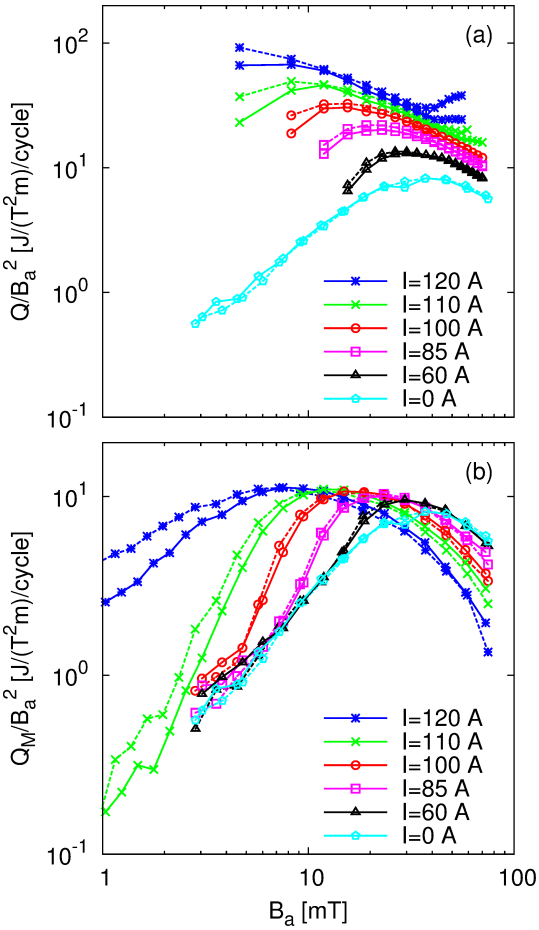

Figure 4.6: The measured losses for tape 2, normalized by the applied field amplitude squared. The dashed and solid lines represent results at frequencies $f = 36$ Hz and $f = 72$ Hz, respectively. (a) The total losses and (b) the magnetization losses.

AC applied fields its contribution to the total loss decreases with increasing transport current as the current saturates the tape cross-section partially.

To compare the measurement and simulation results directly, we linearly interpolated the measurement results to 50 Hz from the 36 Hz and 72 Hz data. The direct comparison of the simulations and measurements for the total loss is presented in figure 4.7. The qualitative agreement between the simulations and measurements is very good, while there are some discrepancies quantitatively. However, for the most part, also the quantitative agreement is acceptable. Note, that the loss factor representation, in which the losses are normalized by the squared amplitude of the applied field, exaggerates the difference between the curves. The measured curves present a slower drop in

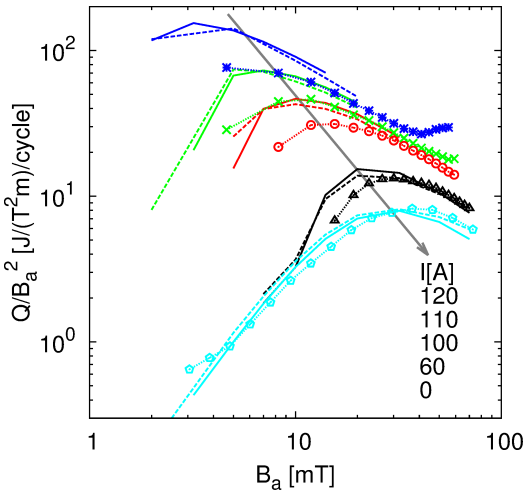

Figure 4.7: The comparison of the total losses obtained from the measurements and simulations for tape 2 carrying several DC, I, normalized by the amplitude of the applied field squared. The solid and dashed lines represent losses obtained using CSM and ECM, respectively, and the lines with markers represent the linearly interpolated measurement results for 50 Hz. The values of DC I are indicated in the figure.

the total loss with decreasing applied field magnitude than the simulated ones. This can be partially explained by possible degradation of J_c near the tape edges [49]. However, as noise is a limiting factor in measurements at such low fields, the reason for the disagreement is not known for sure. As B_a increases, the agreement between simulations and measurements gets better, while as transport DC increases, the agreement gets worse. This indicates that there could be an under-estimation of J_c at low fields in the simulations: the results for 110 A DC agree almost perfectly with 120 A results at the low field end of the graph, suggesting approximately a 10 % error in J_c.

The simulated and measured magnetization losses are compared in figure 4.8. The agreement between simulation and measurement results is better overall for magnetization losses than for the total losses. However, at the lowest fields of the order of 1 mT, the magnetization losses predicted using ECM agree better with the measurements than the ones predicted using CSM, as seen especially in the lower graph. This is partially explained by taking the B-dependence of the n-value into account in ECM. Also, the possible J_c degradation near the tape edges, which was not taken into account in our simulations, can cause higher losses at low field amplitudes.

Unfortunately, no reliable measurement data for transport losses at very

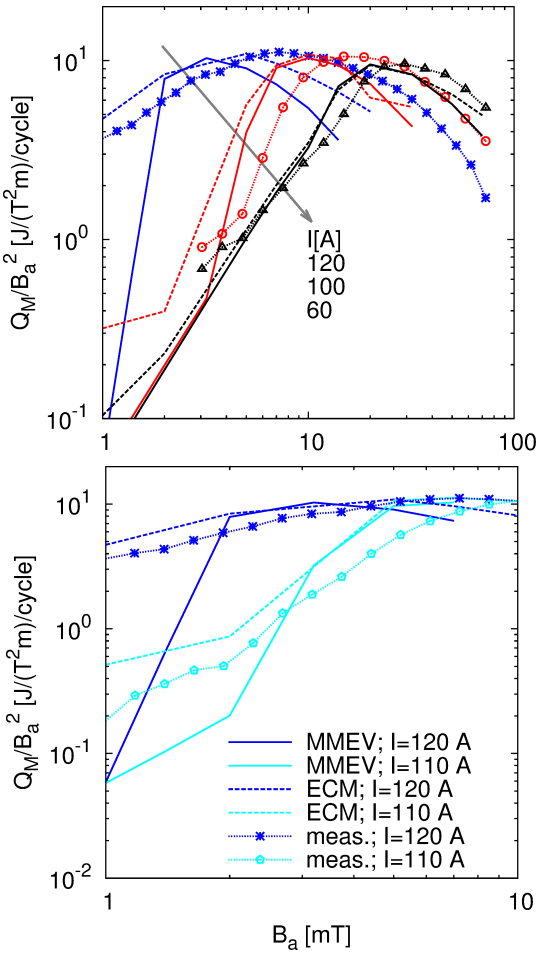

Figure 4.8: The comparison of the magnetization losses obtained from the measurements and simulations for tape 2 carrying several transport DC I, normalized by the amplitude of the applied field squared. The solid, dashed and marked lines have the same meaning as in figure 4.7. The lower figure shows a close-up of some of the measured and computed loss graphs.

low fields was obtained. However, the simulated transport losses were of completely different magnitude in ECM than in CSM, as highlighted in table 4.3. By evaluating the threshold value for dynamic magneto-resistance using (4.2), one obtains $B^* \approx 4$ mT for a superconducting strip of constant $I_c = 120$ A transporting a 100 A DC. This indicates that no transport loss should occur at applied fields of the order of 1 mT. This is the result of CSM, while ECM clearly predicts a high transport loss even at such low fields. The loss related to the DC component could be over-estimated again in ECM, consistently with the results presented previously in this chapter.

Table 4.3: The computed total and magnetization losses for 1 mT AC fields and two transport DC.

Transport DC [A]	Total loss (CSM) [J/m/cycle]	Total loss (ECM) [J/m/cycle]	Magnetization loss (CSM) [J/m/cycle]	Magnetization loss (ECM) [J/m/cycle]
110	6.393×10^{-8}	8.290×10^{-6}	5.691×10^{-8}	5.151×10^{-7}
120	7.157×10^{-8}	1.314×10^{-4}	5.747×10^{-8}	4.715×10^{-6}

4.5 Summary and concluding remarks

Research on the topic of AC losses in DC biased superconductors is important, not only from the viewpoint of application design, but also in the context of the appropriateness of the models used in superconductor modelling. ECM over-estimates the homogenization of the current density profile in a coated conductor tape, leading as well to over-estimation of losses related to DC and low-frequency quantities. The subtle difference of the E-J-relations of ECM and CSM leads to large discrepancies when simulating AC losses in DC biased superconductors at very low AC fields of the order of 1 mT with significant bias fields. However, in comparison with our measurement results, ECM yields a better description of reality in terms of contribution of magnetization loss to the total loss. Nonetheless, more high-precision AC loss measurements for superconductors under DC bias, especially in low AC fields, are needed to gain a better understanding of modelling such situations.

ECM and CSM are both mesoscopic models used for predicting macroscopic quantities observed in systems involving superconductors. Neither one of the models can be regarded as an intrinsic property of high-temperature superconductors. The models reflect different aspects of the behaviour of such materials under different conditions. One could thus claim that neither one of the models employs the *most appropriate* E-J-relation for high-temperature superconductors. However, is it even reasonable to expect a perfect agreement between the predictions of mesoscopic models in terms of observed macroscopic quantitites in systems, in which microscopic phenomena are of ample importance? Not necessarily, but this is not say that we should not strive for better models in the mesoscopic scale, too. The fundamental question of the most appropriate E-J-relation in superconductors is not a pre-meditated issue: in terms of superconductor AC loss modelling, we do not have mesoscopic models leading to predictions that agree with our observations in every case. Model development is still needed in our field of science.

Chapter 5

Possibilities: 2D simulations of hysteresis losses in partially coupled superconducting wires

An important research direction in the field of mesh method based modelling of AC losses in superconductors is that of investigating the possibilities of existing modelling tools. Such research can reveal new ways to utilize different modelling tools as well as situations, in which the utilization of those tools is difficult or impossible. Both kind of outcomes can yield crucial information for both scientific and industrial circles. In this chapter, we discuss the possibility of using a modelling tool comprised of the H-formulation solved using FEM in 2D for simulations of partially coupled superconducting wires.

The research presented in this chapter has been published in **Publication 3**. Here, we discuss the possibility to model hysteresis losses in partially coupled superconducting wires using a 2D H-formulation based simulation tool. We present a heuristic engineering approach for this in simple wire shapes. Furthermore, we compare the results of our approach with 3D simulations.

5.1 Background for this research

In practical magnet applications, multifilamentary superconducting wires are usually twisted to reduce their coupling in applied magnetic fields. Twisted wires can be either coupled, partially coupled or uncoupled with respect to the field, depending, for example, on the twist pitch, matrix resistivity and the magnitude of the applied field. In terms of induced screening currents, in

the fully coupled case the multifilamentary wire behaves like a monofilamentary conductor, whereas in the uncoupled case, each filament carries its own go and return screening currents. When the filaments are *partially coupled* the situation is something in between these two. This is demonstrated in figure 5.1. The difference in the coupling behaviour results in different values of AC losses: coupling currents flowing through the matrix material of the wire cause Ohmic loss, but also the obvious differences in the current density distributions in the filaments affect the hysteresis loss behaviour of the wire. When designing applications, such as superconducting motors [61, 114, 125], transformers [40, 60, 69] and accelerator magnets [5, 34, 131], this must be taken into account. Software implementations for computing losses in the matrix due to eddy currents and the inter-filamentary coupling currents of the wire based on analytical formulae for equivalent magnetization have been introduced, e.g., in the works of De Gersem [33], and in the ROXIE program [109], employed for instance in [8]. However, we shall present a 2D approach based on the H-formulation, with which we obtain qualitative and quantitative information about the changes in the *hysteresis losses* due to inter-filament coupling. Such information can be beneficial, for example, for estimating from measurements, to what extent the filaments are coupled. Our approach does not offer a full 2D simulation tool for modelling such situations as losses in the matrix material are neglected, but could be used as a part of a more complete toolkit for obtaining the full loss information.

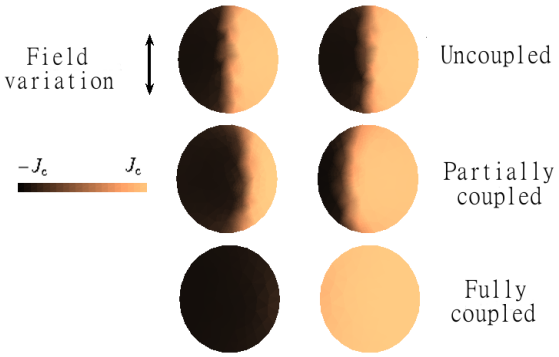

Figure 5.1: Current density distributions in the cross-section of a superconducting wire consisting of two filaments at the peak of external magnetic field with uncoupled, partially coupled, and fully coupled filaments. In the uncoupled case, the filaments both carry zero net currents as the screening currents are induced to them separately In the fully coupled one, the two filaments are filled with current densities in the opposite directions. Note that in this case, the applied field is above the penetration field.

In the typical ECM based hysteresis loss modelling tools, the traditional approach to simulate coupled and uncoupled situations in 2D is to set net current constraint for the whole wire in the coupled case, or separately for each filament in the uncoupled one. However, this leaves the possibility of partial coupling completely out of the question. In 3D simulations, however, one does not have to make such an explicit modelling decision, as the coupling behaviour is a natural consequence of, for example, material properties and the shape of the wire. Unfortunately, 3D simulations are inherently heavier and slower to perform than 2D ones, so 2D simulations would be preferable. Solving for the self-field AC losses of a wire exhibiting helicoidal symmetry is a real 2D problem [120], but this is not true, whenever an applied magnetic field is present. However, one could try to come up with a heuristic approach for performing such simulations. After all, we want to make predictions, and it is valuable if we can do it more easily but still precisely enough.

5.2 An engineering approach to simulate partially coupled superconducting wires in 2D

Looking at a cross-section of a superconducting multifilamentary wire, the question, whether the wire is coupled, partially coupled or uncoupled, can be answered by observing the current density distributions in the filaments (see figure 5.1). In the fully coupled case, a non-zero time-dependent net current $I^i_{\text{coupled}}(t)$ is induced through the cross-sections S_i of the filaments of the wire, even though no current is injected into the conductor: the net current of the *whole wire* remains zero. In the uncoupled case, each filament carries a zero net current. Thus, in the partially coupled case, the net currents of the filaments are in between those of the coupled and uncoupled situations.

To simplify the discussion, we shall consider only wires with round filaments with their centers placed within equal distance on the perimeter of a circle. To simulate such wires with partially coupled filaments in 2D, we need to force currents in between zero and $I^i_{\text{coupled}}(t)$ through the filaments. In a fixed applied field, we define the coupling degree $C^i(t)$ as

$$C^i(t) = I^i_{\text{fil}}(t)/I^i_{\text{coupled}}(t), \tag{5.1}$$

where $I^i_{\text{fil}}(t)$ is the net current through the filament i in a partially coupled case (or in the extreme cases of full coupling or no coupling). As the t-dependence in the definition suggests, C is not constant in time in a 3D simulation: as Faraday's law predicts, the magnitude of coupling currents is proportional to

$\partial_t B$. Thus, to express the coupling degree as a single real number, we define the *effective coupling degree* as

$$C_{\text{eff}} = \bar{I}_{\text{fil}}/\bar{I}_{\text{coupled}} \tag{5.2}$$

where

$$\bar{I}_{\text{fil}} = \frac{\hat{I}_{\text{fil}} + ||\tilde{I}_{\text{fil}}||}{2}, \quad \bar{I}_{\text{coupled}} = \frac{\hat{I}_{\text{coupled}} + ||\tilde{I}_{\text{coupled}}||}{2}. \tag{5.3}$$

The symbols $\hat{I}_{\text{fil}}$ and $\hat{I}_{\text{coupled}}$ denote the positive peak values of $I_{\text{fil}}(t)$ and $I_{\text{coupled}}(t)$, respectively, and similarly, $\tilde{I}_{\text{fil}}$ and $\tilde{I}_{\text{coupled}}$ denote the negative peak values. Note that we have dropped the superscripts related to the filament number here. This is justified, as for the simulated wire shapes, (5.2) has proven to be a reliable way to define to what extent any filament of the wire is coupled: as we altered the matrix resistivity to alter the coupling behaviour in our 3D simulations, the change in C_{eff} was the same, typically within one percent accuracy, in all the filaments. Thus, we can consider C_{eff} as the effective coupling degree of the *whole wire*. Note that this could not necessarily be done for more complicated wire structures.

Thus, to simulate a superconducting wire with a certain effective coupling degree, one would simply first simulate the fully coupled situation, and then force the net currents through the filaments according to the desired C_{eff}. However, the modelling domain we are interested in, a helicoidal multifilamentary wire, is not reducible to a single 2D cross-section of the wire in applied fields. The filaments rotate around each other helicoidally, and as they do so, each cross-section experiences an applied field in a fixed direction differently: the orientation of the field, and hence the current density distribution in the filaments, is different for each transversal cross-section of the wire along one twist pitch, as one travels along the helicoidal paths. This effect is demonstrated in figure 5.2.

However, assuming long enough twist pitches (not comparable to the radius of a filament) we can assume that the cross-sections of the filaments are not substantially deformed in the direction perpendicular to their helicoidal paths, nor in the direction perpendicular to the axis of the wire [50, 124]. With such assumptions, we can model the twisted multifilamentary wire by a 2D cross-section of a wire with round filaments. To take the twisting into account, we simply *alter the direction of the applied field* to obtain different current density distributions confronted in a realistic 3D situation. Hence, we do not need to alter our 2D modelling domain, but we simply compute the losses for a fixed domain, but with applied fields in different directions. We approximate the total loss as the average of the losses obtained at different field directions.

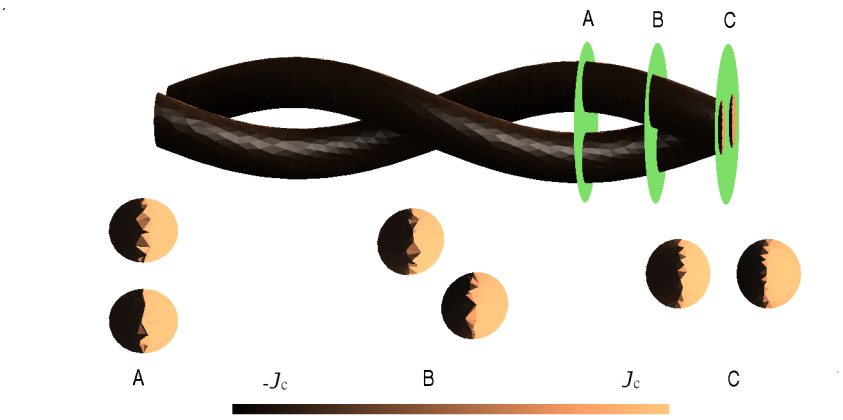

Figure 5.2: J profiles in the axial direction obtained from a 3D simulation for a 2-filament wire with partially coupled filaments in three transversal cross-sections. At the point at which the centers of the filaments are aligned in the direction of the field variation (A) the net currents through the cross-sections are zero. When the centers are aligned perpendicular to the field variation (C), the absolute values of the net currents through filaments reach their maximums.

In our cases, we found it reasonable to take three angles of applied field into account. As the field is rotated, it sees the same filamentary configuration in terms of the loss behaviour after a rotation about an angle α. This is detailed in figure 5.3.

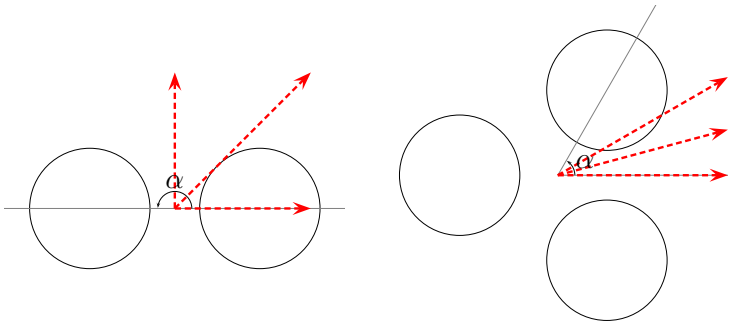

(a) (b)

Figure 5.3: (a) $\alpha = 180°$ for the two-filament wire and (b) $\alpha = 60°$ for the three-filament wire. The dashed arrows indicate the directions of the applied magnetic field in our 2D approach. With respect to the indicated zero angle, the directions are 0, $\alpha/4$, and $\alpha/2$. In terms of the resulting losses, one can multiply the applied field by -1 without changing the results. Hence, in (b) $\alpha = 60°$ instead of 120°.

Combining the discussion so far, we obtain an algorithm for simulating hysteresis losses in twisted multifilamentary superconductors with symmetrically placed round filaments, subject to applied magnetic field, with a predefined C_{eff}:

1. Find the angle α, through which one must rotate the applied magnetic field to yield the repetitive pattern of the filamentary structure. (See figure 5.3.)

2. Compute the fully coupled situation in 2D by forcing a zero net current condition for the *whole wire* using field angles 0, $\alpha/4$, and $\alpha/2$. Add or decrease the number of simulated angles depending on the desired accuracy and the symmetry of the configuration. Save the waveforms of the net currents through the filaments.

3. Compute the desired partially coupled situations for all these cases by forcing net currents according to C_{eff} as $I^i_{\text{fil}}(t) = C_{\text{eff}} I^i_{\text{coupled}}(t)$, for all the filaments S_i.

4. Compute the hysteresis loss Q per cycle and unit length as the average of the losses at different field angles: $Q = (Q_0 + Q_{\alpha/4} + Q_{\alpha/2})/3$, where Q_Υ denotes the loss obtained after applying the external field at angle Υ with respect to the predefined angle 0.

5.3 Results and discussion

Obviously, our engineering approach contains a lot of simplifications and approximations. To investigate its feasibility, it needs to be benchmarked. Hence, we performed 3D simulations for two different superconducting wires consisting of two and three helicoidal superconducting filaments embedded in a cylindrical normal-conducting matrix with a round cross-section, using our H-formulation based FEM modelling tool. The filaments had radii of 0.178412 mm and their centers were placed symmetrically inside the matrix, similarly as in the depiction of figure 5.3, 0.5 mm apart from each other. The filaments' twist pitch was 4 mm and the matrix had a radius of 0.564189 mm yielding a cross-sectional surface area of 1 mm^2. For both wires, we had $J_{\text{c}} = 5 \times 10^9$ A/m^2 and $n = 25$. The end effects were neglected and we used periodic boundary conditions for H to simulate the wires simply along one twist pitch. To obtain uncoupled, partially coupled and coupled situations, we performed simulations for a set of different matrix resistivies ρ_{m} and a set of amplitudes B_{a} of 50 Hz sinusoidal

applied field. Then, we performed the same simulations for the same wires using our engineering approach in 2D. The effective coupling degrees for the 3D cases were computed with respect to the fully coupled situation in 2D at field angle 0. The results are presented in figure 5.4.

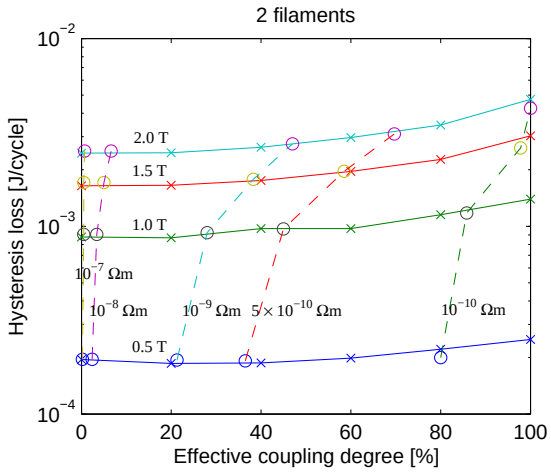

(a)

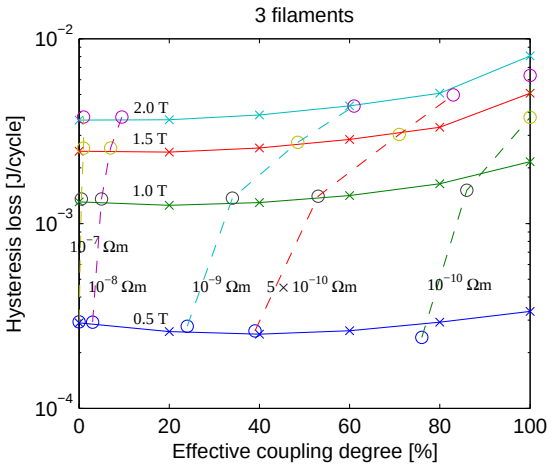

(b)

Figure 5.4: The results for the simulations with different effective coupling degrees for (a) two-filament wire and (b) three-filament wire. The 2D simulation results are denoted by the solid lines with cross markers and the 3D results are denoted by circle markers, and they have been positioned in the graphs according to their effective coupling degrees. The dashed lines represent different values of ρ_{m} in the 3D simulations. The different values of applied field amplitude are also indicated in the graphs. The field amplitude 0.5 T was the only one below full field penetration.

The 2D approach mostly yields similar results qualitatively and quantitatively as the 3D simulations. Especially for the 2-filament wire, the agreement is very good, even though small discrepancies occur at the highest coupling degrees. The largest discrepancies (approximately 20 %) occur for the 3-filament wire at the highest coupling degrees, corresponding to the lowest matrix resistivities. Partially, the worse agreement at low matrix resistivities can be explained by increased shielding provided by the matrix at lower resistivies, as in 2D approach, the matrix was modelled as air. Hence, better results might be obtained by taking the matrix into account in 2D simulations, too. However, as we do not have means for solving the coupling degree beforehand, the question of correct matrix resistivity for each coupling degree would remain. Nonetheless, especially in uncoupled and partially coupled cases, we obtain reliable information about hysteresis losses in twisted wires with this approach. Furthermore, as the number of degrees of freedom is typically of the order of 10^3 for the 2D approach, in comparison to 10^5 of 3D simulations, 2D simulations are significantly faster: the running time of a simulation is a few minutes instead of hours.

5.4 Concluding remarks and future possiblities

We have investigated the possiblity to use an H-formulation based modelling tool for 2D simulations of partially coupled superconducting wires. The engineering approach presented here is the first attempt towards such simulations. It provides an efficient way to obtain reliable information about hysteresis losses in twisted multifilamentary superconductors experiencing different levels of coupling in applied field.

2D simulations offer a speed advantage due to significantly smaller number of degrees of freedom compared to 3D simulations. Still, such a 2D approach has only been proven suitable for simple wire geometries. Furthermore, we cannot solve for the effective coupling degree C_{eff} in 2D using our approach, and associating a correct ρ_{m} for a certain C_{eff} in a fixed applied field is an unsolved issue. Hence, we can only compute losses with predefined coupling degrees and sweep C_{eff} from uncoupled to fully coupled to obtain information about the hysteresis loss behaviour at different coupling degrees. For future development, one possibility is to investigate, whether the effective coupling degree could be solved from a linear problem, as losses in the matrix material of a superconducting wire can be reliably predicted from such 3D simulations [71]. One could first solve for the losses in the matrix from the linear 3D problem and then solve for the hysteresis losses using our 2D engineering approach and

the effective coupling degree obtained from the 3D simulation. This way, one would obtain the full loss information in a quick and reliable manner, without heavy non-linear 3D simulations: only linear (time-harmonic) 3D and non-linear 2D problem would have to be solved. Nonetheless, to fully benefit from the inherent speed advantage of the 2D simulations when modelling partially coupled superconducting wires, there is still a clear need for research in the directions of tool development and possibilities of tools.

Chapter 6

Conclusions

This thesis seeks to push the boundaries of contemporary hysteresis loss modelling in superconductors. At first, the background of mathematical modelling of superconductors was discussed. The discussion emphasized the mathematical structures needed in modelling, as well as the structure of scientific research in this field. Then, we introduced the formulations implemented in our in-house AC loss modelling tool that were used in the research of this thesis. The structural formalism and the chosen level of abstraction allowed us to implement the formulations so, that the resulting simulation tools are dimension-independent: the tools for 2D and 3D simulations were conceived simultaneously in a natural manner. After introducing the formulations, we discussed the properties of two widely used models for hysteresis loss modelling, CSM and ECM, through case studies of DC biased superconductors in AC ripple fields. Finally, we introduced an algorithm to model superconducting wires with partially coupled filaments with respect to external magnetic field in 2D.

In a sense, chapter 2 and **publication 4** structuralize and set up the table for the search of frontiers in our field of science. Chapter 3, based on **Publication 1** and **Publication 6** is related to *formulation* and *tool development*. Especially, it introduces a formulation, which exploits the concepts of homology and cohomology, and which offers a substantial speed advantage over the traditional H-formulation, nowadays most often used for simulating superconductor AC losses. The implementations of the formulations have been done in a dimension-independent manner. **Publication 2** presents an introduction to the theme discussed in chapter 4, which is mainly based on **Publication 5**. This chapter presents *particular case studies*, which suggest that *model development* is still needed in our field. Neither CSM or ECM can be regarded as employing the most appropriate E-J-relation for high-temperature super-

conductors. From a philosophical point of view, we want to emphasize that the models we use should not be regarded as intrinsic properties of nature, but simply formalizations of our intuition, which yield predictions of different accuracy for different situations. Chapter 5, which is based on **Publication 3**, studies the *possiblities of a tool* by presenting an approach for modelling superconductors with partially coupled filaments using an H-formulation based modelling tool in 2D. However, the results also suggest, that more research is needed in the research directions of *tool development* and *possibilities of tools* to fully benefit from the 2D simulations in such cases. The presented algorithm is not valid for arbitrary filamentary structures, nor can one solve beforehand, to what extent the filaments of the wire are coupled.

Even though the research presented in this thesis reaches out to many different directions, it is confined to a well-structured field of science. It provides scientists and industrialists working on AC losses of superconductors with machinery to better tackle problems they face in their everyday work, as well as some insights to the fundamentals of mathematical modelling. Of course, the presented pieces of research represent only the tip of the iceberg in their respective research directions. However, they are useful presentations of new information and valuable discussion openings for important future developments.

Bibliography

[1] Ainslie M D, Zermeno V, Hong Z, Yuan W, Flack T J and Coombs T A 2011 *Supercond. Sci. Technol.* **24** 045005

[2] Amemiya N 2000 *Cryogenics* **40** 303

[3] Amemiya N, Miyamoto K, Banno N, and Tsukamoto O 1997 *IEEE Trans. Appl. Supercond.* **7** 2110

[4] Anderson P W 1962 *Phys. Rev. Lett.* **9** 309

[5] Ang Z *et al* 1999 *IEEE Trans. Appl. Supercond.* **9** 742

[6] `http://fs.magnet.fsu.edu/~lee/plot/plot.htm` Website maintained by Applied Superconductivity Center in Tallahassee, Florida

[7] Auchmann B, De Maria R, Russenschuck S 2008 *IEEE Trans. Appl. Supercond.* **18** 10075083

[8] Auchmann B, Flemisch B and Kurz S 2010 *IEEE Trans. Magn.* **46** 3508

[9] Badía-Majós A, López C and Ruiz H S 2009 *Phys. Rev. B* **80** 144509

[10] The website of professor John C. Baez, section about a mathematics graduate course on classical mechanics given by him. `http://math.ucr.edu/home/baez/classical/`

[11] Baez J and Muniain J P 1994 *Gauge fields, knots and gravity* Series on Knots and Everything: vol 4 (Singapore: World Scientific Publishing)

[12] Bardeen J, Cooper L N and Schrieffer J R 1957 *Phys. Rev.* **108** 1175

[13] Bean C P 1962 *Phys. Rev. Letters* **8** 250

[14] Bednorz J G and Müller K A 1986 *Zeitschrift für Physik B Condensed Matter* **64** 2 189

[15] Bíró O *Comput. Method Appl. M.* **169** 391

[16] Boothby W M 1986 *An introduction to differentiable manifolds and Riemannian geometry* Second edition (Orlando, FL: Academic Press)

[17] Bossavit A 1988 *IEEE Proc.* **135** 493

[18] Bossavit A 1988 *IEEE Trans. Magn.* **38** 341

[19] Bossavit A 1998 *IEEE Trans. Magn.* **34** 2429

[20] Bossavit A 2000 *Physica B* **275** 142

[21] Bossavit A 2005 Discretization of electromagnetic problems: The "generalized finite differences" approach *Handbook of Numerical Analysis* **13** 105-197

[22] Bottura L 2000 *IEEE Trans. Appl. Supercond.* **10** 1054

[23] Brambilla R, Grilli F and Martini L 2007 *Supercond. Sci. Technol.*, **20** 16

[24] Brenner S C and Scott L R 2008 *The mathematical theory of finite element methods* Third edition (New York, NY: Springer Science+Business Media, LLC)

[25] Bruzzone P 2004 *Physica C* **401** 7

[26] Campbell A M 2007 *Supercond. Sci. Technol.* **20** 292

[27] Cardwell D A and Ginley D S Editors 2003 *Handbook of Superconducting Materials* (Bristol: Institute of Physics Publishing)

[28] Ciszek M *et al* 1996 *Supercond. Sci. Technol.* **9** 379

[29] Ciszek M, Tsukamoto O, Ogawa J, and Miyagi D 2002 *Advances in Cryogenic Engineering* **48** 606

[30] Clem J R, Weigand M, Durrel J H and Campbell A M 2011 *Supercond. Sci. Technol.*, **24** 062002

[31] Comsol Multiphysics is a commercial FEM program. `http://www.comsol.com`

[32] Conectus, Consortium of European Companies Determined to Use Superconductivity `http://www.conectus.org/`

[33] De Gersem H, Koch S and Weiland T 2006 *Proceedings of ICAP 2006, Chamonix, France* 90

[34] den Ouden A, Wessel S, Krooshop E, and ten Kate H 1997 *IEEE Trans. Appl. Supercond.* **7** 733

[35] Eckelman H, Däumling M, Quilitz M and Goldacker W 1998 *Physica C* **295** 198

[36] Flanders H 1989 *Differential forms with applications to the physical sciences* (New York: Dover Publications, Inc.)

[37] Foltyn S R *et al* 2007 *Nature Materials* **6** 631

[38] Forrest A M 1983 *Eur J. Phys.* **4** 117 A translation of the original article by Meissner W and Ochsenfeld R 1933 "Ein neuer effekt bei eintritt der supraleitfähigkeit" *Die Naturwissenschaften* **21** 787

[39] Frankel T 2012 *The geometry of physics: an introduction* Third edition (Cambridge: Cambridge University Press)

[40] Funaki K *et al* 2001 *IEEE Trans. Appl. Supercond.* **11** 1578 2001

[41] Gariepy R F and Ziemer W P 1995 *Modern real analysis* (Boston, MA: PWS Publishing Company)

[42] Geroch R 1985 *Mathematical physics* (Chicago and London: The University of Chicago Press)

[43] Geuzaine C and Remacle J-F 2009 *Int. J. Numer. Meth. Eng.* **79** 1309

[44] Grilli F, Brambilla R, Sirois F, Stenvall A and Memiaghe S 2013 *Cryogenics* **53** 142

[45] Grilli F and Pardo E 2010 *Supercond. Sci. Technol.* **23** 115018

[46] Grilli F, Pardo E, Stenvall A, Nguyen D N, Yuan W, and Gömöry F 2014 *IEEE Trans. Appl. Supercond.* **24** 8200433

[47] Gurvitch M, Ghosh A K, Lutz H and Strongin M 1980 *Phys. Rev. B.* **22** 128

[48] Gömöry F and Inanir F 2012 *IEEE Trans. Appl. Supercond.* **22** 4701704

[49] Gömöry F, Vojenčiak M, Pardo E, Solovyov M, and Šouc J 2010 *Supercond. Sci. Technol.* **23** 034012

[50] Hardy M 2004 Geometric transformation for double helical wire rods *M.Sc. thesis* Dept. Mech. Eng., Hawaii Mânoa Univ., Honolulu, HI

[51] Harrington R F 1993 *Field computation by moment methods* (John Wiley & sons, inc.)

[52] Hehl F W, Obukov Y N 2003 *Foundations of classical electrodynamics: charge, flux, and metric* (Boston, MA: Birkhäuser)

[53] Henrotte F and Hameyer K 2003 *IEEE Trans. Magn.* **39** 1167

[54] Herrmann J, Müller K H, Savvides N, Gnanarajan S, Thorley A and Katsaros A 2000 *Physica C* **341** 2493

[55] Hindmarsh A C *et al* 2005 *ACM Trans. Math. Softw.* **31** 363

[56] Hong Z, Campbell A M and Coombs T A 2006 *Supercond. Sci. Technol.* **19** 1246

[57] Hong Z, Yuan W, Ainsile M, Yan Y, Pei R and Coombs T A 2011 *IEEE Trans. Appl. Supercond.* **21** 2466

[58] Honjo S *et al* 2011 *IEEE Trans. Appl. Supercond.* **21** 967

[59] Hull J R and Strasik M 2010 *Supercond. Sci. Technol.* **23** 124005

[60] Iwakuma M *et al* 2001 *IEEE Trans. Appl. Supercond.* **11** 1482

[61] Kalsi S, Gamble B B, Snitchler G and Ige S O 2006 *Power Engineering Society General Meeting, IEEE* 5 pp

[62] Kamihara Y, Watanabe T, Hirano M and Hosono H 2008 *J. Am. Chem. Soc.* **130** 2 3296

[63] Kettunen L, Forsman K and Bossavit A 1998 *Int. J. Numer. Meth. Eng.* **41** 935

[64] Kettunen L, Forsman K and Bossavit A 1998 *IEEE Trans. Magn.* **34** 2551

[65] Kim Y B, Hempstead C F and Strnad A R 1965 *Phys. Rev* **139** A1163

[66] Kincaid D and Cheney W 2002 *Numerical analysis: mathematics of scientific computing* Third edition (Pacific Grove, CA: Brooks/Cole)

[67] Kotiuga P R 1987 *J. Appl. Phys.* **61** 3916

[68] Kurz S and Auchmann B 2012 Differential forms and boundary integral equations for Maxwell-type problems *Fast Boundary Element Methods in Engineering and Industrial Applications: Lecture notes in Applied and Computational Mechanics* **63** 1-62

[69] Lee H J *et al* 2001 *IEEE Trans. Appl. Supercond.* **11** 1486

[70] Lvovsky Y and Jarvis P 2005 *IEEE Trans. Appl. Supercond.* **15** 1317

[71] Lyly M, Lahtinen V, Stenvall A, Rostila L and Mikkonen R 2014 *IEEE Trans. Appl. Supercond.* **24** 8200909

[72] Lyly M, Lahtinen V, Stenvall A, Tarhasaari T and Mikkonen R 2013 *IEEE Trans. Appl. Supercond.* **23** 8200909

[73] Lyly M, Zermeno V, Stenvall A, Lahtinen V and Mikkonen R 2013 *IEEE Trans. Appl. Supercond.* **23** 6000105

[74] Maguire J F *et al* 2007 *IEEE Trans. Appl. Supercond.* **17** 2034

[75] Martini L, Gandini A, Rossi L, Ottoboni V and Zannella S 1996 *Physica C* **261** 196

[76] Masti M , Lehtonen J, Perälä R, Mikkonen R, Söderlund L and Seppälä P 2005 *Meas. Sci. Technol.* **16** 1092

[77] MATLAB is a product of Mathworks. `http://www.mathworks.com`

[78] Maunder C R F 1980 *Algebraic topology* Dover edition (Cambridge: Cambridge University Press)

[79] Maxwell J C 1881 *A treatise on electricity and magnetism* (Clarendon Press)

[80] Mess K H, Sch*ddot*user P and Wolff S 1996 *Superconducting accelerator magnets* Singapore: World Scientific Publishing

[81] Mikitik G P and Brandt E H 2001 *Phys. Rev. B* **54** 092502

[82] Misner C W and Wheeler J A 1957 *Ann. Phys.* **2** 525

[83] Mitchell N *et al* 2008 *IEEE Trans. Appl. Supercond.* **18** 435

[84] Morandi A 2012 *Supercond. Sci. Technol.* **25** 104003

[85] Mota A C, Pollini A and Visani P 1988 *Phys. Scripta* **37** 823

[86] Nguyen D N, Ashworth S P, Willis J O, Sirois F and Grilli F 2010 *Supercond. Sci. Technol.* **23** 025001

[87] Noe M and Steurer M 2007 *Supercond. Sci. Technol.* **20** R15

[88] Norris W T 1970 *J. Phys. D: Appl. Phys.* **3** 489

[89] North J 2009 *J. Phil.* **106** 57

[90] Onnes H K 1911 *Comm. Leiden* **122(b)**

[91] Oomen M P, Leghissa M, Proelss N and Neumuller H 2009 *IEEE Trans. Appl, Supercond.* **19** 3

[92] Pardo E 2008 *Supercond. Sci. Technol.* **21** 065014

[93] Pardo E, Gömöry F, Šouc J and Ceballos J M 2007 *Supercond. Sci. Technol.* **20** 351

[94] Pardo E, Kováč J and Šouc J 2013 *IEEE Trans. Appl. Supercond.* **23** 4701305

[95] Pardo E, Sànchez À, Chen D and Navau C 2005 *Phys. Rev. B* **71** 134517

[96] Pardo E, Šouc J and Vojenčiak M 2009 *Supercond. Sci. Technol.* **22** 075007

[97] Pardo E, Vojenčiak M, Gömöry F and Šouc J 2011 *Supercond. Sci. Technol.* **24** 065007

[98] Pellikka M 2014 Finite element method for electromagnetics on Riemannian manifolds: Topology and differential geometry toolkit *Ph.D. thesis* Tampere University of Technology, Finland `http://urn.fi/URN:ISBN:978-952-15-3285-6`

[99] Pellikka M, Suuriniemi S, Kettunen L and Geuzaine C 2013 *SIAM. J. Sci. Comput.* **35** B1195

[100] Pellikka M, Tarhasaari T, Suuriniemi S and Kettunen L 2013 *J. Comp. Appl. Math.* **246** 225

[101] Polak M, Kvitkovic J, Mozola P, Usak E, Barnes P N and Levin G A 2007 *Supercond. Sci. Technol.* **20** S293

[102] Prigozhin L 1997 *IEEE Trans. Appl. Supercond.* **7** 3866

[103] Raatikainen P, Zalta E N (Ed.) 2013 Gödel's incompleteness theoremss *The Stanford Encyclopedia of Philosophy* Winter 2013 Edition

[104] Rapetti F and Bossavit A 2009 *SIAM J. Numer. Anal.* **47** 2369

[105] Raumonen P 2009 Mathematical structures for dimensional reduction and equivalence classification of electromagnetic boundary value problems *Ph.D. thesis* Tampere University of Technology, Finland `http://urn.fi/URN:NBN:fi:tty-200908196872`

[106] Raumonen P, Suuriniemi S, Tarhasaari T and Kettunen L 2008 *IEEE Trans. Magn.* **44** 1146

[107] Reddy J N and Gartling D K 2001 *The Finite Element Method in Heat Transfer and Fluid Dynamics* Second edition (Boca Raton, FL: CRC Press LLC)

[108] Rossi L 2010 *Supercond. Sci. Technol.* **23** 034001

[109] Roxie is a program for the electromagnetic simulation and optimization of accelerator magnets. `https://espace.cern.ch/roxie/default.aspx`

[110] Runde M, Stenvall A, Magnusson N, Grasso G and Mikkonen R 2008 *J. Phys.: Conference Series* **97** 012159

[111] Sànchez À and Navau C 2001 *Phys. Rev. B* **64** 214506

[112] Sander M and Grilli F. 2010 *JPCS* **234** 022030

[113] Multiple authors, edited by Seeber B 1998 *Handbook of applied superconductivity* IOP Publishing LTD

[114] Sim J *et al* 2003 *IEEE Trans. Appl. Supercond.* **13** 2231

[115] Sirois F and Roy F 2007 *IEEE Trans. Appl. Supercond.* **17** 3836

[116] Sirois F, Roy F and Dutoit B 2009 *IEEE Trans. Appl. Supercond.* **19** 3600

[117] Scnitchler G, Gamble B, King C and Winn P 2011 *IEEE Trans. Appl. Supercond.* **21** 3

[118] Solovyov M, Vojenčiak M and Gömöry F 2009 *IEEE Trans. Appl. Supercond.* **19** 3049

[119] Šouc J, Pardo E, Vojenčiak M and Gömöry F 2009 *Supercond. Sci. Technol.* **22** 015006

[120] Stenvall A, Grilli F and Lyly M 2013 *IEEE Trans. Appl. Supercond.* **23** 8200105

[121] Stenvall A, Siahrang M, Grilli F and Sirois F 2013 *Supercond. Sci. Technol.* **26** 045011

[122] Stenvall A and Tarhasaari T 2010 *Supercond. Sci. Technol.* **23** 075010

[123] Stenvall A and Tarhasaari T 2010 *Supercond. Sci. Technol.* **23** 125013

[124] Stenvall A, Tarhasaari T, Raumonen P, Vojenčiak M and Pellikka M 2013 *Cryogenics* **53** 135

[125] Sugimoto H *et al* 2007 *IEEE Trans. Appl. Supercond.* **17** 1637

[126] SUite for Nonlinear and DIfferential/ALgebraic Equation Solvers (SUNDIALS), available online at: `https://computation.llnl.gov/casc/sundials/`

[127] SuperPower, Inc. http://www.superpower-inc.com/.

[128] Szekeres P 2004 *A course in modern mathematical physics: Groups, Hilbert space and differential geometry* (Cambridge: Cambridge University Press)

[129] Thakur K P, Raj A, Brandt E H, Kvitkovic J and Pamidi S V 2011 *Supercond. Sci. Technol.* **24** 065024

[130] Thakur K P, Raj A, Brandt E H and Sastry P V P S S 2011 *Supercond. Sci. Technol.* **24** 045006

[131] Verweij A P 1997 Review on boundary-induced coupling currents *European Organization for Nuclear Research, European Laboratory for Particle Physics, LHC Project Report 152* 11 pp.

[132] Vinod K, Abhilash Kumar R G and Syamaprasad U 2007 *Supercond. Sci. Technol.* **20** R1

[133] Wakuda T *et al* 1997 *Cryogenics* **37** 381

[134] WAMSDO 2013 – Workshop on Accelerator Magnet, Superconductor, Design and Optimization – January 15-16 2013, CERN. `http://indico.cern.ch/conferenceDisplay.py?confId=199910`

[135] Wan A, Laforest M, Sirois F 2012 Adaptive space-time finite element method based on a power law characteristic for computing AC losses in HTS devices *Applied Superconductivity Conference, October 7-12 2012 (Portland, Oregon)*

[136] Weiland T 1977 *Electronics and Communications* **31** 116

[137] Wilder R L 1965 *Introduction to the Foundations of Mathematics* (Wiley: New York)

[138] Wilson M N 1987 *Superconducting magnets* (USA: Oxford University Press)

[139] Wilson M N 2008 *Cryogenics* **48** 381

[140] Wolsky A M and Campbell A M 2008 *Supercond. Sci. Technol.* **21** 075021

[141] Xu X, Sumption N D, Bhartiya S, Peng X and Collings E W 2013 *Supercond. Sci. Technol.* **26** 075015

[142] Xue X D, Cheng K W E and Sutanto D *Supercond. Sci. Technol.* **20** R31

[143] Yamafuji K, Wakuda T and Kiss T 1997 *Cryogenics* **37** 421

[144] Yee K S 1966 *IEEE Trans. Antennas Propag.* **14** 302

[145] Yosida K 1980 *Functional analysis* Fifth edition (Berlin, Germany: Springer)

[146] Zhang M and Coombs T A 2012 *Supercond. Sci. Technol.* **25** 015009

Tampereen teknillinen yliopisto
PL 527
33101 Tampere

Tampere University of Technology
P.O.B. 527
FI-33101 Tampere, Finland

ISBN 978-952-15-3334-1
ISSN 1459-2045